The final publication is available at

http://dx.doi.org/0.1016/j.aca.2016.10.019

Additional Information

Graphene-based materials for the electrochemical determination of hazardous ions

J. Molina[1], F. Cases[1], L.M. Moretto[2*]

[1]Departamento de Ingeniería Textil y Papelera, EPS de Alcoy, Universitat Politècnica de València, Plaza Ferrándiz y Carbonell s/n, 03801 Alcoy, Spain
[2] Department of Molecular Sciences and Nanosystems, University Ca' Foscari of Venice, Via Torino 155, Venice, Italy

Abstract

The use of graphene in the field of electrochemical sensors is increasing due to two main properties that make graphene and derivatives appealing for this purpose: their conductivity and high surface area. In addition, graphene materials can be easily functionalized with nanoparticles (Au, Pt, etc.) or organic molecules (DNA, polymers, etc.) producing synergies that allow higher sensitivity, lower limit of detection as well as increased selectivity. The present review focuses on the most important works published related to graphene-based electrochemical sensors for the determination of hazardous ions (such as As(III), Cd^{2+}, Pb^{2+}, Hg^{2+}, Cr(VI), Cu^{2+}, Ag^+, etc.). The review presents examples of the use of graphene-based electrodes for this purpose as well as important parameters of the sensors such as: limit of detection, linear range, sensitivity, main interferences, stability, and reproducibility. The application of these graphene-based electrodes in real samples (water or food matrices) is indicated, as well. There is room for improvement of these type of sensors and more effort should be devoted to the use of doped graphene (doped for instance with N, B, S, Se, etc.) since electrochemically active sites originated by doping facilitate charge transfer, adsorption and activation of analytes, and fixation of functional moieties/molecules. This will allow the sensitivity and the selectivity of the electrodes to be increased when combined with other materials (nanoparticles/organic molecules).

Keywords: graphene, nanoparticles, hazardous ions, sensor, electrochemical sensor, electroanalysis.

---

* Corresponding author. Fax: +390412348594; telephone: +390412348585.
E-mail addresses: jamopue@doctor.upv.es (J. Molina), fjcases@txp.upv.es (F. Cases), moretto@unive.it (L.M. Moretto).

Abbreviations:

ABS: Acetate buffer solution; AdDPCSV: Adsorptive differential pulse cathodic stripping voltammetry; ARGO: Activated reduced graphene oxide; ASLSV: Anodic stripping linear sweep voltammetry; ASV: Anodic stripping voltammetry; BF: bismuth film; BFE: Bismuth film electrode; C: Concentration; CC: Chronocoulometry; CPE: Carbon paste electrode; CTAB: Cetyltrimethylammonium bromide; CV: Cyclic voltammetry; CVD: Chemical vapor deposition; DNA: Deoxyribonucleic acid, DPASV: Differential pulse anodic stripping voltammetry; DPV: Differential pulse voltammetry; DTT: Diaminoterthiophene; EDTA: ethylenediaminetetraacetate; EIS: Electrochemical impedance spectroscopy; ERGO: Electrochemically reduced graphene oxide; G: Graphene; GCE: Glassy carbon electrode; GNS: Graphene nanosheets; GO: Graphene oxide; GQD: Graphene quantum dot; GRC: Graphite reinforced carbon; GS: Graphene sheet; HER: Hydrogen evolution reaction; IL: Ionic liquid; ITO: Indium tin oxide; LSV: Linear sweep

voltammetry; MFE: Mercury film electrode; MTU: 5-methyl-2-thiouracil; MWCNTs: Multiwalled carbon nanotubes; nanoG: Nanographene; NP: Nanoparticle; NPC: Nanoporous carbon; ocp: Open circuit potential; OSWV: Osteryoung square wave voltammetry; PAH: polyallylamine hydrochloride; Pani: Polyaniline; PBS: Phosphate buffer solution; PEDOT: Poly(3,4-ethylenedioxythiophene); PEI: Polyethyleneimine; PGE: Pencil graphite electrode; poly-p-ABSA: poly(p-aminobenzene sulfonic acid); po-G: Partially oxidized graphene; PPAA: Plasma polymerized allylamine; PPy: Polypyrrole; PS: Polystyrene; PSA: Potentiometric stripping analysis; PSS: poly(styrenesulfonate); PVDF: polyvinylidene difluoride; PVP: polyvinylpyrrolidone; QCM: Quartz crystal microbalance; QD: Quantum dot; RGO: Reduced graphene oxide; RSD: Relative standard deviation; SA: Sodium alginate; SDS: Sodium dodecyl sulfate; ssDNA: Single stranded DNA; SPCE: Screen printed carbon electrode, SPE: Screen printed electrode; STP: Sulfonate-terminated polymer; SWASV: Square-wave anodic stripping voltammetry; SWV: Square wave voltammetry; WHO: World Health Organization; 3DAGNs: Three-dimensional activated graphene networks.

_____

List of contents

_____

1. Introduction

Graphene, often regarded as the new "miracle material" [1], has emerged as a revolutionary material since its isolation in 2004 by K.S. Novoselov and co-workers [2]. Such consideration arises from properties such as high electron mobility at room temperature ($2.5 \cdot 10^5$ cm^2 V^{-1} s^{-1}), high thermal conductivity (above 3000 W m K^{-1}), Young's Modulus (1 TPa), intrinsic strength (130 GPa), impermeability to any gas, ability to sustain high electric current densities, easy chemical functionalization, etc. [1]. Geim and Novoselov were awarded the Nobel Prize in Physics in 2010 for the "groundbreaking experiments regarding the two-dimensional material, graphene" [3].

Graphene materials have shown an exponential evolution in the production of papers (Fig. 1-a) (the same applies to the production of patents, Fig. 1-c) which gives an idea of the importance of the discovery. The applications pointed out in literature include: flexible electronics (e.g. touch screen displays, transistors, etc.), photonics and optoelectronics (e.g. photodetectors, optical modulators, etc.), spintronics, composite materials, energy generation and storage, biomedical applications, sensors, etc. [1,4]. The application of graphene in these fields is still under investigation and there is much work to be done in order to develop this plethora of possible applications. For this reason the European Union is devoting a great deal of investment (1000 Million €) in the Graphene Flagship within the Horizon 2020 programme. This programme "aims to take graphene and related layered materials from the realm of fundamental science to industrial and societal applications in the space of ten years".
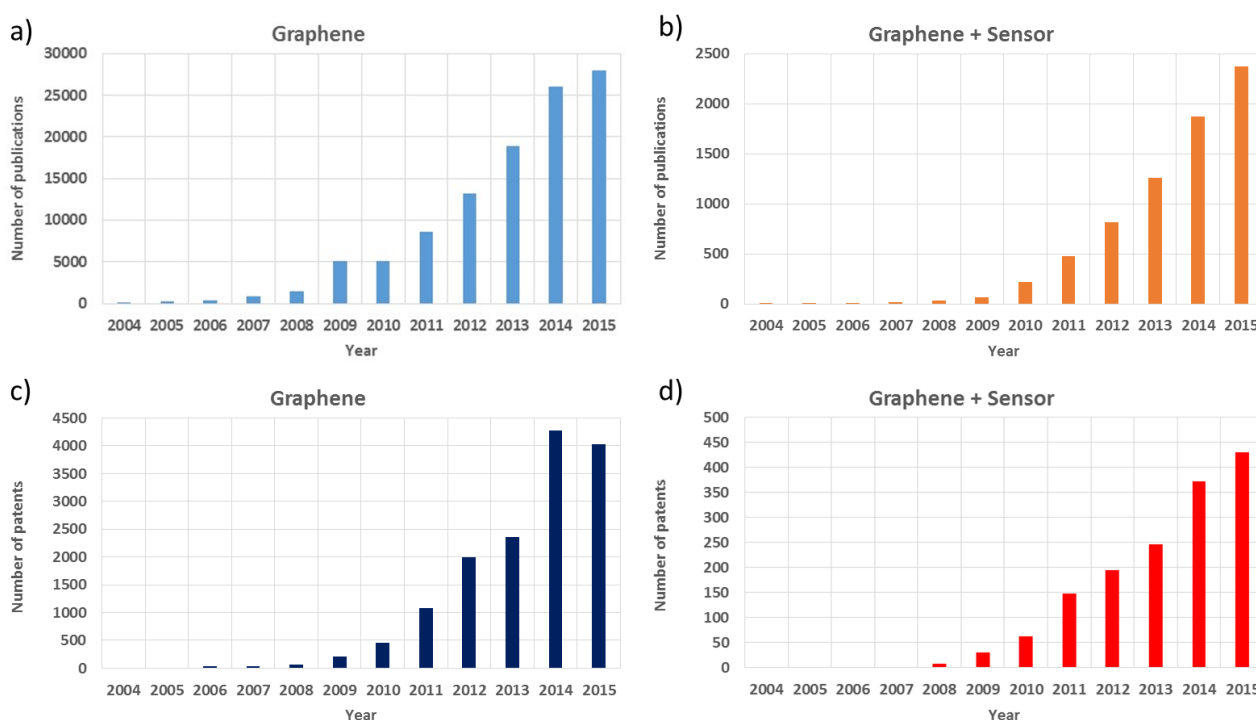

Fig. 1. Number of publications for: a) Graphene, b) Graphene + sensor search. Source: Web of Science, search performed in January 2016. Number of patents for: c) Graphene and d) Graphene + sensor search. Source: World Intellectual Property Association, search performed in August 2016.

Graphene materials have been widely used for the production of sensors and biosensors. An exponential evolution in the production of papers and patents has also been observed for graphene and sensors (Fig. 1-b and Fig. 1-d). Several reviews can be found in literature regarding its use in sensing and biosensing [5-24]. The field of electrochemical sensors for the detection of hazardous metal ions is also an active area in the field, and a progressive growth in the number of publications related to this topic has been observed [25]. The trend in the development of sensors is the use of nanostructured materials and several reviews can be found in the bibliography regarding nanostructured materials for the determination of trace metal ions [25-29]. Different sensitive and accurate analytical techniques have been applied for the determination of metal ions, such as atomic absorption spectrometry, inductively coupled plasma mass spectrometry, inductively coupled plasma atomic emission spectroscopy, X-ray fluorescence spectrometry, etc. However, these techniques require expert operators, are time-consuming, expensive, and cannot be used for in-field measurements. This is why electrochemical techniques have arisen as an alternative due to their low

3

cost, simplicity, rapid analysis, high sensitivity and availability for in-field measurements and monitoring [29]. Among the different electrochemical techniques available, anodic stripping voltammetry (ASV) and its different variants have been used as the preferred technique. In ASV, the metal ions (M^{n+}) are reduced and deposited on the electrode in their metallic form (M^0) applying a cathodic potential in the pre-concentration step for a determined accumulation time. Thereafter, the potential is scanned from negative to positive potential to strip (oxidize) the deposited metal. The peak potential (Ep) is characteristic of the metal and is different for each analyte, which can be used to determine several metal ions at the same time, if there is no overlapping among them. The intensity of the peak current is proportional to the concentration of the metal ion on the surface of the electrode (and consequently in solution). The concentration can be assigned by constructing a calibration plot where the peak current is represented vs. the concentration of M^{n+}. Fig. 2 illustrates the working principle of the ASV technique [30].
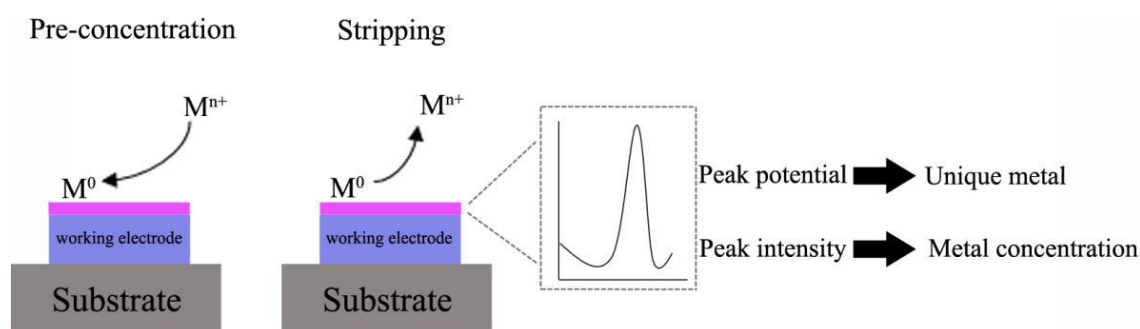

Fig. 2. Anodic Stripping Voltammetry (ASV) principle. Reprinted from Biosensors 2015, 5, 241-275, Gregory March, Tuan Dung Nguyen, Benoit Piro, Modified Electrodes Used for Electrochemical Detection of Metal Ions in Environmental Analysis [30].

Graphene is defined as a one-atom-thick layer of carbon. Regarding the family of graphene materials, different forms have been produced since its isolation [1]. Here follows a brief mention of some of these forms and the method of synthesis. Graphene (G) was first isolated by mechanical cleavage by the Scotch-tape method [2]. Although G obtained by this method is of high-quality and without defects, the quantity of G produced by this method is minimal and is destined for fundamental studies. Other methods of synthesis of G include the CVD method where G is grown on a metallic substrate (normally Cu) [1,4]. In this method, carbon arising from a gas source is dissolved in the metallic substrate that is heated (normally around 1000 ºC). When the temperature drops, carbon solubility decreases and a G film is formed on the surface of the metallic substrate (segregation process). The quality of G grown by CVD is also high, however the cost of producing it is still high and its production is limited and requires the transfer from the metallic substrate to the selected substrate [1]. To increase the production of G materials, chemical methods have arisen as a viable alternative. These methods meet the requirements of different applications (coating, composites, inks, energy storage, biological, transparent conductive layers) due to their higher production capacity and lower cost [1]. These chemical methods include for example the oxidation of graphite by oxidants to produce graphite oxide by Brodie, Staudenmaier and Hummers methods; and the graphite oxide is later exfoliated by simple sonication to produce graphene oxide (GO) [31]. GO is stable in aqueous solution due to the presence of functional groups (negative zeta potential) which cause electrostatic repulsion and stabilize GO in solution [32], which is beneficial for processing. GO is electrically insulating due to the disrupted sp^2 structure, however the conductivity can be partially restored after reduction of the functional groups and the partial restoration of the

4

graphitic network. The material obtained after reduction is known as reduced graphene oxide (RGO). GO reduction can be attained by a range of methods: chemically, thermally, UV-assisted, etc. [31,32]. Reduction of GO can also be performed by means of electrochemical methods, this being a cleaner method than chemical methods since the only reactive used are electrons. The material obtained after electrochemical reduction is known as electrochemically reduced graphene oxide (ERGO). Other liquid-phase exfoliation methods include electrochemical exfoliation, where the electrolyte intercalates between the G sheets and allows their exfoliation [32]. Last development in graphene materials is heterogeneous atom doping [33]. In these materials, other elements at atomic level are inserted into the graphene structure by means of CVD, wet methods, etc. Elements reported to dope graphene include: B, N, P, O, S, F, Cl, Br, I, Se, etc. or the simultaneous co-doping of some of these elements [33]. Heterogeneous atom doping induces electrochemically active sites that facilitate charge transfer, adsorption and activation of analytes, and anchoring of functional moieties or molecules [33].

Two essential properties make the family of graphene materials appealing for the production of electrochemical sensors: firstly, its high active surface area of 2630 m^2 g^{-1} (theoretical value) [1], and secondly, its conductivity, which is necessary to produce the conductive electrodes in order to enhance electron transfer rate. In addition, graphene materials can be easily functionalized by organic or inorganic compounds to produce sensitive and selective electrodes for the electrochemical determination of metal ions.

Metal nanoclusters have proved useful for environmental monitoring due to their electroactivity [34,35]. The high surface area of graphene and its derivatives is helpful for the dispersion of metal nanoparticles in the production of hybrid materials. The interaction between the nanoparticles and graphene materials can be through covalent or non-covalent bonding. In addition, the presence of defects and oxygen-containing functional groups in graphene derivatives such as graphene oxide (GO) or reduced graphene oxide (RGO) make these substrates promising templates for the fixation of metallic nanostructures [36-38]. The combination of graphene materials and nanoparticles produces synergistic effects that allow an increased sensitivity and selectivity [36]. Hence, the combination of these two materials is paving the way toward electrochemical sensors with lower limits of detection (LOD).

The strategy of using nanoparticles offers unique advantages over macroelectrodes for electroanalysis such as: enhancement of mass transport, catalytic properties and high effective surface area [39]. In addition, the presence of functional groups with negative charge in graphene derivatives, such as GO or RGO, enhances the pre-concentration of metal ions (with positive charge) around the surface of the electrode. This property has been used for the adsorption of metallic ions [40].

Another approach used to produce electrochemical sensors for trace metal ions determination is to modify the surface of the electrode with organic substances that are sensitive and/or selective to metal ions. The formation of ligands increases the pre-concentration of the metal ions around the surface of the electrode and hence its electrochemical determination is enhanced. There is an excellent review covering the functionalization of graphene by covalent and non-covalent approaches with different materials [41]. In most of the papers cited in the present review, a perhaps incorrect terminology for graphene materials was used, since in the majority of cases, the name graphene was used instead of other more appropriate terms such as reduced graphene oxide. The terminology of the graphene materials used in the different papers has been adapted according to the current recommendations [42]. The present paper aims to review the most important

bibliography published related to the use of graphene materials in the production of electrochemical sensors for the detection of hazardous ions (mainly trace metal elements) in waters and other matrices [43-160]. Different metals ions have been determined using graphene-based electrodes, such as: As(III) [48-54], Cd^{2+} [56-90], Hg^{2+} [92-111], Pb^{2+} [113-144], Cr(VI)/Cr^{3+} [146-148], Cu^{2+} [150-155], Ag^+ [157,158], etc. In some of the papers, different ions were simultaneously determined, taking into account the selectivity provided by the oxidation potential which is characteristic of each metal ion. These ions normally have an anthropogenic origin and they originate in industry and other human activities (see Table 1 in [29]). However, some of them are also present naturally such as As(III) [43] or Hg^{2+} [96] and are released into the environment. Although water contamination by these ions is present, it is the bioaccumulation within the food web and the consumption of contaminated food that poses a more serious problem. Moreover, the toxicity of the different metal ions has also been briefly highlighted [44,45,55,91,112,145,149,156,159,160]. Up-to-date, no extensive review has been published regarding the use of graphene materials for the production of electrochemical sensors for hazardous ions. A general review was published related to the use of graphene materials as sensors for trace metal elements in water but it included several techniques [25]. The present paper aims to fill this existing gap and to provide new perspectives into the electroanalysis of hazardous ions using graphene materials.

2. Determination of different ions

This review has been divided into different sections devoted to different ions, as indicated in the list of contents. The determination of arsenic, cadmium, mercury, lead and other metal ions (Cr(VI), Cr^{3+}, Cu^{2+}, Ag^+, Zn^{2+} and Tl^+) is studied from section 2.1 to section 2.5, respectively. For each of these sections, a table which synthesizes the most important parameters of the different studies is presented. The tables include important analytical parameters such as: the composition of the electrodes and the synthesis technique used, the electrochemical technique, accumulation time, supporting electrolyte and ion(s) determined LOD, linear range, sensitivity, main interferences, stability, RSD measured with calibrating solutions and applications in real sample measurements. In most of the studies presented, several ions are determined simultaneously, therefore some of the ions studied could be located in the different tables. The reviewed works are organized into the different sections based on what the main ion target is. When determined alone, the sensitivity and LOD are higher since there is no competition for the available active sites and there is no formation of interfering intermetallic compounds. In the majority of papers reviewed, G materials provide high conductivity and high surface area which improve electron transfer kinetics of the electrode. The other materials used improve pre-concentration of metal ions, stability of the electrode, conductivity, etc. Their function will be mentioned as they appear in the different papers of this review. Another factor that has been taken into account is the supporting electrolyte and its pH. These parameters are very important in the determination of metal ions due to the different reactions that can take place (hydrolysis, complexation, etc.). In the column of interferences, the limit ratio where the interference produced is usually below 5 % is presented. Regarding the application of the electrodes in real samples measurement, water and food matrices are the most widely studied samples. Water samples do not normally require a pre-treatment and only if interferent ions/substances are present is a pre-treatment applied (for instance removing Cu^{2+} ions with ferrocyanide) [63,65]. Food samples or other types of samples (liquid or solid) require a digestion with acids to dissolve the organic matrix and obtain a liquid sample. Thereafter, filtration

with a membrane and/or centrifugation are normally applied to separate the solid phase from the liquid. The final liquid samples are normally analysed by the recovery test, in which known concentrations of the target ion are added to the sample and the total content of the ion is determined. The recovery is calculated by means of the ratio between the concentration measured and the concentration added. In addition, the samples obtained are normally compared with other reference methods of analysis (inductively coupled plasma–mass spectrometry, atomic emission spectroscopy, etc.).

Throughout the review, the most important papers have been summarized given the importance of the electrode composition and the synthesis method on the electroanalytical performance obtained.

2.1. Arsenic

Arsenic is a highly toxic substance widely present in nature [43] but also produced by human activity as mentioned previously [29]. The contamination in waters by As is a major global problem, since it is estimated that more than 20 countries in the world present values of As(III) in drinking water above the WHO recommended level, which is 0.01 mg L^{-1} [43]. The incorporation of As(III) in the food chain is produced through irrigation [43], and rice is particularly affected due to the intensive irrigation used for its growth. The detrimental effects of chronic arsenic exposure on health have been reviewed in different papers [44,45] and include weakness, loss of reflexes, weariness, gastritis, colitis, anorexia, weight loss, hair loss, etc. Long-term exposure through food or air results in hyperkeratosis, hyperpigmentation, cardiovascular diseases, disturbance in the peripheral vascular and nervous systems, circulatory disorders, brittle nails, etc. [45]. Arsenic is deposited in hair, skin, nails and bones [45]. Among its different oxidation states and forms, As(III) is 10 times more toxic than As(V) and 70 times more toxic than methylated arsenic compounds [46]. In the case of As(III) determination, acid media is beneficial for such purpose [48]. Electrochemical techniques employing G-based materials as electrodes have been widely used for the determination of As(III) [47-54].

G materials have been used as support onto which different metals or metal oxides such as Au [48-50], Pt [51], Ag [52] and PbO [53] have been deposited for As(III) trace analysis. Au is usually the active material used for As(III) determination since As forms stable intermetallic compounds with Au during the reduction stage, while allowing As to be reproducibly re-oxidized during the stripping step [49]. Au–As intermetallic compounds have the general formula Au_xAs_y (x = 1–3 and y = 2–6) and such compounds enhance the efficiency for cathodic pre-concentration [50]. Regarding the technique of preparation of the electrode, drop casting is the most widely used in the production of sensors, since it is simple and involves only the pre-treatment of the surface of the supporting electrode (normally GCE) and the application of a small volume of liquid containing the electroactive material (G/ GO/ RGO + metal/ metal oxide) [48,51-54]. After drying, the applied material forms an electroactive layer on the supporting electrode. The metal or metal oxide is usually deposited previously on the surface of the G material by means of chemical reduction. Other production techniques used include graphene paste electrodes [49] or electrochemical synthesis, which has several advantages such as more control over the synthesis method, control of the nanoparticle growth and size, etc. [50].

The preparation of the composites of graphene in its different forms and nanoparticles is a critical point to obtain electrodes with good analytical performance. The reduction of GO to RGO and of Au^+ to Au^0 through irradiation with UV light is the method proposed by Li et al. [48] to

7

synthesize Au/RGO composite avoiding the use of additional chemical reductants. Fig. 3 shows a TEM micrograph of GO (A) and a TEM micrograph of the RGO/AuNPs nanocomposite (B) obtained with this procedure. As supporting electrolyte HCl, H_2SO_4 and H_3PO_4 were tested, although the highest currents were obtained with 0.2 M HCl, due to the complexation of As(III) by Cl^- to produce $AsCl_3$, which results in faster electron kinetics. This was also the media used in other works using G and AuNPs [49-51, 53]. One of the problems with real waters measurement is the interference of other inorganic ions or organic substances. Cu^{2+} is known to be the major interference in As(III) determination due to the formation of intermetallic compounds. Modification of the electrode with graphene is one way to minimize such interference, since the Cu^{2+} stripping peak was separated more than 300 mV from that of As(III).

A paste electrode based on AuNPs deposited on G powders using a thiacrown ether (1,4,7-trithiacyclononane) was proposed in the literature to produce high-sensitivity electrodes [49]. The thiacrown ether was able to form strong complexes with As(III), which enhanced the preconcentration of As(III) on the surface of the electrode and lowered the LOD.
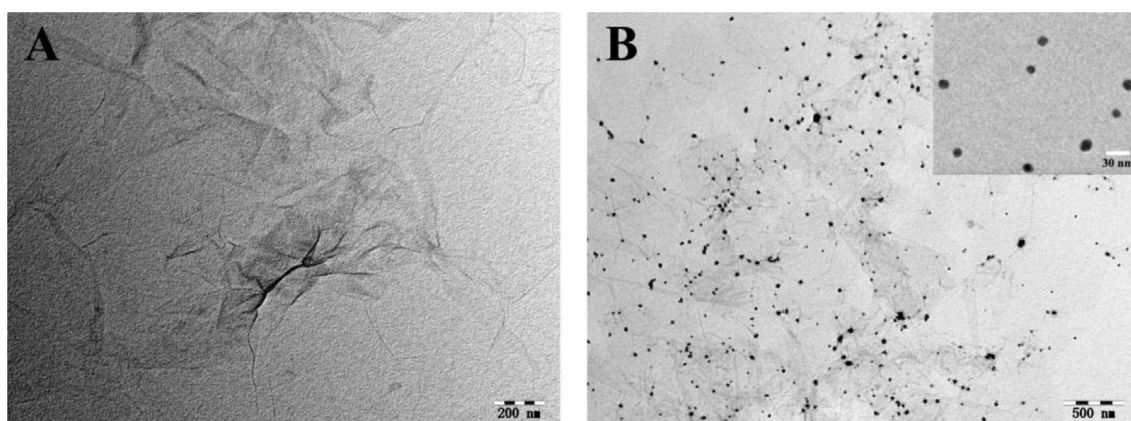

Fig. 3. Representative TEM images of GO (A) and Au-RGO nanocomposite (B). Inset to B: detailed images of Au nanoparticles. Reprinted from Electrochimica Acta, 157, Wei Wei Li, Fen Ying Kong, Jing Yi Wang, Zhi Dong Chen, Hai Lin Fang, Wei Wang, Facile one pot and rapid synthesis of surfactant free Au reduced graphene oxide nanocomposite for trace arsenic (III) detection, 183-190, Copyright (2015), with permission from Elsevier [48].

Liu et al. co-electrodeposited ERGO and AuNPs on a GCE by means of CV [50]. AuNPs size decreased from 100 nm (when no ERGO was deposited on the GCE) to 30 nm (when ERGO was deposited on GCE). The presence of ERGO reduced the size of AuNPs and improved its distribution, thus enhancing the electrochemical surface area. Although GO was electrochemically reduced, functional groups remained in its structure and acted as nucleation and anchoring sites, which explains the lower size and better distribution of the NPs. The Cu^{2+} interference was tested and the separation between Cu^{2+} and As(III) peaks was 200 mV. To reduce the interference of Cu^{2+}, the determination of As(III) was tested in neutral PBS, which showed a better selectivity; however, a degree of sensitivity was sacrificed.

The use of other materials has also been reported [51-53]. Kempegowda et al. synthesized PtNPs supported on RGO [51]. The electrode obtained showed good performance regarding As(III) determination with high selectivity since no interference was observed up to a 2000-fold ratio for Pb^{2+}, Cd^{2+}, Cu^{2+} and Hg^{2+}. The use of AgNPs deposited on RGO has been also reported by Dar et al. [52]. In the case of using AgNPs, better results were observed with H_2SO_4 electrolyte, since HCl

can produce the Ag oxidation to AgCl. No interference of Cu^{2+} was observed up to a concentration of 375 nM, which could serve for the simultaneous determination of As(III) and Cu^{2+}. The interference of organic compounds such as EDTA, Triton X-100 SDS was tested, since these compounds can influence As(III) determination.. Metal oxides, such as PbO have also been used as composite materials for As(III) determination [53]; electrodes prepared by drop-casting GO on GCE followed by simultaneous reduction of GO and $PbNO_3$ produced RGO/PbO hybrid coatings on GCE [53].

Bio-recognition elements for As(III) determination have also been reported [54]. Kumar et al. coated an Au electrode with GO nanosheets, L-leucine and Nafion. The developed electrodes were used for As(III) determination by CV and showed high selectivity.

As(V) ions are less toxic than As(III) ones, as mentioned previously, and this is why in the bibliography more attention is paid to As(III) determination. However, if As(V) content were to be determined, a previous reduction step would be necessary in order to reduce chemically As(V) to As(III), by Na_2SO_3 for instance [49]. The electrochemical response in the determination of As(III) with only graphene materials present in the electrode formulation is lower than when they are combined with metal NPs. In some cases graphene materials alone showed no response for As reduction/oxidation within the potential limits studied [48,51].

Table 1. As(III) determination by electrochemical methods with graphene-based electrodes.

Electrode (Synthesis technique)	Technique (Accumulation time)	Supporting electrolyte (Metal ion)	LOD	Linear range	Sensitivity	Main interferences	Stability (% of initial response) *RSD (in calibrating solutions)*	Application	[Ref]
AuNPs-RGO/GCE (drop casting)	ASLSV (30 s)	0.2 M HCl (As(III))	1.3 nM (As(III))	1.3–267 nM (As(III))	12.2 µA µM^{-1} (As(III)) 174 µA µM^{-1} cm^{-2} (As(III))	No interference: Cu^{2+}, Al^{3+}, Pb^{2+}, Mn^{2+}, Hg^{2+}, Zn^{2+}, Cd^{2+}	Stab: 90.4 % (15 days, refrigerator) *RSD: 5 % (15 cycles)*	Real water samples	[48]
AuNPs-thiacrown ether-GO/Teflon (paste electrode)	PSA (75 s)	1 M HCl (As(III))	8 pM (As(III))	25 pM–34 nM (As(III))	0.2227 s V^{-1} nM^{-1} (As(III))	Interference: Cu^{2+}, Se^{4+}, Sb^{3+} No interference: 100-fold Ag$^+$, Co^{2+}, Ni^{2+}, Zn^{2+}, Fe^{3+}, Cd^{2+}, Ga^{3+}, Sn^{4+}, V^{5+} (0.313 nM As(III))	Stab: 95 % (2 months, room temperature, dry state) *RSD: 2.5 % (15 cycles)*	Pharmaceutical formulations, human hair, sea water, fruits, vegetables, soil and wine samples	[49]
AuNPs-ERGO/GCE (electrochemical synthesis)	ASLSV (400 s)	0.2 M HCl (As(III))	2.7 nM (As(III))	0.01–5 µM (As(III))	12.2 µA µM^{-1} (As(III))	Interference: 5-fold Cu^{2+} (0.5 µM As(III))	Stab: 92 % (1 week, air room temperature) *RSD: 4.9 % (20 cycles)*	Real water samples	[50]
PtNPs-RGO/GCE (drop casting)	SWASV (80 s)	1 M HCl (As(III))	1.1 nM (As(III))	10–100 nM (As(III))	-	No interference: 2000-fold Pb^{2+}, Cd^{2+}, Cu^{2+}, Hg^{2+}, 7600-fold Ba^{2+}, Ca^{2+}, Zn^{2+}, Ni^{2+}, Co^{2+}, Fe^{2+} (50 nM As(III))	*RSD: 4.6 % (15 cycles)*	Borewell water, polluted lake water, agricultural soil, tomato and spinach leaves	[51]
AgNPs-GO/GCE (drop casting)	SWASV (100 s)	0.1 M H$_2$SO$_4$ ((As(III), Cu^{2+})	0.24 nM (As(III))	13.33–375.19 nM ((As(III), Cu^{2+})	Individual: 180.5 µA µM^{-1} (As(III)) Simultaneous: 203 µA µM^{-1} (As(III)) 167 µA µM^{-1} (Cu^{2+})	No interference: Cu^{2+}, EDTA (6.67 mM), Triton X-100, SDS (1.33 mM)	Stab: 94.1 % (90 days, clean and dry environment) *RSD: 3.7-4.2 % (20 cycles)*	Ground and river water samples	[52]
PbO-ERGO/GCE (drop casting/ electrochemical reduction)	SWASV (300 s)	1 M HCl (As(III))	10 nM (As(III))	-	13 µA decade^{-1} (C$_{As(III)}$, M)	-	-	-	[53]
Nafion-L-leucine-GO/Au (drop casting)	CV	0.1 M citrate buffer (pH 5) (As(III))	6.7 µM (As(III))	67–667 µM (As(III))	0.97 µA µM^{-1} cm^{-2} (As(III))	No interference: 1-fold Zn^{2+}, Pb^{2+}, Hg^{2+}, Cd^{2+} (10 ppm As(III))	Stab: Stable for 1 month (0.1 M citrate buffer, stored at 4ºC)	River water, drain of a fertile soil containing pesticides, underground water	[54]

2.2. Cadmium

Cadmium is a toxic element, classified as carcinogenic. Exposure to Cd arises from ingestion of contaminated water and food, and to a significant extent through inhalation and cigarette smoking. Cd primarily affects intestines, liver and kidney and can be maintained in the body for 20 years due to its long biological half-life. Prolonged exposure is carcinogenic to kidney, liver, prostate, lung, hematopoietic and other systems [55]. The limit of Cd^{2+} concentration in drinking waters established by WHO is 0.003 mg L^{-1}.

A lot of work has been done regarding Cd^{2+} determination with G-based electrodes [56-90,113,115,122,131,136,141,144]. Several papers determined Cd^{2+} alone, whilst others determined it simultaneously with other elements (Pb^{2+}, Zn^{2+}, Cu^{2+}, Hg^{2+}), given that the separation between the oxidation peaks was sufficient to allow a proper determination of each metal ion.

Concerning the substrate material, SPCEs or GCEs have been widely used for the production of the electrodes. Traditionally, mercury film electrodes (MFE) have been used in the stripping analysis of metal ions due to their good performance as electrode material. Hg allows the formation of fused-alloys which enhance the LOD of trace metal elements. Three of the papers that determined Cd^{2+} still used Hg in the electrode formulation [56,57,82]. However, due to the toxicity of mercury, MFEs have been progressively replaced by Bi film electrodes (BFEs). BFEs have been widely used with G-based electrodes for Cd^{2+} determination [58-74,113,115,122]. Bi presents low toxicity, high sensitivity, and large cathodic potential, moreover it is not sensitive to dissolved oxygen and a comparable analytical performance to MFEs is obtained. The thickness of the BF has to be optimized, since thick films of Bi hinder the mass transfer of metal ions during the stripping step. Wherever used, the concentration has been indicated in the supporting electrolyte composition in the different tables. Sn films have also been used in the electrode formulation instead of Bi or Hg for the same purpose [75,76]. Other modifiers used in the electrode preparation include Nafion [56,57,60-62,69,70,72,80-82,85,86,136], Pani [72,73], sodium alginate [144], poly(crystal violet) [141], PVP [131], ILs [65,66], other organic molecules [68-71,73-75,77-80], CeO_2 [85], AlOOH [86], SnO_2 [87], Fe_3O_4 [88, 89, 131], AuNPs [68,71,136], MWCNTs [62], SWCNTs [144] and nanoporous carbon [122].

MFEs are still used [56, 57], although they have been progressively replaced by Bi films. A similar electrode composition was used in the two studies mentioned, where RGO-Nafion composite was deposited on the surface of the GCE by drop casting [56, 57]. Finally, a MFE was formed *in situ* at the same time as M^{n+} pre-concentration by reduction. Willemse et al. [56] determined Cd^{2+}, Pb^{2+}, Zn^{2+} and Cu^{2+} individually and simultaneously. Cu^{2+} was not used in the simultaneous analysis to avoid the formation of intermetallic compounds which interfere with the determination (Cu-Zn). The developed sensor had the known advantages of G (conductivity, high surface area) and those of Nafion (antifouling and cation exchange capacity that helps in the pre-concentration of metal ions).

To avoid the use of Hg in the film electrodes, Sahoo et al. [58] deposited BiNPs on RGO by chemical reduction and deposited the composite on the surface of a CPE by

drop casting. The presence of BiNPs avoided re-stacking of RGO sheets. The study was particularly interesting because Cu^{2+} stripping peak appeared before Bi^{3+} one and the normal case is the opposite [62]. Lee et al. [60] also used BFE on ARGO and Nafion (used as solubilising and antifouling agent). ARGO was obtained by treatment of GO with KOH. RGO is smooth and ARGO is porous, which is advantageous for electron transport. The electrode was used to determine Zn^{2+}, Cd^{2+} and Pb^{2+} content individually. Activation showed an increase of 67 % in the sensitivity of the electrodes when compared with bare GO.

The presence of RGO in the electrode composition has been reported to improve the antifouling ability to surfactants of the electrodes, where RGO modified with Nafion was deposited on GCE by drop casting and modified with a BFE [61]. Electrodes could be used in the presence of moderate surfactant concentration and the interference of three surfactants followed this order: Triton X-100 (severe) > (CTAB) (medium) > SDS (low).

3-D structures have also been reported due to their advantage of very high surface area [62,74]. In this sense, Huang et al. deposited a mixture of MWCNTs and GO on a GCE (see Fig. 4) [62]. Nafion was used for its antifouling properties and BFE was deposited in-situ for enhancing the LOD. GO was thereafter electrochemically reduced to ERGO. The presence of MWCNTs avoided re-stacking and curving of ERGO sheets since they acted as spacers. In addition, they provided conductivity and improved conducting pathways by linking the different ERGO sheets, while functional groups of ERGO captured metal ions. The combination of both conducting materials accelerated the electron transfer rate and pre-concentration efficiency of metal ions. The electrodes were used for the simultaneous determination of Cd^{2+} and Pb^{2+}. Copper and zinc determination was also tested, although this presented problems of interference between the different ions, and Cu^{2+} stripping peak appeared after that of Bi^{3+}. In another study, a three-dimensional activated graphene network (3DAGNs) was synthesized and modified with sulfonated terminated polymers (STPs) [74]. The 3DAGNs were synthesized by direct carbonization and simultaneous chemical activation of a cobalt ion-impregnated D113-type ion-exchange resin. STPs can adsorb positively charged anions via electrostatic interaction. The 3DAGNs-STP was deposited on a GCE by drop casting and a BF was also deposited to enhance Cd^{2+} and Pb^{2+} determination.
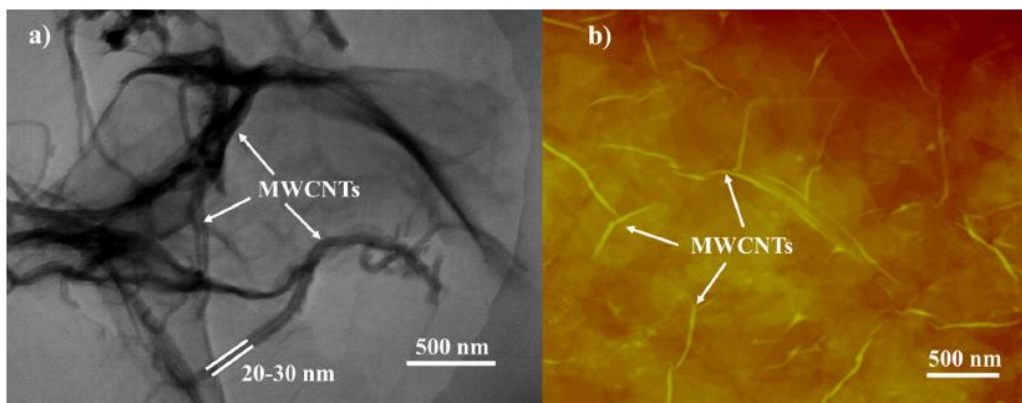
Fig. 4. (a) Typical low magnification TEM and (b) AFM images of GO-MWCNTs nanocomposites. The arrows point to the MWCNTs. Reprinted from Analytica Chimica Acta, 852, Hui Huang, Ting Chen, Xiuyu Liu, Houyi Ma, Ultrasensitive and simultaneous detection of heavy metal ions based on three dimensional graphene carbon nanotubes hybrid electrode materials, 45-54, Copyright (2014), with permission from Elsevier [62].

The use of SPEs for Cd^{2+} determination has been also reported [63-65]. Ping et al. [63] obtained disposable SPEs by potentiostatic deposition of ERGO, followed by in situ deposition of a BF for the determination of metal ions in milk. The Bi-ERGO/SPE electrode improved five-fold the peak current for Cd^{2+} and Pb^{2+} determination when compared with the Bi-SPE electrode. The presence of Bi also produced a 6-fold increase in the currents when compared to ERGO/SPE electrode. In-situ electrochemical reduction of GO proved to be more effective than chemical reduction. The drop casting technique usually uses RGO and the structure obtained is not uniform and compact, which influences the conductivity of the films. On the other hand, electrochemical deposition of ERGO produces a uniform film. The interference of surfactants was high, although Cu^{2+} interference could be eliminated by adding ferrocyanide [63,65]. Huangfu et al. [64] prepared a G/PSS suspension and deposited it by drop casting on a SPE, where later a BF was deposited. PSS was used as G dispersant to avoid precipitation in solution and wrapped around G, providing more adsorbing sites for ions. Wang et al. [65] used an SPE modified with the IL n-octylpyridinum hexafluorophosphate followed by spray-coating deposition of GO and potentiostatic reduction to obtain ERGO. BF was deposited on the top of the electrode surface. The IL improved the mechanical stability and the electron transfer rate of the electrode, since the IL filled the voids between carbon particles. The ERGO film interacted with the IL through hydrophobic interaction and π-π conjugation. The IL and ERGO film decreased the electron charge transfer resistance. The performance of ERGO was better than that of GO. Both, ERGO and GO have a high surface area that allow an increase in the amount of elements deposited on them. In addition, GO has negatively charged functional groups (hydroxyl, epoxide, carbonyl, carboxyl) that can facilitate the non-faradic pre-concentration of metal cations. However, the poor conductivity of GO makes its stripping performance worse than that of G or RGO. Zhao et al. [66] synthesized a similar electrode to Wang et al. [65] for Cd^{2+} on-site determination in soil samples with automatic signal acquisition, processing and detection.

Organic compounds such as selenocysteine [68], thiolated thionine [69], hydroxypropyl-β-cyclodextrin [70], cysteine [71,77,78] or aminophenyl [79] have shown their convenience in electrode composition for Cd^{2+} (and other metal ions) determination. Al-Hossainy et al. [68] used a GCE coated with G, AuNPs, selenocysteine and BF. The complexes formed between the carboxyl group in selenocysteine aminoacid and porous Bi-AuNPs were used as selective ligands for Cd^{2+} and Pb^{2+} quantification. A synergistic effect between selenocysteine and AuNPs-G was observed. Li et al. [69] also deposited a BF on RGO-thiolated thioline composite, firstly GO and thionine were prepared by adsorption due to π-π stacking between thionine dye

13

and GO sheets. Thereafter, the composite was drop-casted on GCE and electroreduced and functionalized by 2-mercaptoethane-sulfonate. Nafion was used as binder and as a permselective film to reduce the interference of anions. ERGO and Nafion also enhanced the adsorbability of metal cations, due to the presence of oxygen groups and large area in the former case, and to the sulfonate groups that can act as a cation-exchanger for electrostatic pre-concentration in the latter case. Thionine and 2-mercaptoethane-sulfonate also interact with the cations due to the presence of S and sulfonate groups. Electrostatic, nanosized and complexation effects were observed due to the synergy among all the components of the electrode. Lv et al. [70] obtained a GCE coated with RGO modified with hydroxypropyl-β-cyclodextrin and Nafion, with a BF deposited on the surface of the electrode for the determination of Cd^{2+} and Pb^{2+}. The presence of RGO increased the conductivity and β-cyclodextrin has host–guest recognition and enrichment properties, thus results in an enhanced detection of both ions when compared with other possible electrode formulations (Fig. 5). Zhu et al. [71] coated a GCE with Bi-cysteine-AuNPs-G nanocomposite. AuNPs were deposited on G by means of chemical reduction by citrate. DL-cysteine was deposited on the G/Au nanocomposite by electrostatic interaction and hydrogen bond with G. Each component had a specific function that contributed to lower the LOD. Citrate anions, which were adsorbed on AuNPs and arise from the chemical reduction of $AuCl_4^-$ to AuNPs, have a great affinity for metal cations. BF also produced an improvement of the peaks for Cd^{2+} and Pb^{2+}, 236 % and 65.1 %, respectively. DL-cysteine can react with many metal ions such as Au^+, Ag^+, Cu^{2+}, Zn^{2+}, Bi^{3+}, Cd^{2+} and Pd^{2+} and produce stable complexes.
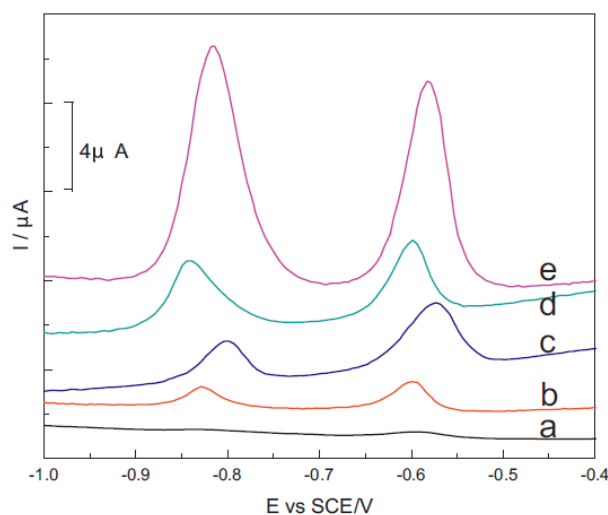
Fig. 5. SWASV for 1.0×10^{-7} mol L^{-1} of Pb^{2+} and Cd^{2+} on (a) bare GCE; (b) Nafion/GCE; (c) HP-β-CD/Nafion/GCE; (d) RGO/Nafion/GCE; (e) HP-β-CD-RGO/Nafion/GCE in 0.1 mol L^{-1} acetate buffer (pH 4.5) by in situ depositing bismuth film (1.0×10^{-6} mol L^{-1}). Deposition potential: −1.2 V (vs. SCE); deposition time: 120 s; frequency: 25 Hz; amplitude: 5 mV; potential step: 5 mV; quite time: 30 s. Reprinted from Electrochimica Acta, 2013, Meijiao Lv, Xianbao Wang, Jing Li, Xuyu Yang, Chang'an Zhang, Jia Yang, Hao Hu, Cyclodextrin reduced graphene oxide hybrid nanosheets for the simultaneous determination of lead(II) and cadmium(II) using square

wave anodic stripping voltammetry, 412-420, Copyright (2013), with permission from Elsevier [70].

Zhou et al. [77] deposited chitosan and RGO on a GCE by drop casting. L-cysteine deposit was formed electrochemically by CV. As observed by SEM, L-cysteine deposit was more ordered on the surface of RGO than on bare GCE; it seems that RGO induced a highly ordered coating. The electrode synthesized enhanced the stripping currents for both Cd^{2+} and Pb^{2+}, when compared with bare GCE due to the presence of RGO. Although L-cysteine deposition decreased the conductivity and electron transfer rate of the film, it promoted the deposition of Cd^{2+} and Pb^{2+} since L-cysteine contains sulfur, nitrogen, and oxygen atoms that coordinate with Cd^{2+} and Pb^{2+}. The electrode was highly selective and it could be simply renewed by CV cycling in acetate buffer solution. Gupta et al. [79] functionalized a GCE with p-nitrophenyl. Thereafter, GO and 1-ethyl-3(3-(dimethlyamino)propyl)-carbodiimide were adsorbed on the surface of the electrode by immersion during 12 h. GO terminated aminophenyl is a multidentate ligand that can form complexes with different metal ions.

Conducting polymers such as Pani have been used in electrode composition due to their conducting properties [72,73]. Ruecha et al. [72] deposited G/Pani nanocomposites on SPEs made of paper or plastic. A Nafion film was also used to pre-concentrate metal ions and an in-situ deposited BF to enhance detection. The deposition methods used were electrospray or drop casting, better results were obtained with electrospray method due to a more uniform distribution of NPs and increased surface-to-volume ratios. The G/Pani composite electrode improved electron transfer kinetics. Cd^{2+}, Pb^{2+} and Zn^{2+} were simultaneously determined. The best performance was observed on plastic substrates since no absorption took place, thus obtaining thicker films with higher conductivity and higher surface roughness. Promphet et al. [73] prepared a SPCE modified with G/Pani/PS fibers obtained by electrospinning on the electrode; a BF was deposited ex-situ prior to the analysis of Pb^{2+} and Cd^{2+}. The modification of the SPE by the nanofibers increased the sensitivity by a factor of three, due to the enhanced specific surface area (12.23 m^2 g^{-1}). Pani was used as a conducting media and PS was a carrier polymer for electrospinning fabrication.

As previously commented, Sn has been used instead of Bi and Hg films for Cd^{2+} determination. Sn has similar electroanalytical properties to Bi; moreover, it is less toxic and cheaper than Bi. Like Bi, Sn can form "fused" alloys with trace metal elements which facilitate the reduction/stripping process. Wang et al. [75] deposited potentiostatically RGO on a GCE, and poly-p-ABSA was deposited on RGO by CV. Afterwards, a Sn deposit was obtained electrochemically prior to determine Cd^{2+}. Although poly-p-ABSA complicates the electron transfer, this film acted as an antifouling agent that avoided contamination by organic compounds. The negatively charged poly-p-ABSA facilitated the non-faradic pre-concentration of Cd^{2+} as well as the nucleation of Sn-Cd alloys due to its large specific surface area and its 3-D macroporous structure. The pH was adjusted to 4 to avoid HER at more acidic pH that damage the Sn film. At more acidic pH, sulfonic groups of poly-p-ABSA would not be deprotonated and less ion exchange sites would be available for pre-concentration of

15

Cd^{2+}, and at a more basic pH Sn would be easily hydrolyzed, for these reasons pH 4 was found to be the optimal one. Lee et al. [76] applied by drop casting a GO/Sn^{2+} composite to a glassy carbon sheet. Thereafter the reduction of GO to ERGO and Sn^{2+} to Sn was performed potentiostatically. SnNPs prevented the stacking of RGO, increased the conductivity and surface area, which enhanced adsorption and improved electrochemical determination of Cd^{2+}, Pb^{2+} and Cu^{2+}.

An interesting study compared two methods of determination, CC and SWASV, for different metal ions [80]. A SPCE coated with GO functionalized with DTT and Nafion (used to protect the sensor from fouling) was used. The metal ions selectively coordinated with the nitrogen atoms of the DTT ligand, and the negative functional groups GO enhanced the interaction with metal ions. The authors compared the traditional SWASV method with CC methods (stripping and deposition methods). Anodic stripping method (from negative to positive potential) showed generally better results than the deposition method (cathodic scan). The LOD was generally better in the SWASV method for Pb^{2+}, Cu^{2+} and Hg^{2+}. However, CC methods require a very short analysis time since no pre-concentration is needed (0.5 s for CC method vs. several minutes for SWASV). This method could be used to achieve the real-time monitoring of trace compounds.

The use of other forms of G, such as nanoG (obtained by ball milling of graphite during 20 h in Ar atmosphere) have been reported [82]. NanoG is hydrophilic due to the presence of hydroxyl and carboxyl groups, which provides good dispersibility in aqueous solutions. NanoG was functionalized with Nafion and applied by drop casting onto a GCE. The electrode was finally coated with a mercury film to carry out Cd^{2+} determination. In this study the authors compared the performance of nanoG and MWCNTs. The specific surface area of both materials as measured by the BET method was 905 m^2 g^{-1} and 77.6 m^2 g^{-1} for nanoG and MWCNTs, respectively. NanoG improved the specific surface area of the electrode and the electron transfer rate, which facilitated the deposition of Cd^{2+} from solution. The LOD was 3.5 ng L^{-1} and 25 ng L^{-1} for electrodes modified with nanoG and MWCNTs, respectively. NanoG electrodes demonstrated higher reproducibility and lower background noise. Liquid phase exfoliated GNS also produced better results than RGO-modified electrodes for Cd^{2+} and Pb^{2+} determination [83]. This result was attributed to a higher density of edge plane-like sites and defects, resulting in larger active areas and faster electron transfer. The electrodes were used as single use electrodes, since strong adsorption of the metal ions was observed.

Nitrogen-doped G has been recently reported for the simultaneous determination of Cd^{2+}, Pb^{2+}, Cu^{2+} and Hg^{2+} [84]. This was the first report of the use of N-doped G in the electrochemical determination of metal ions; nitrogen doping enhances the electroactivity of carbon nanomaterials. N-doped G was deposited by electroreduction of GO in ammonia solution at -1.3 V for 400 s and the effective surface area of N-doped G was 1.6 times higher than that of RGO. This was explained by the formation of nanospheres of N-doped G (3-D structure), instead of a more planar structure for RGO (Fig. 6). As shown in Fig. 7, N-doped G electrode showed better analytical performance

than GCE and GCE/RGO due to the presence of nitrogen functional groups and its 3-D structure with enhanced active surface area.
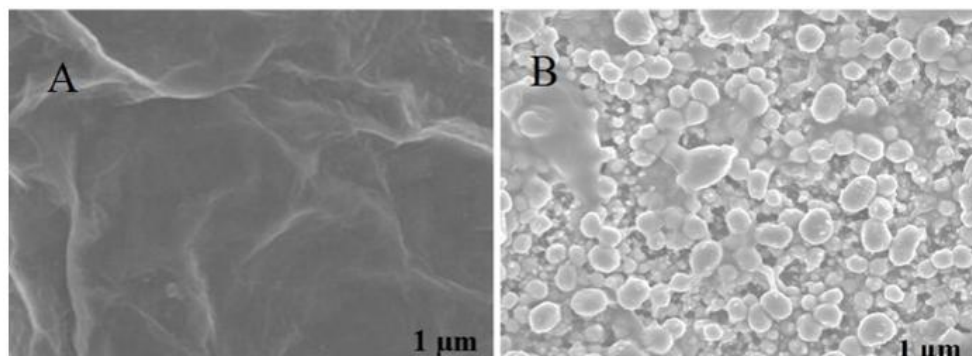
Fig. 6. SEM images of RGO (A) and NG (B). All the samples were deposited on indium tin oxide (ITO) substrates. Adapted from Journal of Electroanalytical Chemistry, 760, Huakun Xing, Jingkun Xu, Xiaofei Zhu, Xuemin Duan, Limin Lu, Wenmin Wang, Youshan Zhang, Taotao Yang, Highly sensitive simultaneous determination of cadmium (II), lead (II), copper (II), and mercury (II) ions on N-doped graphene modified electrode, 52-58, Copyright (2016), with permission from Elsevier [84].
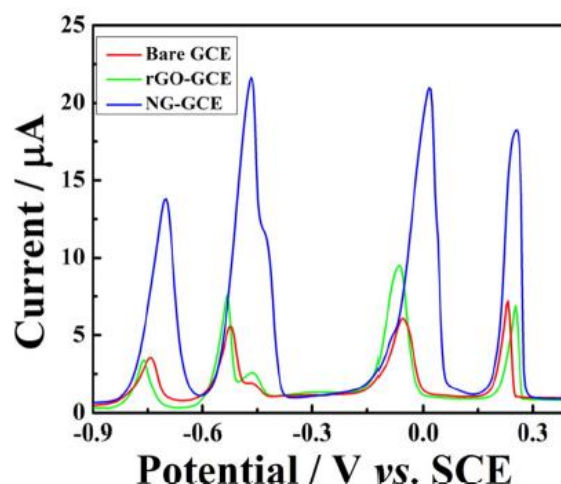
Fig. 7. DPSV curves at the bare GCE, RGO/GCE and NG/GCE in the presence of 3 μM Hg^{2+}, 3 μM Cu^{2+}, 3 μM Cd^{2+} and 6 μM Pb^{2+} together in 0.1 M acetate buffer (pH 4.5). Deposition potential: −1.1 V, deposition time: 300 s, pulse amplitude: 50 mV, pulse width: 50 ms. Reprinted from Journal of Electroanalytical Chemistry, 760, Huakun Xing, Jingkun Xu, Xiaofei Zhu, Xuemin Duan, Limin Lu, Wenmin Wang, Youshan Zhang, Taotao Yang, Highly sensitive simultaneous determination of cadmium (II), lead (II), copper (II), and mercury (II) ions on N-doped graphene modified electrode, 52-58, Copyright (2016), with permission from Elsevier [84].

The use of inorganic materials in electrode composition has been also reported for Cd^{2+} determination [85-89]. RGO/CeO_2 hybrid material obtained by the solvent-thermal method have been deposited on a GCE by drop casting [85]. Functional groups of RGO helped to anchor the NPs on both sides of RGO sheets. CeO_2 acted as spacer avoiding re-stacking of RGO layers which enhanced the electrode surface area. The

17

stripping currents increased substantially due to the synergistic effect between RGO and CeO_2 (Fig. 8). Cd^{2+}, Pb^{2+}, Cu^{2+} and Hg^{2+} could be simultaneous determined since the corresponding peaks were separated enough to perform simultaneous determination, as is clearly shown in the voltammograms in Fig. 9.
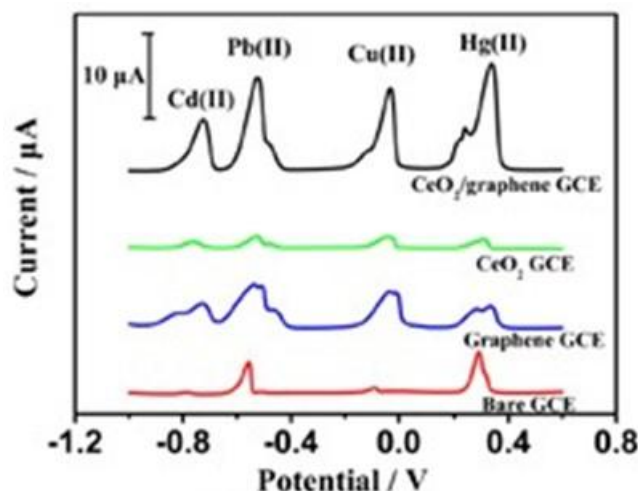
Fig. 8. DPASV for 1.0 μM each of Cd(II), Pb(II), Cu(II), and Hg(II) on bare, CeO_2, graphene, and graphene/CeO_2 hybrid nanocomposite modified GCE in 0.1 M acetate buffer (pH 5.0), vs. SCE. Reprinted from Journal of Electroanalytical Chemistry, 757, Yu-Long Xie, Su-Qing Zhao, He-Lin Ye, Jing Yuan, Ping Song, Shu-Qing Hu, Graphene/CeO_2 hybrid materials for the simultaneous electrochemical detection of cadmium(II), lead(II), copper(II), and mercury(II), 235-242, Copyright (2015), with permission from Elsevier [85].
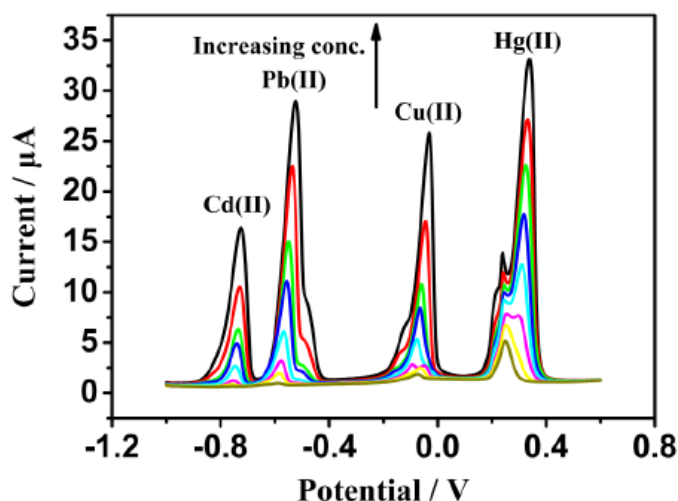
Fig. 9. DPASV response of the graphene/CeO_2 hybrid nanocomposite modified GCE for the simultaneous analysis of Cd(II), Pb(II), Cu(II), and Hg(II) over a concentration range of 0.2 to 2.5 μM for each metal ion, vs. SCE. Reprinted from Journal of Electroanalytical Chemistry, 757, Yu-Long Xie, Su-Qing Zhao, He-Lin Ye, Jing Yuan, Ping Song, Shu-Qing Hu, Graphene/CeO_2 hybrid materials for the simultaneous electrochemical detection of cadmium(II), lead(II), copper(II), and mercury(II), 235-242, Copyright (2015), with permission from Elsevier [85].

18

The use of AlOOH-RGO nanocomposite, synthesized by the one-pot hydrothermal method and deposited on GCE by drop casting, has been also reported [86]. AlOOH nanoplates intercalated between RGO nanosheets and avoid re-stacking. AlOOH has proven to be good adsorbent for metallic ions, however it is an insulating material. RGO played here a key role, connecting electrically the different AlOOH nanoplates. Cd^{2+} and Pb^{2+} were determined individually and simultaneously. Cu^{2+}, Zn^{2+} and Hg^{2+} interfered in the analysis due to the non-selectivity of AlOOH adsorbent. Similarly, RGO/SnO_2 hybrid material was deposited on GCE by drop casting to produce electrodes for the simultaneous determination of Cd^{2+}, Pb^{2+}, Cu^{2+} and Hg^{2+} [87]. Interference between metal ions was observed. For instance, the presence of Cd^{2+} and Pb^{2+} enhanced the sensitivities towards Hg^{2+} and Cu^{2+} due to the formation of intermetallic compounds. The sensitivity of Cu^{2+} was also enhanced in the presence of Hg^{2+} due to the same reason.

RGO/Fe_3O_4 nanocomposites have been used for Cd^{2+} individual determination [88,89] or with the presence of other metal ions [89]. The diameter of the $Fe_3O_4$ nanoparticles was lower when deposited on the surface of RGO than when no RGO was used (60 nm *vs* 110 nm) [89]. This could be attributed to the presence of functional groups on the RGO surface that can act as nucleation points and produce lower diameter NPs. Cd^{2+} determination was influenced by the presence of Hg^{2+} and Pb^{2+}, due to the preferential occupation of the nucleation sites by the latter ions [89]. The mutual interference between the different ions was further studied by pairs of ions (Cd^{2+}, Hg^{2+}), (Pb^{2+}, Hg^{2+}), (Cd^{2+}, Pb^{2+}) [89].

The interference of surfactants (sodium cholate, in this case) used during the manufacturing process of G sheets (by density gradient ultracentrifugation) in Cd^{2+} determination has also been reported [90]. The hydrophobic nature of G makes it prone to adsorb surfactants that block its surface and prevent the proper determination of Cd^{2+}. Hence, the method of synthesis of G materials has great influence on their properties.

Table 2. Cd^{2+} determination by electrochemical methods with graphene-based electrodes.

Electrode (Synthesis technique)	Technique (Accumulation time)	Supporting electrolyte (Metal ions)	LOD	Linear range	Sensitivity	Main interferences (target ion(s) concentration)	Stability (% of initial response) *RSD (in calibrating solutions)*	Application	[Ref]
Hg-nafion-RGO/GCE (drop casting)	SWASV (120 s)	0.1 M ABS (pH 4.6) [10 mg L^{-1} Hg^{2+}] (Cd^{2+}, Pb^{2+}, Zn^{2+}, Cu^{2+})	Individual: 0.71 nM (Cd^{2+}) 0.34 nM (Pb^{2+}) 1.07 nM (Zn^{2+}) 2.05 nM (Cu^{2+}) Simultaneous: 1.16 nM (Cd^{2+}) 0.34 nM (Pb^{2+}) 2.14 nM (Zn^{2+})	Individual: 8.9–62.3 nM (Cd^{2+}) 4.9–33.8 nM (Pb^{2+}) 15.3–107.1 nM (Zn^{2+}) 0.31–2.83 μM (Cu^{2+})	Individual: 60.8 μA μM^{-1} (Cd^{2+}) 340 μA μM^{-1} (Pb^{2+}) 81.7 μA μM^{-1} (Zn^{2+}) 823 μA μM^{-1} (Cu^{2+}) Simultaneous: 62.6 μA μM^{-1} (Cd^{2+}) 352 μA μM^{-1} (Pb^{2+}) 49.6 μA μM^{-1} (Zn^{2+})	Mutual interference, formation Cu-Zn intermetallic compounds	-	Lake water	[56]
Hg-RGO-nafion/GCE (drop casting)	DPASV (120 s)	0.1 M ABS (pH 4.5) [100 mg L^{-1} Hg^{2+}] (Cd^{2+})	44 pM (500 s preconcentration) (Cd^{2+})	1.8–133 nM (Cd^{2+})	-	-	*RSD: 0.65 % (10 cycles)*	Sewerage samples	[57]
BiNPs-RGO/CPE (drop casting)	DPASV (400 s)	0.1 M ABS (pH 5.5) (Cd^{2+}, Pb^{2+}, Zn^{2+}, Cu^{2+})	Individual: 25 nM (Cd^{2+}) 2.65 nM (Pb^{2+}) 260 nM (Zn^{2+}) 409 nM (Cu^{2+})	Individual: 0.18–1.07 μM (Cd^{2+}) 0.1–0.58 μM (Pb^{2+}) 1.53–6.12 μM (Zn^{2+}) 0.31–1.57 μM (Cu^{2+})	-	-	*RSD: 2.5 % (6 cycles)*	Ground water	[58]
Bi-ERGO/PGE (electrochemical synthesis)	SWASV (120 s)	0.1 M ABS (pH 4.6) [0.8 mg L^{-1} Bi^{3+}] (Cd^{2+}, Pb^{2+}, Zn^{2+})	(2-20 μg L^{-1}): Individual: 0.88 nM (Cd^{2+}) 0.56 nM (Pb^{2+}) 3.04 nM (Zn^{2+}) Simultaneous 0.96 nM (Cd^{2+}) 0.61 nM (Pb^{2+}) 3.90 nM (Zn^{2+}) (10-100 μg L^{-1}): Individual: 0.86 nM (Cd^{2+}) 0.56 nM (Pb^{2+})	Individual/ simultaneous: 2–20 μg L^{-1} (Cd^{2+}, Pb^{2+}, Zn^{2+}): 17.8–178 nM Cd^{2+}; 9.7–97 nM Pb^{2+}; 30.6–306 nM Zn^{2+} 10–100 μg L^{-1} (Cd^{2+}, Pb^{2+}, Zn^{2+}): 89–890 nM Cd^{2+}; 48.3–483 nM Pb^{2+}; 153–1530 nM Zn^{2+}	(2-20 μg L^{-1}): Individual: 96.1 μA μM^{-1} (Cd^{2+}) 139.4 μA μM^{-1} (Pb^{2+}) 35.90 μA μM^{-1} (Zn^{2+}) Simultaneous: 122.5 μA μM^{-1} (Cd^{2+}) 170.5 μA μM^{-1} (Pb^{2+}) 85.01 μA μM^{-1} (Zn^{2+}) (10-100 μg L^{-1}): Individual: 202 μA μM^{-1} (Cd^{2+}) 23.8 μA μM^{-1} (Pb^{2+})	-	-	Tap water	[59]

Electrode	Technique	Conditions	LOD	Linear range	Sensitivity	Interference	Stability/RSD	Sample	Ref
			3.20 nM (Zn^{2+}) Simultaneous: 0.92 nM (Cd^{2+}) 0.77 nM (Pb^{2+}) 4.00 nM (Zn^{2+})		32.9 µA µM^{-1} (Zn^{2+}) Simultaneous: 273 µA µM^{-1} (Cd^{2+}) 315 µA µM^{-1} (Pb^{2+}) 179 µA µM^{-1} (Zn^{2+})				
Bi-nafion-ARGO/GCE (drop casting)	DPASV (300 s)	0.1 M ABS (pH 4.5) [400 µg L^{-1} Bi^{3+}] (Cd^{2+}, Pb^{2+}, Zn^{2+})	Individual: 0.62 nM (Cd^{2+}) 0.44 nM (Pb^{2+}) 8.72 nM (Zn^{2+})	Individual: 0.04–0.89 µM (Cd^{2+}) 0.02–0.48 µM (Pb^{2+}) 0.08–1.53 µM (Zn^{2+})	Individual: 91.9 µA µM^{-1} (Cd^{2+}) 127 µA µM^{-1} (Pb^{2+}) 48.2 µA µM^{-1} (Zn^{2+})	No mutual interference at 10-fold concentrations of the other metal ions (Cd^{2+}, Pb^{2+}, Zn^{2+})	*RSD: 0.8 % (Zn^{2+}, Cd^{2+}), 1.6 % (Pb^{2+}) (10 cycles)*	Tap water	[60]
Bi-nafion-RGO/GCE (drop casting)	DPASV (120 s)	0.1 M ABS (pH 4.5) [0.4 mg L^{-1} Bi^{3+}] (Cd^{2+}, Pb^{2+})	Simultaneous: 0.18 nM (Cd^{2+}) 0.1 nM (Pb^{2+})	Simultaneous: 13.34–267 µM (Cd^{2+}) 2.41–241 nM (Pb^{2+})	Simultaneous: 127 µA µM^{-1} (Cd^{2+}) 197 µA µM^{-1} (Pb^{2+})	Interference: Triton X-100 > CTAB > SDS	-	Lake water samples	[61]
Bi-nafion-MWCNTs-ERGO/GCE (drop casting)	DPASV (180 s)	0.1 M ABS (pH 4.5) [500 µg L^{-1} Bi^{3+}] (Cd^{2+}, Pb^{2+}, Zn^{2+}, Cu^{2+})	Simultaneous: 0.9 nM (Cd^{2+}) 0.97 nM (Pb^{2+})	Simultaneous: 4.45–267 nM (Cd^{2+}) 2.41–145 nM (Pb^{2+})	Simultaneous: 26.5 µA µM^{-1} (Cd^{2+}) 39.7 µA µM^{-1} (Pb^{2+})	Mutual interference, formation of Cu-Zn and other intermetallic compounds	-	Water from electroplating effluent	[62]
Bi-ERGO/SPE (electrochemical deposition) (Cd^{2+}, Pb^{2+})	SWASV (150 s)	0.1 M ABS (pH 4.5) [0.8 mg L^{-1} Bi^{3+}]	Simultaneous: 4.45 nM (Cd^{2+}) 3.86 nM (Pb^{2+})	Simultaneous: 8.90–534 nM (Cd^{2+}) 4.83–290 nM (Pb^{2+})	Simultaneous: 28.2 µA µM^{-1} (Cd^{2+}) 43.9 µA µM^{-1} (Pb^{2+})	Severe interference: 300-fold Cu^{2+}; 15 mg L^{-1} Trit. X-100, CTAB, SDS No interference: 300-fold Fe^{2+}, Co^{2+}, Ni^{2+}, Ag^+ (0.27 µM Cd^{2+}, 0.14 µM Pb^{2+})	*RSD: 6.1 % (Cd^{2+}), 5.9 % (Pb^{2+}) (10 cycles)*	Milk	[63]
Bi-PSS-G-SPE (screen printed electrode) (Cd^{2+}, Pb^{2+})	DPSV (120 s)	ABS (pH 4.5) [0.5 mg L^{-1} Bi^{3+}]	Simultaneous: 0.37 nM (Cd^{2+}) 0.43 nM (Pb^{2+})	Simultaneous: 4.44 nM–1.07 µM (Cd^{2+}) 2.41 nM–0.58 µM (Pb^{2+})	Simultaneous: 1.35 µA V µM^{-1} (Cd^{2+}) 1.45 µA V µM^{-1} (Pb^{2+})	No interference: 10-fold Sn^{2+}, 4-fold Ni^{2+}, 1-fold Cu^{2+} (0.27 µM Cd^{2+}, 0.14 µM Pb^{2+})	*RSD: 2.56 % (Cd^{2+}), 3.37 % (Pb^{2+}) (8 cycles)*	Deionized water, lake water, tap water	[64]
Bi-ERGO-ionic liquid/SPE (screen printed electrode) (Cd^{2+}, Pb^{2+})	SWASV (120 s)	0.1 M ABS (pH 4.5) [0.6 mg L^{-1} Bi^{3+}]	Simultaneous: 0.7 nM (Cd^{2+}) 0.5 nM (Pb^{2+})	Simultaneous: 8.90–712 nM (Cd^{2+}) 4.83–386 nM (Pb^{2+})	Simultaneous: 133 µA µM^{-1} (Cd^{2+}) 152 µA µM^{-1} (Pb^{2+})	Severe interference: 2-fold Cu^{2+} No interference: 100-fold K^+, Na^+, Ca^{2+}, Mg^{2+}, Al^{3+}, Mn^{2+}, Cr^{3+}, Ba^{2+}, NH_4^+, 30-fold Fe^{3+}, Zn^{2+} (0.27 µM Cd^{2+}, 0.14 µM Pb^{2+})	Stab: 94.8 % (Cd^{2+}), 95.3 % (Pb^{2+}) (30 days, ambient conditions) *RSD: 2.2 % (Cd^{2+}) 1.9 % (Pb^{2+}) (5 cycles)*	Rice	[65]
Bi-ionic liquid-ERGO/SPE (screen printed electrode)	SWASV (600 s)	0.1 M PBS (pH 7) [4 µg L^{-1} Bi^{3+}] (Cd^{2+})	26.7 nM (Cd^{2+})	44.5–623 nM (Cd^{2+})	36.2 µA µM^{-1} (Cd^{2+})	-	-	Soil	[66]
Bi-G/CPE (blending)	SWASV Flow-based monitoring	0.05 M HCl [0.9 mg L^{-1} Bi^{3+}] (Cd^{2+}, Pb^{2+})	Simultaneous: 0.6 nM (Cd^{2+}) 0.19 nM (Pb^{2+})	Simultaneous: 0.89–445 nM (Cd^{2+}) 0.48–241 nM (Pb^{2+})	Simultaneous: 74 µA µM^{-1} (Cd^{2+}) 164 µA µM^{-1} (Pb^{2+})	-	-	Tap water Sea bash fish and undulated surf clam tissues	[67]
Bi-selenocysteine-G-	SWASV	ABS (pH 4.8) [275	Simultaneous:	Simultaneous:	Simultaneous:	No interference:	Stab: 95 % (15	Underground	[68]

21

AuNPs/GCE (drop casting)	(14 min)	ppb Bi^{3+}] (Cd^{2+}, Pb^{2+})	0.7 nM Cd^{2+} 0.24 nM Pb^{2+}	4.45–890 nM (Cd^{2+}) 2.41–483 nM (Pb^{2+})	140 µA µM^{-1} (Cd^{2+}) 105 µA µM^{-1} (Pb^{2+})	100-fold excess Fe^{3+}, Cu^{2+}, Ca^{2+}, Cr^{3+}, Zn^{2+} (0.18 µM Cd^{2+}, 0.10 µM Pb^{2+})	cycles), 90 % (30 cycles)	water, soil, leaves, stems and roots	
Bi-nafion-thiolated thionine-ERGO/GCE (drop casting)	SWASV (300 s)	0.1 M ABS (pH 4.5) [400 µg L^{-1} Bi^{3+}] (Cd^{2+}, Pb^{2+})	Simultaneous: 0.9 nM (Cd^{2+}) 0.24 nM (Pb^{2+})	Simultaneous: 8.90–356 nM (Cd^{2+}) 4.83–193 nM (Pb^{2+})	Simultaneous: 1017 µA µM^{-1} cm^{-2} (Cd^{2+}) 1935 µA µM^{-1} cm^{-2} (Pb^{2+})	No interference: 30-fold Co^{2+}, Ni^{2+}, Zn^{2+}, Ag^+, Cu^{2+}, Hg^{2+} (0.18 µM Cd^{2+}, 0.10 µM Pb^{2+})	RSD: 4.4 % (Cd^{2+}), 5.3 % (Pb^{2+}) (5 cycles)	Tap water, spring water, river water	[69]
Bi-nafion-RGO-hydroxypropyl-β-cyclodextrin /GCE (drop casting)	SWASV (120 s)	0.1 M ABS (pH 4.5) [1.5 µM Bi^{3+}] (Cd^{2+}, Pb^{2+})	Simultaneous: 67.3 pM (Cd^{2+}) 94.2 pM (Pb^{2+})	Simultaneous: 0.5–9 nM (Cd^{2+}) 0.1–9 nM (Pb^{2+})	Simultaneous: 281 µA µM^{-1} (Cd^{2+}) 223 µA µM^{-1} (Pb^{2+})	-	RSD: 1.93 % (Pb^{2+}) (10 cycles)	-	[70]
Bi-cysteine-AuNPs-G/GCE (drop casting)	SWASV (800 s)	0.1 M ABS (pH 4.5) [0.3 mg L^{-1} Bi^{3+}] (Cd^{2+}, Pb^{2+})	Simultaneous: 0.9 nM (Cd^{2+}) 0.24 nM (Pb^{2+})	Simultaneous: 0.89–356 nM (Cd^{2+}) 0.48–193 nM (Pb^{2+})	Simultaneous: 171 µA µM^{-1} (Cd^{2+}) 120 µA µM^{-1} (Pb^{2+})	No interference: 50-fold Co^{2+}, Fe^{3+}, Ni^{2+}, Cr^{3+}, Zn^{2+}, Cu^{2+}, In^{2+}, Sn^{2+} (0.18 µM Cd^{2+}, 0.10 µM Pb^{2+})	Stab: 95 % (10 cycles), 88 % (20 cycles)	Spring water	[71]
Bi-nafion-G-Pani/SPE (electrospraying or drop-casting)	SWASV (140 s)	0.1 M ABS (pH 4.5) [500 µg L^{-1} Bi^{3+}] (Cd^{2+}, Pb^{2+}, Zn^{2+})	Simultaneous: 0.9 nM (Cd^{2+}) 0.48 nM (Pb^{2+}) 15.3 nM (Zn^{2+})	Simultaneous: 8.9 nM–2.67 µM (Cd^{2+}) 4.83 nM–1.45 µM (Pb^{2+}) 15.29 nM–4.59 µM (Zn^{2+})	Simultaneous: 4.28 µA µM^{-1} (Cd^{2+}) 7.31 µA µM^{-1} (Pb^{2+}) 1.44 µA µM^{-1} (Zn^{2+})	No interference: 25-fold Fe^{3+}, 50-fold Co^{2+}, 200-fold Ni^{2+}, etc. (1.78 µM Cd^{2+}, 0.97 µM Pb^{2+}, 3.06 µM Zn^{2+})	Stab: 82 % (3 weeks) RSD: 7.8 % (Cd^{2+}), 4.8 % (Pb^{2+}), 9.2 % (Zn^{2+}), (10 cycles)	Human serum	[72]
Bi-PS nanofibers-Pani-G/SPCE (electrospining)	SWASV (180 s)	0.1 M HCl (pH 1) [0.9 mg L^{-1} Bi^{3+}] (Cd^{2+}, Pb^{2+})	Simultaneous: 39.4 nM (Cd^{2+}) 15.9 nM (Pb^{2+})	Simultaneous: 89 nM–4.45 µM (Cd^{2+}) 48 nM–2.41 µM (Pb^{2+})	Simultaneous: 103.6 µA µM^{-1} (Cd^{2+}) 194 µA µM^{-1} (Pb^{2+})	No interference: 250-fold Ba^{2+}, Ca^{2+}, NO_3^{2-}, 20-fold Ni^{2+}, 1-fold Zn^{2+}, Cu^{2+} (0.44 µM Cd^{2+}, 0.24 µM Pb^{2+})	RSD: 3.52 % (Cd^{2+}), 4.67 % (Pb^{2+}) (10 cycles)	River waters	[73]
Bi-STP-3DGANs/GCE (drop casting)	DPV (300 s)	0.1 M ABS (pH 4) [500 µg L^{-1} Bi^{3+}] (Cd^{2+}, Pb^{2+})	Simultaneous: 0.9 nM (Cd^{2+}) 1 nM (Pb^{2+})	Simultaneous: 9–623 nM (Cd^{2+}) 5–338 nM (Pb^{2+})	Simultaneous. 1020 µA µM^{-1} cm^{-2} (Cd^{2+}) 1293 µA µM^{-1} cm^{-2} (Pb^{2+}) Individual: 1017 µA µM^{-1} cm^{-2} (Cd^{2+}) 1297 µA µM^{-1} cm^{-2} (Pb^{2+})	-	RSD: 4.7 % (Cd^{2+}), 4.1 % (Pb^{2+}) (3 cycles)	-	[74]
Sn-poly(p-aminobenzene-sulfonic acid-RGO/GCE (electrochemical synthesis)	SWASV (120 s)	0.1 M ABS (pH 4) [3 mg L^{-1} Sn^{2+}] (Cd^{2+})	0.44 nM (120 s pre-concentration) (Cd^{2+}) 0.11 nM (300 s pre-concentration) (Cd^{2+})	9–623 nM (Cd^{2+})	107 µA µM^{-1} (Cd^{2+})	Severe interference: 2-fold Cu^{2+} No interference: 100-fold Ca^{2+}, Ag^+, Mg^{2+}, Mn^{2+}, Zn^{2+}, Al^{3+}, 30-fold Fe^{3+} (0.45 µM Cd^{2+})	Stab: 95.6 % (14 days, ambient conditions) RSD: 1.2 % (Cd^{2+}) (6 cycles)	Industrial wastewater, lakewater, and farmland irrigation water	[75]
Sn-ERGO/GCS (drop casting)	SWASV (150 s)	0.1 M ABS (pH 5) (Cd^{2+}, Pb^{2+}, Cu^{2+})	Individual: 0.63 µM (Cd^{2+})	Individual/ simultaneous: 10 nM–100 nM (Cd^{2+}, Pb^{2+}, Cu^{2+})	Individual: 289.16 µA µM^{-1} (Cd^{2+})	Mutual interference, formation of Cd-Cu and Pb-Cu intermetallic compounds	-	Tap water	[76]

22

			0.60 µM (Pb^{2+})		367.73 µA µM^{-1} (Pb^{2+})				
			0.52 µM (Cu^{2+})		145.36 µA µM^{-1} (Cu^{2+}) Simultaneous: 43.572 µA µM^{-1} (Cd^{2+})				
			Simultaneous: 7.56 µM (Cd^{2+}) 6.77 µM (Pb^{2+}) 5.62 µM (Cu^{2+})		173 µA µM^{-1} (Pb^{2+}) 86.217 µA µM^{-1} (Cu^{2+})				
L-cysteine-RGO/GCE (drop casting)	DPASV (120 s)	0.1 M ABS (pH 4.5) (Cd^{2+}, Pb^{2+})	Simultaneous: 4 nM (Cd^{2+}) 0.6 nM (Pb^{2+})	Simultaneous: 5–598 nM (Cd^{2+}) 5–300 nM (Pb^{2+})	Simultaneous: 49.1 µA µM^{-1} (Cd^{2+}) 154.4 µA µM^{-1} (Pb^{2+})	No interference: 100-fold phenolic compounds, Cl$^-$, NO$_3^-$, SO$_4^{2-}$, Na$^+$, Al^{3+}, Cu^{2+}, Mg^{2+}, K$^+$, Zn^{2+}, Ca^{2+}.	Stab: 95 % (7 days, 4ºC), 91 % (6 cycles) *RSD: 2.77 % (Cd^{2+}), 2.86 % (Pb^{2+}) (8 cycles)*	Rice, honey	[77]
L-cysteine-RGO/GCE (drop casting)	DPASV (450 s)	0.1 M ABS (pH 6) (Cd^{2+}, Pb^{2+}, Cu^{2+}, Hg^{2+})	Individual: 0.138 nM (Cd^{2+}) 1.04 nM (Pb^{2+}) 4.743 nM (Cu^{2+}) 4.958 nM (Hg^{2+}) Simultaneous: 3.252 nM (Cd^{2+}) 2.013 nM (Pb^{2+}) 4.104 nM (Cu^{2+}) 5.547 nM (Hg^{2+})	Individual/ simultaneous: 0.2–1.6 µM (Cd^{2+}) 0.2–1.2 µM (Pb^{2+}) 0.2–1 µM (Cu^{2+}) 0.2–1.6 µM (Hg^{2+})	Individual: 2.744 µA µM^{-1} (Cd^{2+}) 4.731 µA µM^{-1} (Pb^{2+}) 4.000 µA µM^{-1} (Cu^{2+}) 5.551 µA µM^{-1} (Hg^{2+}) Simultaneous: 2.226 µA µM^{-1} (Cd^{2+}) 4.759 µA µM^{-1} (Pb^{2+}) 2.356 µA µM^{-1} (Cu^{2+}) 2.179 µA µM^{-1} (Hg^{2+})	-	-	Industrial effluent, pond water, lake water	[78]
1-ethyl-3(3-(dimethlyamino)propyl)-carbodiimide-GO-p-nitrophenyl/GCE (immersion)	SWASV (15 min ocp adsorption, 30 ºC)	0.1 M ABS (pH 4.5) (Cd^{2+}, Cu^{2+})	Simultaneous: 3.3 pM (Cd^{2+}, Cu^{2+})	Simultaneous: 10 pM–500 pM (Cd^{2+}, Cu^{2+})	Simultaneous: 3851 µA µM^{-1} (Cd^{2+}) 1805 µA µM^{-1} (Cu^{2+})	No interference: 100-fold Pb^{2+}, Fe^{2+}, Co^{2+}, Hg^{2+}, Ag$^+$ (1.6 µM Cd^{2+}, Cu^{2+})	Stab: 96.37 % (Cd^{2+}), 95.14 % (Cu^{2+}) (2 months)	Tap water, human urine	[79]
Nafion-diaminoterthiophene-G-SPCE (drop casting)	CC (0 s) SWASV (300 s)	ABS (pH 5.4) (Cd^{2+}, Pb^{2+}, Cu^{2+}, Hg^{2+})	Individual: CC method: 16.9 nM (Cd^{2+}) 13.5 nM (Pb^{2+}) 12.6 nM (Cu^{2+}) 13 nM (Hg^{2+}) SWASV: 63.2 nM (Cd^{2+}) 9.2 nM (Pb^{2+}) 6.3 nM (Cu^{2+}) 3.5 nM (Hg^{2+})	Individual: CC method: 8.89 nM–89 µM (Cd^{2+}) 4.83 nM–48 µM (Pb^{2+}) 15.74 nM–157 µM (Cu^{2+}) 4.99 nM–150 µM (Hg^{2+}) SWASV: 8.89 nM–22 µM (Cd^{2+}) 4.83 nM–12 µM (Pb^{2+}) 15.74 nM–39 µM (Cu^{2+}) 4.99 nM–12 µM (Hg^{2+})	-	No interference: 50-fold Mn^{2+}, Ni^{2+}, Zn^{2+}, Ag$^+$ (0.89 µM Cd^{2+}, 0.48 µM Pb^{2+}, 1.57 µM Cu^{2+}, 0.50 µM Hg^{2+})	Stab: 95 % (24 days), 70 % (2 cycles), 30 % (3 cycles)	Urine standard reference material, tap water, ground water, stream water	[80]

Nafion-RGO/GCE (drop casting)	DPASV (60 s)	0.01 M HCl (Cd^{2+}, Pb^{2+}, Cu^{2+})	Individual: 0.1 μM (Cd^{2+}) 10 pM (Pb^{2+}) 10 nM (Cu^{2+})	-	-	-	-	-	[81]
Hg-nanoG-nafion/GCE (drop casting)	DPASV (120 s)	0.1 M ABS (pH 5) [10 mg L^{-1} Hg^{2+}] (Cd^{2+})	31.1 pM (Cd^{2+})	2.2–44.5 nM (Cd^{2+})	-	No interference: Zn^{2+}, Mn^{2+}, Ni^{2+}, Al^{3+}, etc.	RSD: 0.29 % (8 cycles)	Tap water	[82]
GNS/GCE (drop casting)	ASV (120 s)	0.1 M ABS (pH 4.6) (Cd^{2+}, Pb^{2+})	Simultaneous: 9.61 nM (Cd^{2+}) 8.78 nM (Pb^{2+})	Simultaneous: 22.2–890 nM (Cd^{2+}) 12.1–483 nM (Pb^{2+})	Simultaneous: 22.93 μA $μM^{-1}$ (Cd^{2+}) 35.01 μA $μM^{-1}$ (Pb^{2+})	No interference: 0.01 mM Hg^{2+}, Bi^{3+}; 0.01 M, Ni^{2+}, Fe^{3+} (0.44 μM Cd^{2+}, 0.24 μM Pb^{2+})	Stab: 1 cycle (strong absorption)	Water samples	[83]
N-doped G/GCE (electrochemical synthesis)	DPSV (300 s)	0.1 M ABS (pH 4.5) (Cd^{2+}, Pb^{2+}, Cu^{2+}, Hg^{2+})	Individual: 0.03 μM (Cd^{2+}) 0.002 μM (Pb^{2+}) 0.001 μM (Cu^{2+}) 0.01 μM (Hg^{2+}) Simultaneous: 0.05 μM (Cd^{2+}) 0.005 μM (Pb^{2+}) 0.005 μM (Cu^{2+}) 0.05 μM (Hg^{2+})	Individual: 0.05–9 μM (Cd^{2+}) 0.007–9 μM (Pb^{2+}) 0.009–5 μM (Cu^{2+}) 0.07–9 μM (Hg^{2+}) Simultaneous: 0.1–9 μM (Cd^{2+}) 0.01–9 μM (Pb^{2+}) 0.01–5 μM (Cu^{2+}) 1–9 μM (Hg^{2+})	Individual: 2.842 μA $μM^{-1}$ (Cd^{2+}) 4.517 μA $μM^{-1}$ (Pb^{2+}) 7.281 μA $μM^{-1}$ (Cu^{2+}) 15.734 μA $μM^{-1}$ (Hg^{2+}, UPD) 4.241 μA $μM^{-1}$ (Hg^{2+}, BD) Simultaneous: 3.337 μA $μM^{-1}$ (Cd^{2+}) 4.946 μA $μM^{-1}$ (Pb^{2+}) 8.821 μA $μM^{-1}$ (Cu^{2+}) 17.073 μA $μM^{-1}$ (Hg^{2+}, UPD) 3.689 μA $μM^{-1}$ (Hg^{2+}, BD)	No interference: 50-fold K^+, Ca^{2+}, Mg^{2+}, Na^+, Al^{3+}, Ni^{2+}, Zn^{2+}, Mn^{2+}, Co^{2+}, Li^+ (5 μM Cd^{2+}, Pb^{2+}, Cu^{2+}, Hg^{2+})	Stab: 95 % (3 weeks)	Tap water	[84]
Nafion-CeO$_2$-RGO/GCE (drop casting)	DPASV (120 s)	0.1 M ABS (pH 5) (Cd^{2+}, Pb^{2+}, Cu^{2+}, Hg^{2+})	Individual: 0.2344 nM (Cd^{2+}) 0.1046 nM (Pb^{2+}) 0.1124 nM (Cu^{2+}) 0.0218 nM (Hg^{2+}) Simultaneous: 0.1944 nM (Cd^{2+})	Individual: 0.02–2.5 μM (Cd^{2+}) 0.01–2.5 μM (Pb^{2+}) 0.04–1.0 μM (Cu^{2+}) 0.002–0.12 μM (Hg^{2+}) Simultaneous: 0.2–2.5 μM (Cd^{2+})	Individual: 5.5461 μA $μM^{-1}$ (Cd^{2+}) 9.5301 μA $μM^{-1}$ (Pb^{2+}) 14.7197 μA $μM^{-1}$ (Cu^{2+}) 103.4819 μA $μM^{-1}$ (Hg^{2+}) Simultaneous:	Mutual interference, formation of Cd-Hg and Pb-Hg intermetallic compounds	-	-	[85]

24

			0.1057 nM (Pb^{2+})	0.2–2.5 µM (Pb^{2+})	6.6886 µA µM^{-1} (Cd^{2+})				
			0.1636 nM (Cu^{2+})	0.2–2.5 µM (Cu^{2+})	9.4289 µA µM^{-1} (Pb^{2+})				
			0.2771 nM (Hg^{2+})	0.2–2.5 µM (Hg^{2+})	10.1134 µA µM^{-1} (Cu^{2+})				
					8.1339 µA µM^{-1} (Hg^{2+})				
AlOOH-RGO/GCE (drop casting)	SWASV (120 s)	0.1 M ABS (pH 6) (Cd^{2+}, Pb^{2+})	Individual: 44.6 pM (Cd^{2+}) 76 pM (Pb^{2+}) Simultaneous: 35.2 pM (Cd^{2+}) 93.2 pM (Pb^{2+})	Individual: 0.1–0.8 µM (Cd^{2+}) 0.3–0.11 µM (Pb^{2+}) Simultaneous: 0.2–0.8 µM (Cd^{2+}, Pb^{2+})	Individual: 5.38 µA µM^{-1} (Cd^{2+}) 2.97 µA µM^{-1} (Pb^{2+}) Simultaneous: 4.83 µA µM^{-1} (Cd^{2+}) 3.49 µA µM^{-1} (Pb^{2+})	Interference: Humic acid (10 ppm), 20-fold Zn^{2+}, 5-fold Cu^{2+}, 1-fold Hg^{2+} (1.5 µM Cd^{2+}, Pb^{2+})	*RSD: 2.21 % (15 cycles)*	Water from a reservoir	[86]
SnO$_2$-RGO/GCE (drop casting)	SWASV (120 s)	0.1 M ABS (pH 5) (Cd^{2+}, Pb^{2+}, Cu^{2+}, Hg^{2+})	Individual: 0.1141 nM (Cu^{2+}) 0.0344 nM (Hg^{2+}) Simultaneous: 0.1015 nM (Cd^{2+}) 0.1839 nM (Pb^{2+}) 0.2269 nM (Cu^{2+}) 0.2789 nM (Hg^{2+})	Individual: 0.2–0.6 (Cu^{2+}) 0.1–1.3 (Hg^{2+}) Simultaneous: 0.3–1.2 µM (Cd^{2+}, Pb^{2+}, Cu^{2+}, Hg^{2+})	Individual: 2.766 µA µM^{-1} (Cu^{2+}) 5.16 µA µM^{-1} (Hg^{2+}) Simultaneous: 18.4 µA µM^{-1} (Cd^{2+}) 18.6 µA µM^{-1} (Pb^{2+}) 14.98 µA µM^{-1} (Cu^{2+}) 28.2 µA µM^{-1} (Hg^{2+})	Mutual interference, formation of Cu-Hg, Cd-Cu, Cd-Hg, Pb-Cu, Pb-Hg intermetallic compounds	-	-	[87]
Fe$_3$O$_4$-RGO/GCE (drop casting)	SWASV (120 s)	0.1 M ABS (pH 5) (Cd^{2+})	0.056 µM (Cd^{2+})	0.4–0.8 µM (Cd^{2+})	14.82 µA µM^{-1} (Cd^{2+})	Severe interference: 2.5-fold Zn^{2+}, Cu^{2+}, Pb^{2+}, Hg^{2+} (0.8 µM Cd^{2+})	*RSD: 8.47 % (16 cycles)*	-	[88]
Fe$_3$O$_4$-RGO/GCE (drop casting)	SWASV (120 s)	0.1 M ABS (pH 5) (Cd^{2+}, Pb^{2+}, Hg^{2+})	Individual: 8 nM (Cd^{2+}) 6 nM (Pb^{2+}) 4 nM (Hg^{2+}) Simultaneous: 28 nM (Cd^{2+}) 8 nM (Pb^{2+}) 17 nM (Hg^{2+})	Individual: 0.3–3 µM (Cd^{2+}) 0.2–1.3 µM (Pb^{2+}) 0.4–1.8 µM (Hg^{2+}) Simultaneous: 0.1–1.7 µM (Cd^{2+}, Pb^{2+}, Hg^{2+})	Individual: 14.87 µA µM^{-1} (Cd^{2+}) 19.13 µA µM^{-1} (Pb^{2+}) 24.19 µA µM^{-1} (Hg^{2+}) Simultaneous: 5.43 µA µM^{-1} (Cd^{2+}) 14.33 µA µM^{-1} (Pb^{2+}) 8.18 µA µM^{-1} (Hg^{2+})	Mutual interference, formation of intermetallic compounds No interference: 60-fold As(III), As(V), Cu^{2+}, Ni^{2+}, Zn^{2+}, Cr^{3+}, K$^+$, Ca^{2+}, Na$^+$, Cr(VI), Mn^{2+}, Bi^{3+}, Gd^{2+}.	Stab: 95 % (72 h) *RSD: 4 % (4 cycles)*	Soil samples	[89]

25

2.3. Mercury

Mercury pollution is caused by human activity primarily but it is also present naturally in the environment [96]. The toxicity of mercury varies with its form; inhaled mercury primarily affects the brain, mercurous and mercuric salts damage the gut lining and the kidney, and methyl mercury is widely distributed throughout the body [91]. Low-level exposure can produce nonspecific symptoms such as weakness, fatigue, anorexia, weight loss, and gastrointestinal disturbance. With higher exposure levels, mercurial tremor can appear. Erethism may also appear: severe behaviour and personality changes, emotional excitability, loss of memory, insomnia, depression, fatigue, and, in severe cases, delirium and hallucination [91]. The limit of Hg^{2+} concentration in drinking water established by the WHO is 0.001 mg L^{-1}.

Hg^{2+} has been determined in different studies using graphene-based electrodes [78,80,84,85,87,89,92-111,119,120,134]. Materials used in the electrode formulation for the electrochemical determination of Hg^{2+} include: ILs [92,99,134], chitosan [93,95,103], Nafion [80,85,97], other organic molecules [78,80,95,102, 104,106,107,109,119,120], AuNPs [92-98], CeO_2 [85], SnO_2 [87], Fe_3O_4 [89], Al_2O_3 [99], Cu_2O [108], ferrocene [100], DNA [100-103,105,107,108], phosphorous ylide [134], ion imprinted polymer [99], Pani [101], PPy [110], PEDOT [111], PVP [93], and PSS [111]. Au has been usually employed as electrode material or as a component in Hg^{2+} determination as it has great affinity for this metal, which enhances the pre-concentration effect.

Among the major components in the electrode formulation, ILs are used as binders as they improve the ionic conductivity [92,99,134], whereas carbon materials (G, RGO, GQDs, etc.) improve electronic conductivity. Chitosan has been used as a stabilizer to produce stable RGO solutions [93], to protect GO [95] or to complex Hg^{2+} with the amino groups in chitosan [103]. Nafion has been used as a dispersant [85], protective layer [80,97] and cation exchanger membrane [97]. AuNPs provide active sites and favours the pre-concentration of Hg^{2+} [92-98]. DNA has been used as a highly selective and sensitive agent for Hg^{2+} determination [100-108]. The rest of the inorganic and organic compounds usually increase the pre-concentration effect of Hg^{2+} on the surface of the electrode.

Fig. 10 shows a SEM micrograph of RGO surface prior and after AuNPs synthesis [93]. RGO was applied onto the GCE by drop casting of a solution stabilized by chitosan (Fig. 10-A), and subsequently the synthesis of AuNPs was performed by CV (Fig. 10-B). Such a good distribution of small AuNPs allowed a very low LOD (3 pM for 300 s pre-concentration) to be achieved.
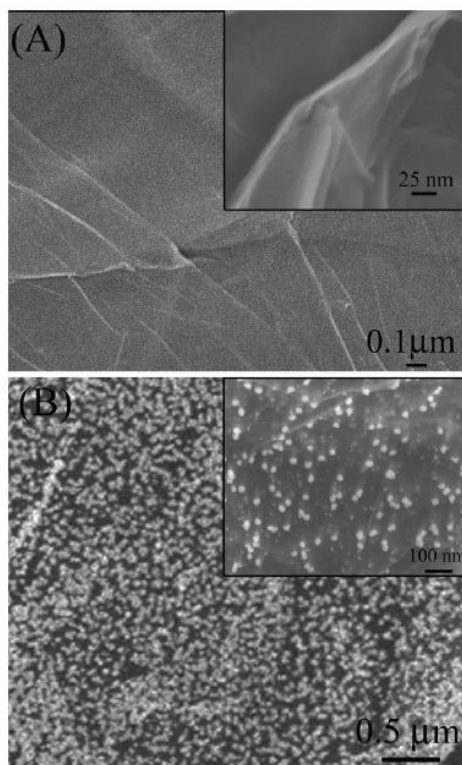
Fig. 10. Typical SEM images of (A) the as-synthesized chi-graphene; (B) AuNPs coated chi-graphene/GCE. Reprinted from Sensors and Actuators B: Chemical, 150, Jingming Gong, Ting Zhou, Dandan Song, Lizhi Zhang, Monodispersed Au nanoparticles decorated graphene as an enhanced sensing platform for ultrasensitive stripping voltammetric detection of mercury(II), 491-497, Copyright (2010), with permission from Elsevier [93].

Fig. 11 shows TEM micrographs of AuNPs, GO and GO-AuNPS hybrid materials [95]. 5-methyl-2-thiouracil (MTU) was thereafter applied by drop casting and fixed on AuNPs via strong S-Au interactions. MTU has a similar interaction to that of Timine-Hg^{2+}-Timine, which forms complexes with Hg^{2+} but not with other metal ions. The electrode presented a synergistic effect between GO/AuNPs and the selective binding of MTU with Hg^{2+}, which improved Hg^{2+} determination. Hg^{2+} ions were fixed to MTU through simple adsorption for 300 s and were subsequently determined by DPV.
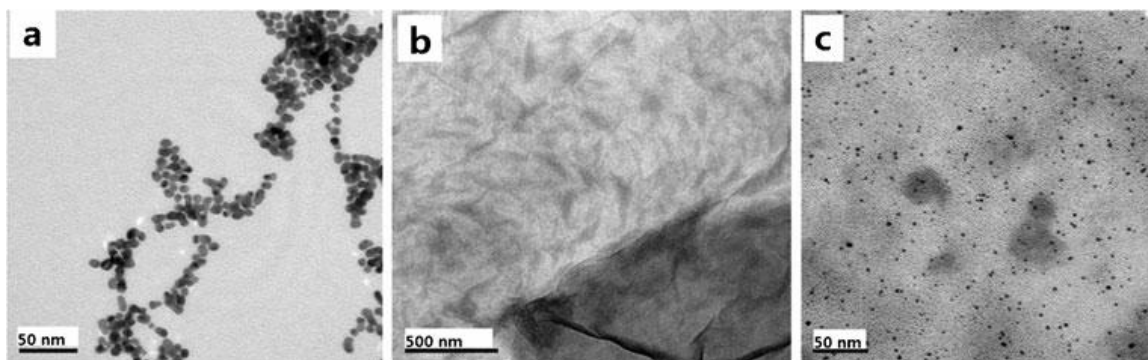
Fig. 11. TEM morphologies of (a) AuNPs, (b) GO and (c) GO-AuNPs nanocomposites with the aid of chitosan. Microchimica Acta, Highly sensitive and selective voltammetric detection of mercury(II) using an ITO electrode modified with 5-methyl-2-thiouracil, graphene oxide and gold nanoparticles, 180, 2013, 493-499, Na Zhou, Hao Chen, Jinhua Li, Lingxin Chen, "With permission of Springer" [95].

SPCE has been also used as a substrate onto which GO and AuNPs have been deposited [96]. The determination of Hg^{2+} was performed in the first underpotential deposition (UPD) peak. Hg^{2+}, As(III) or Pb^{2+} present the UPD process that happens due to strong interaction between the metal and Au after the reduction of the metallic ion, resulting in the formation of an adlayer of the reduced metal. When the films grow due to the increase of the deposition time or an increase of the concentration of metal ions, bulk deposition (BD) takes place. The technique used was highly selective, because the first UPD was observed at + 0.3 V, where only Hg^{2+} was reduced. In this way, the interference of other metallic ions such as Cu^{2+}, Se^{4+}, Zn^{2+}, Cd^{2+} and Pb^{2+} was avoided. The UPD and BD processes have been also observed on AuNPs/GQDs [97] or N-doped G [84] electrodes.

Other type of sensor for Hg^{2+} determination based on G materials include potentiometric sensors [99]. The electrode consisted of a CPE containing graphite powder, RGO, Al_2O_3-NPs and 1-butyl-1-methylpyrrolidinium bis(trifluoromethylsulfonyl)imide ([BMP]Tf_2N) as the conductive binder (IL). An Hg^{2+}-ion imprinted polymer was also included in the mixture as a highly selective sensing material towards Hg^{2+} ions, and resorcinol was used as the selective ligand for Hg^{2+} determination. Hg^{2+} ions were included in the polymer formation and were subsequently removed from the polymer matrix prior to the analysis, in this way the functional sites for Hg^{2+} adsorption were available. The potentiometric sensor was stable in the pH range 3 - 4.5 and a slope of 29.72 mV decade^{-1} was obtained. The response time was about 5 s and it was reversible (from higher to lower concentrations), although the response time was higher (about 15 s).

Among the different electrode formulations, those which contain DNA have demonstrated to have higher selectivity and sensitivity, due to the reaction which are based on [100-108], consequently LOD as low as 5 pM have been reported [100]. The working principle of this type of electrodes is shown in Fig. 12 [100]. In this particular electrode formulation, RGO was deposited on a GCE by drop casting. Thereafter ssDNA was derivatized with ferrocene and was drop casted onto an RGO-GCE electrode. ssDNA was adsorbed on RGO surface due to hydrophobic forces and $\pi-\pi$ stacking interaction. In the absence of Hg^{2+}, ferrocene could approach the surface of RGO due to the flexible random-coil conformation of single stranded oligonucleotides and produce the electron transfer. However, when Hg^{2+} was present, it was fixed on Thimine (T) base pairs forming a T-Hg^{2+}-T duplex with the target DNA (added before the measurement) forming double stranded DNA. This complex is relatively rigid (as duplex DNA) and has low affinity for the RGO surface, and it suffers a conformational reorganization that moves the ferrocene groups away from the electrode surface. As a result, there is a decrease of the redox current signal due to the increased electron-

tunnelling distance. In this case, the dependence of the current on the Hg^{2+} concentration was logarithmic. Therefore, to determine Hg^{2+}, the decrease of the redox current was the analytical parameter measured (signal suppression). The electrode was highly selective and showed little signal suppression for other metal ions, and could be regenerated with good reproducibility.
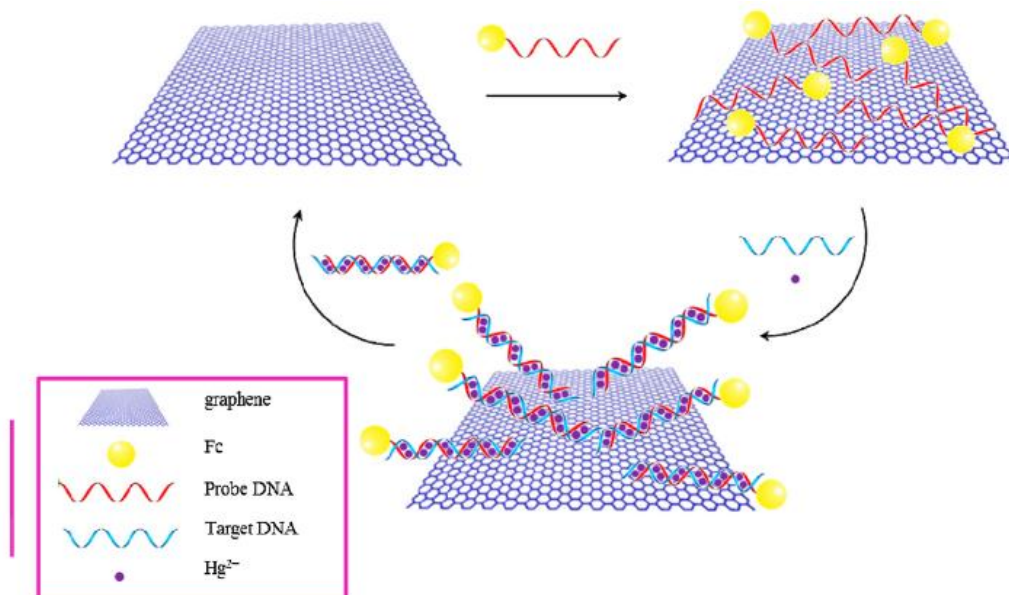

Fig. 12. Schematic illustration of the electrochemical biosensor fabrication and Hg^{2+} detection. Reprinted from Electrochimica Acta, 170, Yanli Zhang, Jinling Xie, Yanpei Liu, Pengfei Pang, Lili Feng, Hongbin Wang, Zhan Wu, Wenrong Yang, Simple and signal-off electrochemical biosensor for mercury(II) based on thymine-mercury-thymine hybridization directly on graphene, 210-217, Copyright (2015), with permission from Elsevier [100].

The EIS technique has been used to measure the increase in the interfacial charge transfer resistance (R_{ct}) on DNA-Pani-RGO/Au electrodes when Hg^{2+} content is increased. The dependence of the R_{ct} on the concentration of Hg^{2+} was also logarithmic [101]. The same technique and principle were used for electrodes composed of 3D-RGO structure with chitosan and DNA [103]. The 3D structure offers large surface area, rapid charge transfer and mass transport kinetics. Three kinds of interaction were obtained on the electrode: the formation of surface complexes of Hg^{2+} ion with the amino group in chitosan, the electrostatic interaction between the negatively charged surface of 3D-RGO and Hg^{2+}, and the formation of the T-Hg^{2+}-T coordination compounds between Hg^{2+} and DNA strands. An increasing amount of Hg^{2+} produced an increase of the charge transfer resistance (Fig. 13). The EIS technique has been also used in other works with DNA-based electrodes to determine Hg^{2+} content [105,106,108].
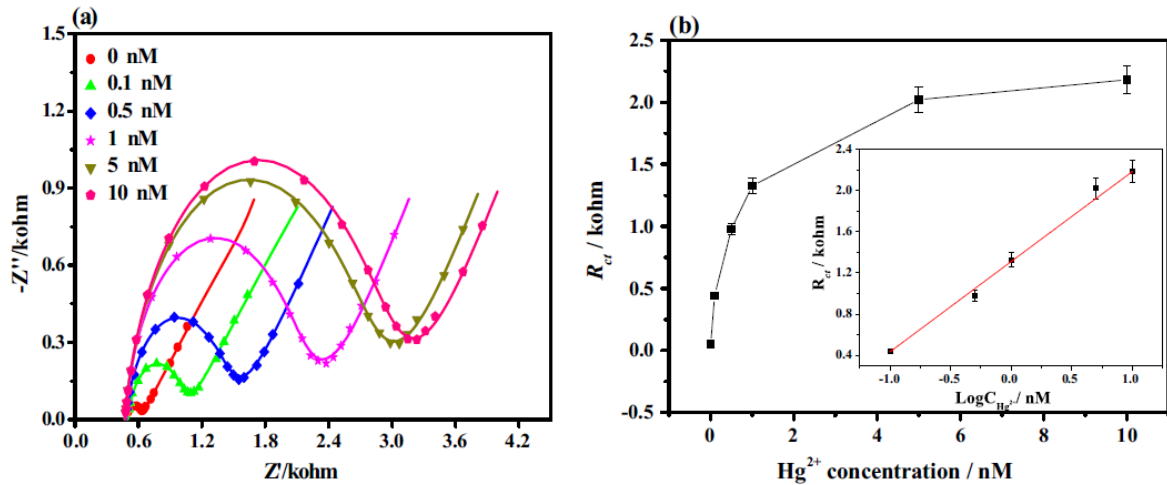
Fig. 13. (a) EIS Nyquist plots for the detection of different concentrations of Hg^{2+} ions: 0, 0.1, 0.5, 1.0, 5.0, and 10.0 nM. (b) The linear fit plots of ΔR_{ct} (charge transfer resistance) as function of the logarithm of Hg^{2+} concentration. Error bar represents the standard deviation of three parallel experiments. Reprinted from Sensors and Actuators B: Chemical, 225, Zhihong Zhang, Xiaoming Fu, Kunzhen Li, Ruixue Liu, Donglai Peng, Linghao He, Minghua Wang, Hongzhong Zhang, Liming Zhou, One-step fabrication of electrochemical biosensor based on DNA-modified three-dimensional reduced graphene oxide and chitosan nanocomposite for highly sensitive detection of Hg(II), 453-462, Copyright (2016), with permission from Elsevier [103].

The selectivity of DNA-based electrodes as commented before is very high. For example, highly selective electrodes for Hg^{2+} and Pb^{2+} determination have been obtained with DNA modification [105]. This type of electrode showed no significant interference from the presence of other ions in a 10000-fold excess concentration [105].

Indirect methods of determination of Hg^{2+} based on DNA-modified electrodes are proposed in the literature [106]. For this purpose, the surface of an Au-coated glass was modified with thiol-functionalized poly-T-oligonucleotides via the formation of Au-S bonds. When Hg^{2+} was present in solution, it formed T-Hg^{2+}-T bonds which induced a conformational change in DNA from single strand to double helix, as previously mentioned. Thereafter, GO was deposited on the surface of the modified electrode. The conformational change produced by the presence of Hg^{2+} influenced the amount of GO that could be deposited on the surface of the electrode, ssDNA has stronger π-π interactions with GO than double helix DNA has with GO. Hence, with lower Hg^{2+} concentration, more ssDNA was present and more GO could be deposited on the surface of the electrode. Since GO is an insulating material, when its quantity increases, the charge transfer resistance measured by EIS increases. Conversely, when the amount of Hg^{2+} increases, more double helix DNA was formed and less GO was deposited on the electrode, obtaining a lower charge transfer resistance. Authors also used CV as a monitoring technique to quantify the amount of Hg^{2+}, in which the intensity of the reduction peak at -0.9 V, which corresponds to the reduction of GO to RGO, was monitored vs. the Hg^{2+} concentration. The CV method showed better performance than the EIS one.

DNA-based sensors are not always based on signal suppression [107]. In this work, a DNA probe modified at the 5′-end with an alkylamino modifier (NH$_2$-ssDNA) was grafted on RGO/polydopamine surface via the Michael addition reaction. In the presence of Hg^{2+}, ssDNA hybridized with probe DNA and led to an increase of the redox mediator ([Ru(NH$_3$)$_6$]$^{3+}$) peak current measured by DPV. The hybridization of DNA in the presence of Hg^{2+} produced an increase of the content of anionic phosphate due to the formation of double stranded DNA. Therefore, more [Ru(NH$_3$)$_6$]$^{3+}$ molecules could bind to the electrode and an increase in the DPV current was recorded.

Other types of modifiers have been used to lower the LOD [109-111]. GO has been modified with cysteamine by nucleophilic ring opening reaction between the epoxy group on GO and the amino group of cysteamine in KOH solution [109]. GO was reduced to RGO at the same time by KOH and Au-S bonds allowed the immobilization of the modified RGO on the Au electrode. Mercapto groups on the surface of modified RGO allowed the selective interaction with Hg^{2+}. The use of the conducting polymer PPy combined with RGO has been also reported as a way to improve the determination of Hg^{2+} due to their synergy; RGO and PPy provided good conductivity and Hg^{2+} coordinated selectively with the nitrogen of the pyrrole units [110]. Partially oxidized G (po-G) obtained by means of electrochemical exfoliation in HClO$_4$/NaCl medium has been also used in the fabrication of electrodes [111]. The po-G provided high surface area and conductivity, and it was combined with PEDOT-PPS. PSS was used as a copolymer to produce a conductive, stable and flexible polymer when combined with PEDOT (a conductive polymer). Thiol groups in PEDOT and sulfonic groups in PSS produced an increase in the oxidation current of Hg due to its affinity for these functional groups. Regeneration or electrode activation was not necessary, which is an advantage when compared with AuNPs based sensors, which require regeneration of the surface with EDTA due to amalgam formation. Other regeneration procedures are applied for Hg^{2+} electrodes, such as: application of a potential of 0.8 V for 60s in a solution containing 1.0 mM HNO$_3$, 1.0 M KCl and 1.0 mM EDTA [92]; immersion of the electrode in a stirred solution containing 1.0 M HNO$_3$, 1.0 KCl and 1.0 mM EDTA for 1 min [101]; soaking the electrode with 100 mM EDTA solution during 30 min [104] or in a cysteine solution to disrupt the T-Hg^{2+}-T sandwich structure [108].

Table 3. Hg^{2+} determination by electrochemical methods with graphene-based electrodes.

Electrode (Synthesis technique)	Technique (Accumulation time)	Supporting electrolyte (Metal ion)	LOD	Linear range	Sensitivity	Main interferences (target ion(s) concentration)	Stability (% of initial response) *RSD (in calibrating solutions)*	Application	[Ref]
AuNPs-IL-GO/GCE (drop casting, electrochemical synthesis)	DPV (660 s)	0.1 M HCl (Hg^{2+})	0.03 nM (Hg^{2+})	0.1–100 nM (Hg^{2+})	-	No interference: 50-fold Co^{2+}, Cd^{2+}, Cu^{2+}, Fe^{3+}, Zn^{2+}, Na^+, K^+, Ca^{2+}, Cl^-, I^-	*RSD: 2.6 % (7 cycles)*	Tap water, bottled water, seawater	[92]
AuNPs-Chitosan-PVP-RGO/GCE (drop casting)	SWASV (120 s)	1 M HCl (Hg^{2+})	30 pM (120 s preconcentration) (Hg^{2+}) 3 pM (300 s pre-concentrat.) (Hg^{2+})	0.04−0.25 nM (Hg^{2+}) 0.5−299 nM (Hg^{2+})	142078 µA µM^{-1} (0.04−0.25 nM) (Hg^{2+}) 1478 µA µM^{-1} (0.5−299 nM) (Hg^{2+})	No interference: 20-fold Fe^{3+}, Cu^{2+}, Co^{2+}, Cd^{2+}, Zn^{2+}, I^- (5 nM Hg^{2+})	Stab: 80 % (30 days, 4ºC)	River water	[93]
AuNPs-RGO/GCE (electrochemical synthesis)	ASV (600 s)	0.01 M HCl (Hg^{2+})	0.6 nM (Hg^{2+})	1–150 nM (Hg^{2+})	79 µA µM^{-1} (Hg^{2+})	No interference: 50-fold Ca^{2+}, Na^+, K^+, Zn^{2+}, Co^{2+}, Ni^{2+}, Mg^{2+}, Cd^{2+}, Cu^{2+}, Cl^- (60 nM Hg^{2+})	*RSD: 1.5 % (3 cycles)*	Tap water	[94]
5-methyl-2-thiouracil-AuNPs-Chitosan-GO/ITO (drop casting)	DPV (300 s OCP)	0.1 M PBS (pH 1) (Hg^{2+})	0.78 nM (Hg^{2+})	5–110 nM (Hg^{2+})	-	No interference: 50-fold K^+, Na^+, Ca^{2+}, Fe^{3+}, Cu^{2+}, Co^{2+}, Pb^{2+}, Zn^{2+}, Ag^+, Pt^{4+} (100 nM Hg^{2+})	-	Tap water, bottle water, lake water	[95]
AuNPs-GO/SPCE (drop casting)	SWASV (200 s)	0.1 M HCl (Hg^{2+})	9.47 nM (Hg^{2+})	10–249 nM (Hg^{2+})	47.5 µA µM^{-1} (Hg^{2+}) (UPD)	No interference: 1000-fold Cu^{2+}, Zn^{2+}, Cd^{2+}, Pb^{2+}, Se^{4+} (50 nM Hg^{2+})	Stab: 85 % (30 days)	Tap water, river water	[96]
GCE/GQDs/AuNPs-Nafion (drop casting)	ASV (120 s)	0.1 M HCl (Hg^{2+}, Cu^{2+})	Individual: 0.02 nM (Hg^{2+}) 0.05 nM (Cu^{2+})	Individual: 0.02–1.5 nM (Hg^{2+}) (UPD) 1.5–100 nM (Hg^{2+}) (BD) 0.05 nM–0.5 µM (Cu^{2+})	Individual: 2470 µA µM^{-1} (Hg^{2+}) (UPD) 467 µA µM^{-1} (Hg^{2+}) (BD) 3690 µA µM^{-1} (Cu^{2+})	-	Stab: >95 % Hg^{2+}, Cu^{2+} (1 week)	-	[97]
AuNPs-RGO/CPE (drop casting)	DPASV (500 s)	0.1 M KCl (pH 3.5) (Hg^{2+})	2.04 nM (Hg^{2+})	5–40 nM (Hg^{2+})	-	Interference: 200-fold Ag^+ No interference: 200-fold Cd^{2+}, Pb^{2+}, Cu^{2+}, Bi^{3+}, As(III), Cr(VI)	*RSD: 3.5 % (6 cycles)*	Soil samples	[98]
CPE (Graphite, RGO, ionic liquid, Al_2O_3, ion imprinted polymer)	Potentiometry	Mercury nitrate solutions (Hg^{2+})	1.95 nM (Hg^{2+})	4 nM–1.3 mM (Hg^{2+})	29.72 mV decade^{-1} (C_{Hg2+}, M)	No interference: Zn^{2+}, Co^{2+}, Pb^{2+}, Cu^{2+}, Cd^{2+}, Ag^+, etc.	Stab: Stable for 18 weeks	Tap water, river water, industrial wastewater, metallurgy wastewater, dental amalgam, tuna fish,	[99]

								shrimp, human hair	
ssDNA-Ferrocene-RGO/GCE (drop casting)	DPV (1.5 h in the Hg^{2+} + 0.1 mM target DNA solution at 25ºC)	pH 7.4 in 50 mM Tris-HCl + 0.3 M NaCl (Hg^{2+})	5 pM (Hg^{2+})	25 pM–10 μM (Hg^{2+})	5.074 μA decade^{-1} (C_{Hg2+}, μM)	No interference: 100-fold Na^+, K^+, Ba^{2+}, Mg^{2+}, Zn^{2+}, Pb^{2+}, Mn^{2+}, Co^{2+}, Ni^{2+}, Fe^{2+}, Fe^{3+}, Al^{3+} (50 nM Hg^{2+})	Stab: 96.1 (5 cycles) *RSD: 1.6 % (5 cycles)*	Tap water, lake water, river water	[100]
ssDNA-Pani-RGO/Au (drop casting)	EIS (2 h in 10 mM PBS + 0.5 M NaCl (pH 7.4) + Hg^{2+})	10 mM PBS (pH 7.4) + 5 mM $K_3[Fe(CN)_6]/K_4[Fe(CN)_6]$ (1:1) (Hg^{2+})	0.035 nM (Hg^{2+})	0.1–100 nM (Hg^{2+})	0.392 kΩ decade^{-1} (C_{Hg2+}, nM)	No interference: 100-fold Pb^{2+}, Ni^{2+}, Ca^{2+}, Ag^+, Co^{2+}, Mn^{2+}, Ca^{2+}, Fe^{3+} (0.1 μM Hg^{2+})	*RSD: 4.5 % (10 cycles)*	River water	[101]
ssDNA-PPAA-G-1-octadecanethiol/Au (self assembly, plasma polymerization)	QCM DPV	PBS + 0.1 M KCl (pH 7.4) (Hg^{2+})	0.031 nM (QCM) (Hg^{2+}) 0.017 nM (DPV) (Hg^{2+})	0.1–200 nM (QCM) (Hg^{2+}) 0.1–100 nM (DPV) (Hg^{2+})	QCM: 46.00868 Hz decade^{-1} (C_{Hg2+}, nM) (QCM) DPV: 1.36523 mA decade^{-1} (C_{Hg2+}, nM)	No interference: 1000-fold Co^{2+}, Cu^{2+}, Fe^{3+}, Mg^{2+}, Ni^{2+}, Pb^{2+}, Zn^{2+} (100 nM Hg^{2+})	Stab: 88% (10 cycles)	-	[102]
DNA-RGO-Chitosan/Au (drop casting)	EIS (incubation with Hg^{2+})	5 mM $Fe(CN)_6^{3-}/^{4-}$ + 1 M KCl + 140 mM NaCl in 0.1 M PBS (pH 7.4) (Hg^{2+})	0.016 nM (Hg^{2+})	0.1–10 nM (Hg^{2+})	0.905 kΩ decade^{-1} (C_{Hg2+}, nM)	No interference: 10-fold Co^{2+}, Cu^{2+}, Ca^{2+}, Fe^{2+}, Fe^{3+}, Mg^{2+}, Ni^{2+}, Pb^{2+}, Zn^{2+}, Ag^+, Ba^{2+}, Mn^{2+}, K^+, Ca^{2+}, Na^+ (10 nM Hg^{2+})	Stab: 96.1 % (10 cycles) *RSD: 1.6 % (10 cycles)*	Tap water, river water	[103]
Thymine-1-acetic acid-Cysteamine-AuNPs-ERGO/GCE (drop casting, electrochem. synthesis)	DPV (15 min incubation) (120 s reduction)	PBS + 0.5M NaCl (pH 7.0) (Hg^{2+})	7.5 pM (Hg^{2+})	0.05 nM–5 nM (Hg^{2+})	1604 μA μM^{-1} (Hg^{2+})	No interference: 10-fold Zn^{2+}, Cd^{2+}, Pb^{2+}, Cu^{2+}, Ni^{2+}, Co^{2+} (50 nM Hg^{2+})	Stab: 92 % (30 cycles)	Tap water	[104]
DNA-NH$_2$-RGO/Au (drop casting)	EIS	20 mM PBS (pH 7.4) (Hg^{2+}, Pb^{2+})	Individual: 5.4 pM (Hg^{2+}) 7.8 pM (Pb^{2+})	Individual: 0.01–100 nM (Hg^{2+}, Pb^{2+})	Individual: 0.116 kΩ decade^{-1} (C_{Hg2+}, nM) (Hg^{2+}) 0.152 kΩ decade^{-1} (C_{Pb2+}, nM) (Pb^{2+})	No interference: 10000-fold Ca^{2+}, Mg^{2+}, Zn^{2+}, Mn^{2+}, Co^{2+}, Ni^{2+} (0.01 nM Hg^{2+}, Pb^{2+})	-	Human serum and tomato juice	[105]
GO-thiol-functionalized poly-T-oligonucleotides/Au-coated glass (adsorption)	EIS/ CV (1.5 h ocp adsorption Hg^{2+} in PBS)	$Fe(CN)_6^{4-}/Fe(CN)_6^{3-}$ (1 mM, 1:1 molar ratio) (Hg^{2+})	1 nM (CV) (Hg^{2+})	1–300 nM (EIS, CV) (Hg^{2+})	0.1468 kΩ decade^{-1} (C_{Hg2+}, nM) (EIS) 0.0853 kΩ decade^{-1} (C_{Hg2+}, nM) (CV)	No interference: 1-fold Hg^{2+}, Ba^{2+}, Cd^{2+}, Co^{2+}, Ni^{2+}, Zn^{2+} (300 nM Hg^{2+})	-	-	[106]
NH$_2$-	DPV	10 mM Tris-HCl (pH	5 nM (Hg^{2+})	8–100 nM	-	No interference:	Stab: Stable for several	River water	[107]

Electrode	Technique	Electrolyte	LOD	Linear range	Sensitivity	Interference	Stability/RSD	Real sample	Ref.
ssDNA/Polydopamine-RGO/GCE (drop casting)	(30 min adsorption in Hg^{2+} solution at 40°C)	7.4) + 50 μM [Ru(NH$_3$)$_6$]$^{3+}$ (Hg^{2+})		(Hg^{2+})		1-fold Zn^{2+}, Cu^{2+}, Ag$^+$, Cd^{2+}, Pb^{2+}, Fe^{3+}, Fe^{2+}, Co^{2+}, Mn^{2+}, Mg^{2+}, Ca^{2+}, Ni^{2+} (10 μM Hg^{2+})	months, stored at 4°C *RSD: 1.02 % (4 cycles)*		
DNA-Cu$_2$O-RGO/Au (drop casting)	EIS	5 mM K$_3$[Fe(CN)$_6$]/ K$_4$[Fe(CN)$_6$] (1:1) in PBS (pH 7.4, + 0.1 M KCl) (Hg^{2+})	8.6 pM (Hg^{2+})	0.05–40 nM (Hg^{2+})	0.19005 kΩ decade^{-1} (C$_{Hg2+}$, nM)	No interference: 10-fold Ba^{2+}, Ca^{2+}, Cu^{2+}, Ni^{2+}, Mg^{2+}, Mn^{2+} (50 nM Hg^{2+})	Stab: 95 % (10 cycles)	River water	[108]
Cysteamine-RGO/Au (adsorption)	SWASV (2 h ocp adsorption Hg^{2+} solutions) (10 s reduction)	0.1 M HCl (Hg^{2+})	3 nM (Hg^{2+})	5–40 nM (Hg^{2+})	13.3 μA μM^{-1} (Hg^{2+})	No interference: 2-fold Cu^{2+}, 200-fold Zn^{2+}, Co^{2+}, Fe^{2+}, Mn^{2+} (50 nM Hg^{2+})	-	-	[109]
PPy-RGO/GCE (drop casting)	SWASV (20 min)	0.01 M HNO$_3$ + 0.3 M KCl (pH 7) (Hg^{2+})	15 nM (Hg^{2+})	10–100 nM (Hg^{2+})	124 μA μM^{-1} (Hg^{2+})	No interference: 10-fold Zn^{2+}, Cd^{2+}, Pb^{2+}, Cu^{2+} (2 μM Hg^{2+})	-	-	[110]
PSS-PEDOT/Partially oxidized G flakes/GCE (drop casting)	DPSV (120 s)	0.05 M HNO$_3$ (Hg^{2+})	0.19 μM (Hg^{2+})	0.2–14 μM (Hg^{2+})	8.72 μA μM^{-1} (Hg^{2+})	No interference: 330-fold Cd^{2+}, As(III), Ni^{2+}, Zn^{2+}, 16-fold Cu^{2+}, 10-fold Fe^{2+} (6 μM Hg^{2+})	*RSD: 0.93 % (10 cycles)*	Laboratory waste samples	[111]

2.4. Lead

Lead ion (Pb^{2+}) is a cause of poisoning for humans and animals producing different detrimental effects on the hematopoietic, renal, reproductive and central nervous systems, mainly through increased oxidative stress [112]. The limit of Pb^{2+} concentration in drinking water established by the WHO is 0.01 mg L^{-1}.

Pb^{2+} has been determined in different studies using graphene-based electrodes [56,58-65,67-74,76-78,80,81,83-87,89,105,113-144]. In addition to G materials, other materials used in the electrode formulation for Pb^{2+} determination include: Bi [58-74,113,115,122,123,137], Sn [76], Hg [56,126,128,129,139], AuNPs [68,71,123-125,136], porous Au [127], Fe_3O_4 [89,130,131], SnO_2 [87], AlOOH [86], CeO_2 [85], ZnO [132], phosphorous ylide [134], SWCNTs [144], MWCNTs [62], DNA [105], chitosan [123], ILs [65,134], Nafion [56,60,62,69,70,72,80,81,85,121,128,129,136,140], PSS [64,126], PVP [131], PPy [138,139], Pani [72,73,113,140], poly(cristal violet) [141], STPs [74], PS [73], PVDF [143], nanoporous carbon [122], sodium alginate [144] and other organic compounds [68-71,77,78,80,117,119,120, 125,129,138,142].

One of the methods of synthesis used for G ultrathin films consists of solid state carbon-diffusion from amorphous carbon on Si wafers [113-115]. By this technique, a layer of Ni was deposited on the amorphous carbon and the carbon atoms dissolved into the Ni layer at a high temperature (800-1100 °C). Thereafter, a G layer was formed by segregation during the cooling due to the diminished solubility of carbon in the Ni layer. In [113], a conductive polymer (Pani) was deposited electrochemically on the G layer to increase corrosion protection and minimize passivation by surfactants or other organic species. On top of the Pani/G coating, a film of Bi was deposited to obtain higher response and sensitivity to determine Pb^{2+} (quantitatively) and Cd^{2+} (qualitatively). Ultralow concentrations of Pb^{2+} (0.33 - 5 nM) were measured in UPD conditions. The LOD of the electrode was lower than when using bare G electrode (0.33 nM vs. 7 nM, respectively) [114]. The electrodes just coated with G showed lower sensitivity to Pb^{2+} even though they have a high resistance to surfactants which could induce passivation, such as SDS [114]. The best performance was obtained when Si wafers were used rather than Si/SiO_2 wafers. SiO_2 could affect the conductivity of the electrode, and the roughness of the G layer was also lower than when using Si. In [115] the same electrodes (G-Ni/Si) coated with Bi were used for the simultaneous electroanalysis of Cd^{2+}, Pb^{2+} and Cu^{2+}. For Pb^{2+} individual electroanalysis UPD and BD processes were also observed, which is demonstrated in Fig. 14. In the concentration range of 0 - 0.3 µM, UPD was observed and a monolayer of Pb^{2+} was formed on the electrode. At higher Pb^{2+} concentration BD was observed, and the sensitivity obtained was lower. Comparing the LODs presented in the three papers [113-115], the best results were obtained when Pani and BiNPs were deposited on the G-Ni/Si electrodes [113].

The importance of defects and functional groups on G materials was stated in a study were G was grown by CVD [116]. A high value of LOD for Pb^{2+} was obtained, and it should be taken into account that CVD graphene presents low defects. Thus, the high LOD could be ascribed to the absence of oxygen-containing groups that help in the process of metal ion adsorption as mentioned throughout the present review. This was

35

confirmed for Pb^{2+} determination in a study where Au electrodes were modified with L-cysteine and finally with GO [119]. The presence of GO on the electrode improved its sensitivity by two orders of magnitude when compared with the Au/L-cysteine electrode. The negative functional groups of GO helped in the adsorption/coordination process of Pb^{2+}, Hg^{2+} and Cu^{2+} ions. Other studies used a similar approach, with GO on the surface of the electrode to favour the pre-concentration effect [120,133].
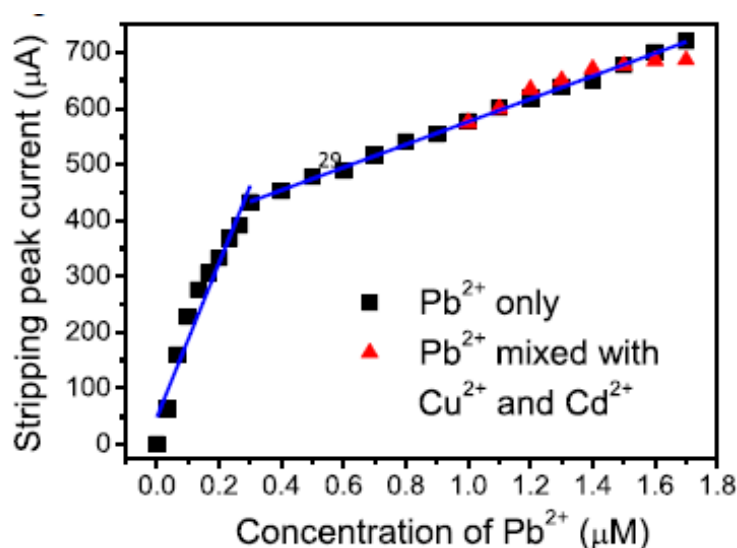
Fig. 14. Anodic stripping peak currents with respect to concentration of Pb^{2+} (0 – 1.7 μM). All the results were measured at a Bi/ graphene electrode in 0.1 M acetate buffer solutions (pH 5.3) with a step increment of 0.1 μM of each target metal. Adapted from Thin Solid Films, 544, Zhaomeng Wang, Pui Mun Lee, Erjia Liu, Graphene thin film electrodes synthesized by thermally treating cosputtered nickel–carbon mixed layers for detection of trace lead, cadmium and copper ions in acetate buffer solutions, 341-347, Copyright (2013), with permission from Elsevier [115].

The use of other forms of carbon combined with G materials has also been studied [121,122]. Modified G carbon nanosheets were obtained by pyrolysis of GO and carbon precursors (resorcinol and formaldehyde) at 800ºC in N_2 atmosphere for 2 h [121]. The porous carbon obtained has a high adsorption capacity of metal ions but has low conductivity; RGO plays a key role providing high electrical conductivity to the layered structure. The coating formed a 3-D structure due to the presence of macropores and the layered structures provided a large surface area that could enhance Pb^{2+} diffusion kinetics. The optimal thickness of the carbon layers (34 ± 4 nm) showed a moderate conductivity, which was beneficial as low background current was observed, which allowed good sensitivity. The enlargement of surface area and the decrease of conductivity was beneficial for lowering the LOD. In another work [122] NPC was synthesized on GS by pyrolysis of zeolitic imidazolate framework-8 (ZIF-8) deposited on GO. Due to the nanoscale cavities and open channels, ZIF-8 is a good template to synthesize NPC by carbonization. The surface area of the GS-NPC nanocomposite was calculated to be 1251 m^2 g^{-1} which enhanced electron transfer kinetics. Thereafter, BiNPs were chemically synthesized in-situ on the GS-NPC composite. The active

36

material was finally deposited on a GCE by drop casting technique. No mutual interference was observed between Pb^{2+} and Cd^{2+}. In addition, Tl^+ could also be determined due to the adequate potential separation between peaks (a quantitative analysis was performed).

AuNPS have also been used in the electrode formulation, although in less extension than with the determination of other metal ions [123,124]. The obtained electrodes combined the benefits of RGO (enlarged active surface area and high electronic conductivity) and AuNPs (high affinity). Chitosan was used in the formulation due to its excellent film–forming ability, good water permeability and strong adsorption of metal ions [123].

Other forms of G, such as N-doped G have been recently applied to Pb^{2+} determination by electrochemical methods [125]. N-doped G was synthesized from the hydrothermal treatment of GO and urea as the reducing and doping agent. Colloidal AuNPs were added subsequently and a hybrid material AuNPs-N-doped G was obtained and applied by drop casting onto a GCE. The electrode obtained was immersed in L-cysteine solution that was fixed through S-Au bonds. The –CN groups in N-doped G caused an increase of the chelation with Pb^{2+} ions; AuNPs increased the effective surface area and conductivity; L-cysteine provided the active –COOH groups which are known to bind strongly with Pb^{2+}. All these factors contributed to an increment in the stripping current.

Although Hg tends to be eliminated from electrode formulation due to its toxicity, some works still use it for Pb^{2+} determination [56,126,128,129,139]. Very low LODs have been obtained using Hg in the electrode formulation (as low as 0.1 pM [129]). Along similar lines, Hg-GQDs-PSS modified electrodes have been reported. GQDs solution was mixed with the PSS surfactant to avoid aggregation, and it was applied on a GCE by drop casting technique [126]. Fig. 15 shows TEM micrographs of GO (Fig. 15-a) and the GQDs (Fig. 15-b) obtained. The presence of defects in the structure of GQDs and their high surface area, as well as the negative charges of PSS enhance the adsorption process of metal ions. Finally, an Hg film was also co-deposited during the analysis, which helped in the stripping process.
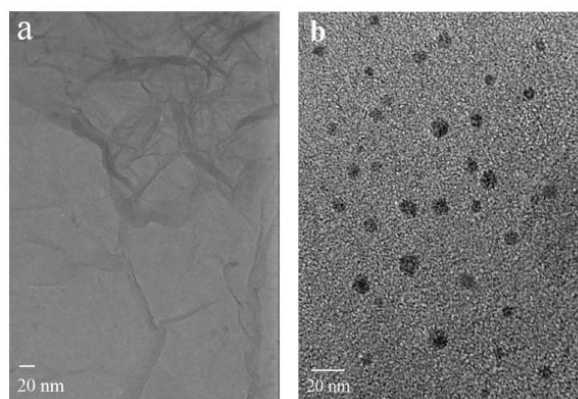
Fig. 15. Transmission electron microscopy (TEM) images of (a) pristine GO and (b) GQDs. Reprinted from Colloids and Surfaces B: Biointerfaces, 118, Chengfeng Zhou, Wei Jiang, Brian K. Via, Facile synthesis of soluble graphene quantum dots and its

improved property in detecting heavy metal, 72-76, Copyright (2014), with permission from Elsevier [126].

In another study [128] a GO/Hg^{2+} composite was dispersed in Nafion to obtain stable suspension and was deposited on a GCE by drop casting technique. Thereafter, electrochemical reduction of GO/Hg^{2+} produced the reduction of Hg^{2+} to Hg nanodroplets. GO helped to attach Hg^{2+} ions due to the presence of negative charged functional groups. In this way, Hg was fixed on the structure of the electrode and toxicity could be reduced when compared with traditional MFEs. The electrode obtained was 167% more sensitive than the Hg/MWCNTs electrode, which can be explained by the high surface area of GO when compared to MWCNTs.

The covalently modified GO with p-phenylenediamine, producing amine functionalized graphene oxide (AGO), is presented as an alternative to increase the analytical sensitivity towards Pb^{2+} [129]. The aminated GO showed enhanced detection due to both the negative functional groups of GO that attract metallic ions and to the nitrogen atoms in the $-NH_2$ bonds that can offer lone pairs of electrons, which effectively attract metallic cations. The good conductivity obtained during the amination process, where GO was partially reduced, and the large surface area and the good mobility of the amino groups enhanced sensitivity. The co-deposition of a Hg film with Pb^{2+} on the surface of the electrode makes the electrode highly selective to Pb^{2+} even in the presence of other metal ions (Zn^{2+}, Cd^{2+}, Cu^{2+}). The influence of amino groups in the detection process was certified by its thermal removal. In another study, PPy/RGO nanocomposite has shown selective adsorption towards Hg^{2+} and provided a large number of nucleation sites for the deposition of Hg^0 during the pre-concentration step, due to the large surface area of the nanocomposite [139].

Inorganic compounds have been also used as sensing material in electrode formulation, such as the composite made by Fe_3O_4/RGO NSCs, where RGO mainly provided the conductivity of the electrode surface [130-132]. The structure of the inorganic material was a key factor to maximize the active area. In [130] the optimal formulation contained 3% RGO, as a higher RGO content induced a change in the Fe_3O_4 structure from rose-like to spherical, which decreased the area and the number of pores. In [131] various shapes of Fe_3O_4-decorated RGO were prepared (band, spherical and rod) by adjusting the Fe^{2+}/Fe^{3+} molar ratio. The electrode was used in the determination of Pb^{2+} and the influence of the Fe_3O_4 morphology on the sensitivity of the electrode was demonstrated. The functional groups on the surface of RGO controlled the diffusion, growth and agglomeration of Fe_3O_4 nanoparticles. The sensitivity obtained followed the order band Fe_3O_4 > spherical Fe_3O_4 > rod Fe_3O_4.

The use of ZnO nanotubes/RGO coatings has also been reported [132]. ZnO nanotubes have higher surface area and porosity than nanofibers. The hydroxy groups on the surface of ZnO nanotubes can be used as adsorbents for metal ions. The poor conductivity of ZnO is compensated by the presence of RGO and allowed the use of ZnO as electrode material.

38

Ionic liquids have been demonstrated to be helpful modifiers [134]. A CPE containing graphite, the IL 1-n-octylpyridinum hexafluorophosphate and a new phosphorus ylide [2,4-Cl$_2$C$_6$H$_3$C(O)CHPPh3] that acted as a selective adsorbent for the determination of Pb^{2+}, Hg^{2+} and Tl$^+$ was prepared. The conductive performance of the electrode was improved as it had two conducting pathways, electronic (carbon) and ionic (due to the IL). With this electrode the authors succeeded in separating the three peaks sufficiently and no mutual interference among them was observed. The proper separation of these peaks was difficult to achieve with other electrodes, where overlapping was observed.

Other type of sensor for Pb^{2+} determination includes potentiometric sensors [142]. In this case, ERGO was deposited on a GCE by CV. Thereafter, an electrode membrane was deposited by immersion of the electrode to construct a potentiometric sensor (ion selective electrode). The ionophore 1,2-bis(N'-benzoylthioureido) benzene acted as the selective ligand which forms a complex with Pb^{2+}. The membrane obtained had a loose structure with channels through which Pb^{2+} ions could diffuse. The measured potentials were independent of the pH in the range 4.0 to 8.0, the time of response was less than 15 s and the sensor was highly selective.

The creation of 3-D structures is of particular interest due to their high surface area. Along these lines a 3-D SA (sodium alginate)-SWCNTs-RGO aerogel prepared hydrothermally has been reported [144]. SWCNTs avoided re-stacking of RGO sheets, enhanced electron transfer and created a 3-D structure of the composite with very high surface area. SA is a natural polysaccharide extracted from the cell wall of brown seaweed and showed excellent adsorption of metal ions. In addition, SA helped in decreasing the background current and improving the signal/noise ratio. The surface area of the SA-MWCNTs-RGO composites was 702 m^2 g^{-1}, larger than that of RGO (558 m^2 g^{-1}) and RGO-SA composites (510 m^2 g^{-1}). Other 3-D structures include G nanodots-encaged porous Au electrodes via ion beam sputtering deposition [127]. The higher the thickness of the film, the higher the G nanodot content. However, the diffusion was hindered as the thickness of the film increased, so the optimal thickness of the electrode was limited to 40 nm.

Table 4. Pb^{2+} determination by electrochemical methods with graphene-based electrodes.

Electrode (Synthesis technique)	Technique (Accumulation time)	Supporting electrolyte (Metal ion)	LOD	Linear range	Sensitivity	Main interferences (target ion(s) concentration)	Stability (% of initial response) *RSD (in calibrating solutions)*	Application	[Ref]
Bi-Pani-G-Ni/Si (solid state carbon diffusion)	SWASV (180 s)	0.1 M ABS (pH 5.3) [1.25 µM Bi^{3+}] (Pb^{2+}) (Cd^{2+}, qualitative)	0.33 nM (Pb^{2+})	0.33–5 nM (Pb^{2+}, UPD) 0.1–1.1 µM (Pb^{2+}, BD)	670 µA µM^{-1} (Pb^{2+}, UPD) 490 µA µM^{-1} (Pb^{2+}, BD)	Interference: > 2 mg L^{-1} SDS (1µM Pb^{2+})	Stab: Stable 32 cycles	-	[113]
G-Ni/Si (solid state carbon diffusion)	SWASV (180 s)	0.1 M ABS (pH 5.3) + 0.1 M KNO_3 (Pb^{2+})	7 nM (Pb^{2+})	7–1200 nM (Pb^{2+})	490 µA µM^{-1} (Pb^{2+})	Interference: SDS	Stab: Stable 11 cycles with 8 mg L^{-1} SDS *RSD: 6.2 % (46 cycles)*	-	[114]
Bi-G-Ni/Si (solid state carbon diffusion)	SWASV (180 s)	0.1 M ABS (pH 5.3) + 0.1 M KNO_3 [2.5 µM Bi^{3+}] (Pb^{2+}, Cd^{2+}, Cu^{2+})	Individual: 0.03 µM (UPD) (Pb^{2+}) Simultaneous: 0.1 µM (Cd^{2+}) 0.1 µM (Cu^{2+})	Individual: 0–0.03 µM (UPD) (Pb^{2+}) 0.03–1.7 µM (BD) (Pb^{2+}) Simultaneous: 1–1.7 µM (Pb^{2+}) 0.1–0.7 µM (Cd^{2+}) 0.1–0.7 µM (Cu^{2+})	Individual: 1375.78 µA µM^{-1} (UPD) (Pb^{2+}) 203.99 µA µM^{-1} (BD) (Pb^{2+}) Simultaneous: 23.5 µA µM^{-1} (Cd^{2+}) 196.68 µA µM^{-1} (Cu^{2+})	No mutual interference	*RSD: ~0.6 % (34 cycles)*	-	[115]
G-Ni/Oxidised Si wafer (CVD)	SWV (40 s)	HCl (pH 1.5) (Pb^{2+})	1.93 µM (Pb^{2+})	1.93–9.65 µM (Pb^{2+})	3.33 µA µM^{-1} (Pb^{2+})	Interference: Ni from substrate	*RSD: 4.8 % (3 cycles)*	-	[116]
RGO-pyrene-diazonium salt/Au (adsorption)	OSWV	Ammonium acetate buffer (pH 7) (Pb^{2+}, Cu^{2+})	Individual: 0.4 nM (Pb^{2+}) 1.5 nM (Cu^{2+})	Individual: 0.4–20 nM (Pb^{2+}) 1.5–20 nM (Cu^{2+})	-	Interference: 100-fold Cd^{2+}, Co^{2+}, Ni^{2+}, Zn^{2+}, Ca^{2+} (20 nM Cu^{2+}, Pb^{2+})	Stab: 96.4 % (Cu^{2+}), 91.9 % (Pb^{2+}) (2 weeks) 77.6 % (Cu^{2+}), 83.8 % (Pb^{2+}) (4 weeks)	-	[117]
ERGO/GRC (drop casting, electrochemical reduction)	SWV (600 s)	0.1 M HCl + 0.1 M citrate buffer (pH 2) (Pb^{2+})	0.5 nM (Pb^{2+})	3–15 nM (Pb^{2+})	31.02 µA µM^{-1} (Pb^{2+})	Interference: 1000-fold Cu^{2+} (severe) No interference: 1000-fold Bi^{3+}, Al^{3+}, Cl^-, Zn^{2+} (1 µM Pb^{2+})	Stab: 95 % (1 week, 4ºC), 99% (100 cycles) *RSD: 3.5 % (8 cycles)*	Tap water, river water, sea water	[118]
GO-L-cysteine/Au (coupling)	SWV	Ammonium acetate buffer (pH 7) + 50 mM KCl (Pb^{2+}, Cu^{2+}, Hg^{2+})	Individual: 1.93 nM (Pb^{2+}) 3.99 nM (Hg^{2+}) 18.88 nM (Cu^{2+})	Individual: 0–247 nM (Pb^{2+}) 0–63.8 nM (Hg^{2+})	Individual: 5.01 µA µM^{-1} (Pb^{2+}) 14.64 µA µM^{-1} (Hg^{2+})	Severe interference: 4-fold Zn^{2+}, Ni^{2+}, Fe^{3+}, Cu^{2+}, Hg^{2+} (0.12 µM)	-	-	[119]

40

Material (method)	Technique	Electrolyte	LOD	Linear range	Sensitivity	Interference	Stability/RSD	Real samples	Ref
				0–3.15 µM (Cu²⁺)	1.61 µA µM⁻¹ (Cu²⁺)				
GO-4-phenyl diazonium salt/Au (electrochemical)	OSWV (600 s ocp adsorption)	50 mM ammonium acetate buffer (pH 6.8) + 50 mM KCl (Pb²⁺, Cu²⁺, Hg²⁺)	Simultaneous: 1.45 nM (Pb²⁺) 8.47 nM (Hg²⁺) 26.75 nM (Cu²⁺)	Simultaneous: 1.45–241 nM (Pb²⁺) 8.47–748 nM (Hg²⁺) 26.75–1574 nM (Cu²⁺)	Simultaneous: 6.26 µA µM⁻¹ (Pb²⁺) 2.31 µA µM⁻¹ (Hg²⁺) 1.11 µA µM⁻¹ (Cu²⁺)	Interference: Ba²⁺, Cu²⁺, Ni²⁺, Zn²⁺, Cd²⁺	Stab: 96.5 % (30 days in 50 mM ammonium acetate buffer) -0.001 µA (1 cycle per day, 20 days)	-	[120]
Nafion-G-carbon nanosheets/GCE (pyrolysis, drop casting)	SWASV (400 s)	0.01 M ABS (pH 5.5) (Pb²⁺)	1.12 nM (Pb²⁺)	0.5–50 µM (Pb²⁺)	92.86 µA µM⁻¹(Pb²⁺)	Interference: 1-fold Hg²⁺ (1 µM Pb²⁺), formation intermetallic compound (Pb-Hg)	-	-	[121]
Bi-NPC-GS/GCE (drop casting)	SWASV (180 s)	0.1 M ABS (pH 5.0) (Pb²⁺, Cd²⁺) (Tl⁺, qualitative)	Simultaneous: 3.2 nM (Pb²⁺) 4.1 nM (Cd²⁺)	Simultaneous: 0.06–0.6 µM (Pb²⁺) 0.08–0.8 µM (Cd²⁺)	Simultaneous: 46.27 µA µM⁻¹ (Pb²⁺) 36.78 µA µM⁻¹ (Cd²⁺)	Interference: > 1 µM Cu²⁺, Hg²⁺ (0.2 µM Pb²⁺, 0.4 µM Cd²⁺) formation intermetallic compound	Stab: 95 % (Pb²⁺), 93 % (Cd²⁺) (6 weeks) RSD: 2.6 % (Pb²⁺), 3.0 % (Cd²⁺) (10 cycles)	Tap water, lake water	[122]
Bi-Chitosan-AuNPs-RGO/GCE (electrodeposition)	DPASV (600 s)	0.1 M ABS (pH 4.5) [3 mg L⁻¹ Bi³⁺] (Pb²⁺)	48.3 pM (Pb²⁺)	2.41–483 nM (Pb²⁺)	24.9 µA µM⁻¹ (Pb²⁺)	No interference: 100-fold Cu²⁺, Cd²⁺, 1000-fold Mg²⁺, Ag⁺, Co²⁺, Ca²⁺, Zn²⁺, Al³⁺, Ni²⁺ (0.48 µM Pb²⁺)	RSD: 2.06 % (6 cycles)	River water	[123]
AuNPs-ERGO/GCE (electroreduction)	SWASV (180s)	0.1 M ABS (pH 5.3) (Pb²⁺, Cu²⁺)	Individual: 0.8 nM (Pb²⁺) Simultaneous: 2.39 nM (Pb²⁺) 5.18 nM (Cu²⁺)	Individual: 10–150 nM (Pb²⁺) Simultaneous: 10–100 nM (Pb²⁺) 10–100 nM (Cu²⁺)	Individual: 455.83 µA µM⁻¹ (Pb²⁺) Simultaneous: 218.68 µA µM⁻¹ (Pb²⁺) 62.206 µA µM⁻¹ (Cu²⁺)	Mutual interference, formation Pb-Cu intermetallic compound	-	Tap water	[124]
L-cysteine-AuNPs-N doped G/GCE (drop casting)	SWV (600 s)	0.1 M ABS (pH 4.5) (Pb²⁺)	0.27 nM (Pb²⁺)	4.83–386 nM (Pb²⁺)	151 µA µM⁻¹ (Pb²⁺)	Interference: 5-fold Cd²⁺, 1-fold Cu²⁺, Ag⁺ (96.5 nM Pb²⁺)	-	River water, tap water	[125]
Hg-GQDs-PSS/GCE (drop casting)	DPV (300 s ocp adsorption of Pb²⁺ and Hg²⁺ ions) (60 s reduction)	0.01 M HCl [50 µM Hg²⁺] (Pb²⁺)	7 nM (Pb²⁺)	0.8 µM–10 µM (Pb²⁺)	7.5438 µA µM⁻¹ (Pb²⁺)	-	-	-	[126]
Porous Au-G nanodots (ion beam sputtering deposition)	OSWV	Ammonium acetate buffer (pH 5) (Pb²⁺, Cu²⁺)	Individual: 6 nM (Pb²⁺) 9 nM (Cu²⁺)	Individual: 0.006–2.5 µM (Pb²⁺). 0.009–4 µM (Cu²⁺)	-	Interference: 4-fold Cd²⁺, Co²⁺, Ni²⁺, Ca²⁺, Mg²⁺ (2.5 µM Pb²⁺, Cu²⁺)	Stab: 97.97 % (Cu²⁺), 99.24 % (Pb²⁺) (2 weeks) 88.5 % (Cu²⁺), 89.9 % (Pb²⁺) (40 days)	-	[127]
Hg-GO-Nafion/GCE (drop casting)	SWASV (150 s)	0.1 M ABS (Pb²⁺)	0.63 pM (Pb²⁺)	24–338 pM (Pb²⁺) 0.48–48 nM (Pb²⁺)	79150 µA µM⁻¹ (24–338 pM) (Pb²⁺) 6775 µA µM⁻¹ (0.48–48 nM) (Pb²⁺)	No interference: 120-fold Al³⁺, 110-fold Ca²⁺, 90-fold Ba²⁺, 15-fold Co²⁺, 10-fold Ni²⁺, 2-	-	Tap water, pool water, river water, lake water	[128]

41

						fold Cu^{2+} (24.1 nM Pb^{2+})			
Hg-Nafion-GO-p-phenylenediamine/GCE (drop casting)	DPASV (300 s ocp adsorption of Pb^{2+} and Hg^{2+} ions) (120 s reduction) (Pb^{2+})	0.01 M HCl + 0.01 M NaOH (pH 4) [50 μM Hg^{2+}]	0.1 pM (Pb^{2+})	0.1–8 pM (Pb^{2+}) 0.5–50 μM (Pb^{2+})	39600 μA μM^{-1} (0.1–8 pM) (Pb^{2+}) 1.488 μA μM^{-1} (0.5–50 μM) (Pb^{2+})	No interference: 1-fold Cu^{2+}, Pb^{2+}, Cd^{2+}, Zn^{2+} (1 nM, 100 nM Pb^{2+})	-	Tap water	[129]
Fe$_3$O$_4$-RGO/GCE (hydrothermal process, drop casting)	DPV	0.1 M ABS (pH 6) (Pb^{2+})	0.082 nM (Pb^{2+})	0.05–1.5 nM (Pb^{2+})	55.4 μA cm^{-2} μM^{-1} (Pb^{2+})	No interference: 50-fold Ni^{2+}, Zn^{2+}, Cr^{2+}, Bi^{3+}, 40-fold Cu^{2+}, Ag^+, Hg^{2+} (5 μM Pb^{2+})	Stab: 91.8 % (10 days) *RSD: 1.2-3 %*	-	[130]
Fe$_3$O$_4$-PVP-RGO/GCE (co-precipitation method, drop casting)	SWASV	0.1 M ABS (pH 5) (Pb^{2+}, Cd^{2+}, Cu^{2+})	Individual: 0.073 μM (spherical Fe$_3$O$_4$) (Pb^{2+}) 0.033 μM (rod Fe$_3$O$_4$) (Pb^{2+}) 0.17 μM (band Fe$_3$O$_4$) (Pb^{2+}) 0.04 μM (band Fe$_3$O$_4$) (Cd^{2+}) 0.05 μM (band Fe$_3$O$_4$) (Cu^{2+})	Individual: 0.7–1.2 μM (spherical Fe$_3$O$_4$) (Pb^{2+}) 0.8–1.2 μM (rod Fe$_3$O$_4$) (Pb^{2+}) 0.4–1.5 μM (band Fe$_3$O$_4$) (Pb^{2+}) 0.4–1.1 μM (band Fe$_3$O$_4$) (Cd^{2+}) 0.5–1.5 μM (band Fe$_3$O$_4$) (Cu^{2+})	Individual: 7.387 μA μM^{-1} (spherical Fe$_3$O$_4$) (Pb^{2+}) 2.362 μA μM^{-1} (rod Fe$_3$O$_4$) (Pb^{2+}) 13.57 μA μM^{-1} (band Fe$_3$O$_4$) (Pb^{2+}) 4.35 μA μM^{-1} (band Fe$_3$O$_4$) (Cd^{2+}) 10.1 μA μM^{-1} (band Fe$_3$O$_4$) (Cu^{2+})	-	-	-	[131]
ZnO-Nafion-RGO/GCE (drop casting)	SWSV (600 s)	0.1 M ABS (pH 4.6) (Pb^{2+})	0.48 nM (Pb^{2+})	2.4 nM–480 nM (Pb^{2+})	202.7 μA μM^{-1} (Pb^{2+})	Interference: 50-fold Fe^{3+}, 1-fold Cd^{2+}, Hg^{2+}, Cu^{2+} (0.24–0.48 μM Pb^{2+})	*RSD: 8.56 % (5 cycles)*	Tap water, lake water	[132]
GO-CPE (paste electrode)	SWASV (90 s)	0.1 M HCl (pH 1) (Pb^{2+})	21.8 nM (Pb^{2+})	0.1–70 μM (Pb^{2+})	4.01 μA μM^{-1} (Pb^{2+})	No interference: 10-fold Zn^{2+}, Hg^{2+}, Cd^{2+}, Cu^{2+}, Ni^{2+}, Co^{2+} (5 μM Pb^{2+})	-	Fish (Rainbow Trout)	[133]
CPE (Graphite-G-1-n-octylpyridinum Hexafluorophosphate-phosphorous ylide) (paste electrode)	SWASV (90 s)	0.2 M ABS (pH 4) (Pb^{2+}, Hg^{2+}, Tl^+)	Simultaneous: 0.45 nM (Pb^{2+}) 0.386 nM (Hg^{2+}) 0.357 nM (Tl^+)	Simultaneous: 1.25 nM–0.2 μM (Pb^{2+}, Hg^{2+}, Tl^+)	Simultaneous: 305.78 μA μM^{-1} (Pb^{2+}) 342.95 μA μM^{-1} (Hg^{2+}) 400.34 μA μM^{-1} (Tl^+)	Interference: 0.18 μM Cd^{2+} No interference: 0.35 μM Cu^{2+}, Zn^{2+}, K^+, Na^+, Ca^{2+}, Mg^{2+}, Al^{3+}, Ni^{2+}, Mn^{2+}, Co^{2+}, Cr^{3+}, In^{3+}, Ba^{2+}, Fe^{3+}, etc. (0.13 μM Tl^+)	Stab: 95.2 % (Tl^+), 94.4 % (Pb^{2+}), 95.1 % (Hg^{2+}) (28 days, ambient conditions) *RSD: 3.6 % (Tl^+), 3.2 % (Pb^{2+}), 2.9 % (Hg^{2+}) (5 cycles)*	Tap water, river water, soil	[134]
ERGO/SPCE (drop casting, electrochemical synthesis)	SWASV (420 s)	0.1 M ABS (pH 4.5) (Pb^{2+})	4.83 nM (Pb^{2+})	24–965 nM (Pb^{2+})	66 μA μM^{-1} (Pb^{2+})	Interference: 0.5-fold Cd^{2+} No interference: 1-fold Cu^{2+} (0.48 μM Pb^{2+})	-	Tap water, juice, preserved eggs, tea	[135]
AuNPs-Nafion-	DPSV	0.1 M ABS (pH 4.5)	Simultaneous:	Simultaneous:	Simultaneous:	No interference:	*RSD: 1.5 % (Pb^{2+}),*	River water,	[136]

42

Electrode	Method	Electrolyte	LOD	Linear range	Sensitivity	Interference	Stability/RSD	Sample	Ref
RGO/SPCE (drop casting, electrosynthesis)	(240 s)	(Pb^{2+}, Cd^{2+})	1.11 nM (Pb^{2+}) 3.11 nM (Cd^{2+})	2.42–290 nM (Pb^{2+}) 7.11–445 nM (Cd^{2+})	116 µA µM^{-1} (Pb^{2+}) 66 µA µM^{-1} (Cd^{2+})	500-fold Al^{3+}, Mn^{2+}, Ni^{2+}, Na^+, Ca^{2+}, Mg^{2+}, K^+, NO_3^-, SO_4^{2-}, 200-fold Fe^{3+}, Zn^{2+}, Co^{2+}, 100-fold Fe^{2+}, As(III)), Cr^{3+} (10 nM Pb^{2+}, Cd^{2+})	1.7 % (Cd^{2+}) (10 cycles)	pond water	
Bi-RGO/SPE (drop casting, electroreduction)	DPV (300 s)	0.1 M ABS (pH 4.5) (Pb^{2+})	6.8 nM (Pb^{2+})	0.05–20 µM (Pb^{2+})	1.57 µA µM^{-1} (Pb^{2+})	No interference: 100-fold K^+, Na^+, Ca^{2+}, Mg^{2+}, Mn^{2+}, Cr^{3+}, Cl^-, NO_3^-, 50-fold Fe^{3+}, Zn^{2+}, 20-fold Cu^{2+}, 15-fold Sn^{2+}, Cd^{2+}	Stab: 83.5 % (3 days, used each day twice times) RSD: 4.6 % (Pb^{2+}) (8 cycles)	Coastal sediment pore waters	[137]
Cysteine-GO-PPy/SPE (electropolymerization)	DPASV (600 s)	0.1 M ABS (pH 5.0) (Pb^{2+})	0.33 nM (Pb^{2+})	6.8–135 nM (Pb^{2+}) 135 nM–1.35 µM (Pb^{2+}) 1.35–67.5 µM (Pb^{2+})	3.81 µA µM^{-1} (6.8–135 nM) (Pb^{2+}) 2.18 µA µM^{-1} (135 nM–1.35 µM) (Pb^{2+}) 0.89 µA µM^{-1} (1.35–67.5 µM) (Pb^{2+})	No interference: 1-fold Na^+, K^+, Ag^+, Cd^{2+}, $Cu2+$, Hg^{2+}, Ca^{2+}, Mg^{2+}, Fe^{3+}, Co^{2+}, Ni^{2+}, Zn^{2+}, Ba^{2+}. Minimal interference: 1-fold Cd^{2+}, Cu^{2+}, Hg^{2+} (67.6 nM Pb^{2+}), formation of Pb-Hg and Pb-Cu intermetallic compounds.	Stab: Stable for 1 month RSD: 3 % (Pb^{2+}) (3 cycles)	Real water samples from a local company	[138]
Hg-RGO-PPy/GCE (drop casting)	SWASV (120 s)	0.1 M HCl/KCl buffer (pH 3) [1 µM Hg^{2+}] (Pb^{2+})	4 pM (Pb^{2+})	5–60 nM (Pb^{2+})	642 µA µM^{-1} (Pb^{2+})	No interference: 50-fold Mg^{2+}, Zn^{2+}, Cu^{2+} 10-fold Cd^{2+}, 133-fold As(III)	-	-	[139]
Nafion-G-Pani/GCE (drop casting)	DPV (5 min ocp adsorption) (120 s reduction)	0.01 M HCl (Pb^{2+})	10 nM (Pb^{2+})	10 µM–1 nM (Pb^{2+})	-	No interference: 1-fold Cd^{2+}, Cu^{2+} (10 µM Pb^{2+})	Stab: Stable after 30 cycles	-	[140]
Poly(crystal violet)-nanoG/GCE (drop casting/ electrosynthesis)	DPV	ABS (pH 4.6) (Pb^{2+}, Cd^{2+})	Simultaneous: 6 nM (Pb^{2+}) 10 nM (Cd^{2+})	Simultaneous: 0.020–19.5 µM (Pb^{2+}) 0.040–55.8 µM (Cd^{2+})	Simultaneous: 1.87 µA µM^{-1} (Pb^{2+}) 0.59 µA µM^{-1} (Cd^{2+})	No interference: 1000-fold K^+, Na^+, Ca^{2+}, NH_4^+, 500-fold Al^{3+}, NO_3^-, Cl^-, 100-fold Ni^{2+}, Mn^{2+},	Stab: 99.4 % (Pb^{2+}), 99.2 % (Cd^{2+}) (30 days, air) RSD: 3 % (Pb^{2+}, Cd^{2+})	River water, lake water	[141]
1,2-bis(N'-benzoylthioureido) benzene-ERGO/GCE (electroreduction, dipping)	Potentiometry	pH 4.0-8.0 (NaOH-HCl) (Pb^{2+})	25.1 nM (Pb^{2+})	63.1 nM–39.8 mM (Pb^{2+})	30.37 mV decade^{-1} (C_{Pb2+}, M) (Pb^{2+})	No interference until high concentration of interferents (Na^+, Li^+, Ag^+, K^+, NH_4^+, Cs^{2+}, Ni^{2+}, Co^{2+}, Fe^{2+}, Zn^{2+}, Ca^{2+}, Hg^{2+}, Cu^{2+}, Cd^{2+}, Fe^{3+}, Al^{3+})	Stab: Stable for 10 weeks RSD: 1% (3 cycles)	Milk	[142]
PVDF-ERGO-GRC (drop casting, electroreduction)	Electromembrane extraction + SWV	0.1 M HCl (Pb^{2+})	0.09 nM (Pb^{2+})	0.25–2 nM (Pb^{2+})	1209.5 µA µM^{-1} (Pb^{2+})	-	Stab: 87 % (1 week, 4ºC), 85% (100 cycles) RSD: 8.3 % (5	Tap water, river water, sea water	[143]

43

							cycles)		
Sodium alginate-SWCNTs-RGO/GCE (drop casting)	DPASV (300 s)	ABS (pH 4.6) (Pb^{2+}, Cd^{2+}, Cu^{2+})	20 pM (Pb^{2+}) 0.75 nM (Cd^{2+}) 6.2 nM (Cu^{2+})	Simultaneous: 1 nM–10 µM (Pb^{2+}) 0.1–8 µM (Cd^{2+}) 0.2–2 µM (Cu^{2+})	Simultaneous: 8.75331 µA µM^{-1} (Pb^{2+}) 1.7223 µA µM^{-1} (Cd^{2+}) 4.7506 µA µM^{-1} (Cu^{2+})	-	Stab: 95 % (2 weeks, dry conditions) *RSD: 1.2 % (5 cycles)*	-	[144]

44

2.5. Other metal ions

2.5.1. Chromium

Exposure to chromium arises from ingestion, dermal contact or inhalation. Chromium effects include bronchial asthma, lung and nasal ulcers and cancers, skin allergies, reproductive and developmental problems [145]. The limit established by the WHO for Cr(VI) and Cr^{3+} concentrations in drinking water is 0.05 mg L^{-1}.

AuNPs-chitosan-RGO-PVP/Au electrodes have been used applying CV to determine Cr(VI) content [146]. The electrochemical response of these electrodes is improved 100-fold with respect to that of bare Au. The application of CV for Cr^{3+} determination has been also reported [147], using a GCE modified with RGO/Fe_3O_4 nanocomposite. The RGO and Fe_3O_4 contents were optimized in order to obtain the lower crystallite size and enhance the active surface area. On-line determination is also important to achieve real time analysis and thus, the use of an Autopret system coupled with a portable Mini potentiostat to perform on-line determination of Cr(VI) by LSV has been reported [148]. A SPC electrode coated with Pani/GQDs was used. The method of determination was very rapid and up to 90 samples per hour could be analysed.

2.5.2. Copper

When copper intoxication occurs, it is deposited firstly in the liver and disrupts the liver's ability to detoxify elevated copper level in the body. This affects adversely the nervous and reproductive systems, adrenal function, connective tissue, learning ability of new born babies, etc. [149]. In addition, copper is a powerful inhibitor of enzymes. The limit established by the WHO for Cu^{2+} concentration in drinking water is 2 mg L^{-1}.

In previous sections different works where Cu^{2+} was determined with other ions were presented [56,58,62,76,78-81,84,85,87,97,115,117,119,120,124,127,131,144]. In the present section, other works dealing with individual Cu^{2+} determination are presented [150-155]. In addition to G materials, other components of electrode formulation include: Rhodamine-B hydrazide [150], SA [144], PVP [131], Nafion [56,62,80,81,85,97,154], polyethyleneimine [154], other organic compounds [78-80,117,119,120,152,155], AuNPs [97,124,151], porous Au [127], Hg [56], Bi [58,62,115], Sn [76], CeO_2 [85], SnO_2 [87], Fe_3O_4 [131], CdS [153], MWCNTs [62] and SWCNTs [144].

Rhodamine-B hydrazide-GO/Au electrodes have been used for Cu^{2+} determination [150], in which GO provided the conductivity and Rhodamine-B contributed to the selective adsorption of Cu^{2+} ions. Cu^{2+} content was determined by EIS and correlated with the charge transfer resistance. When the concentration of Cu^{2+} in solution increased, there was an increase of Cu^{2+} adsorbed on the electrode surface and the charge transfer resistance rose. The regeneration of the electrode was simply accomplished in 0.1 M EDTA solution. Electrophoresis has been used as the deposition technique of GO on GCE [151], which was later electrochemically reduced to ERGO by CV. Thereafter, AuNPs were potentiostatically deposited. Synergy between the two components was observed: RGO provided a large surface area, good conductivity and

nucleation sites where Cu^{2+} could be adsorbed and AuNPs provided extraordinary conductivity, large surface area and good stability.

Less usual sensors include a photoelectrochemical sensor based on an RGO-CdS coating on carbon cloth [153]. The presence of RGO increased the photocurrent generated by three and two orders of magnitude when compared with CdS/ITO and CdS/carbon cloth electrodes, respectively. RGO wrapped around the CdS nanoparticles (Fig. 16) maximized interfacial contact, which improved electron conductivity. In addition, the presence of RGO enhanced the electron-hole pair lifetime due to the effective separation of the charges during the photogeneration process due to its good electron conductivity. Triethanolamine was used as a hole scavenger to avoid recombination of electron/hole pairs. The electrode showed a decrease of the photocurrent intensity in the presence of Cu^{2+}. This can be attributed to the formation of Cu_xS (x = 1,2) compounds which have lower solubility than CdS, fact that promoted the recombination of the pairs electron/hole which led to a decrease of the generated photocurrent.
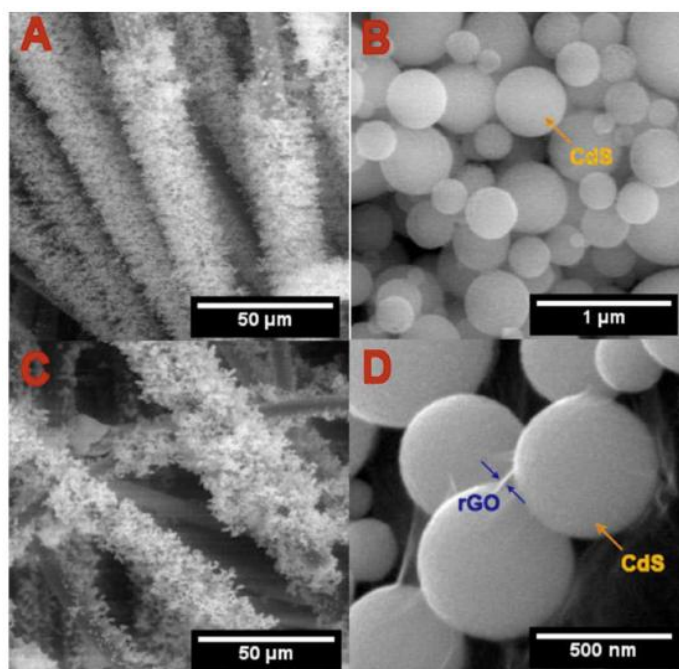
Fig. 16. FESEM images of CdS/CC and CdS/rGO/CC electrodes (A and C) at low magnification. Higher magnification of these two electrodes are shown in B and D, respectively. Adapted from Journal of Hazardous Materials, 304, C.Y. Foo, H.N. Lim, A. Pandikumar, N.M. Huang, Y.H. Ng, Utilization of reduced graphene oxide/cadmium sulfide-modified carbon cloth for visible-light-prompt photoelectrochemical sensor for copper (II) ions, 400-408, Copyright (2016), with permission from Elsevier [153].

Another electrode formulation includes a Nafion-PEI-RGO composite on a GCE [154]. PEI is a cationic polymer and the lone pairs of electrons in nitrogen atoms in the N–H bonds can effectively attract metallic cations. The electrode displayed high selectivity since PEI is a highly selective chelating agent towards Cu^{2+} and only Pb^{2+} was found to interfere.

46

A further type of deposition technique for the preparation of electrodes is layer by layer self-assembly deposition [155]. A GCE was immersed in a solution containing PAH (positive charge) for 30 min; subsequently the electrode was introduced in a solution containing GO (negative charge) for 30 min. This two-step process was repeated until a desired number of cycles; the optimal number of deposition cycles found was 12. The coatings were formed due to self-assembly induced by local interactions such as hydrogen-bonding, van der Waals forces, electrostatic and hydrophobic interactions. The prepared [PAH-GO]$_n$ coating was reduced to obtain [PAH-RGO]$_n$. The electrode showed good performance towards Cu^{2+} determination due to the high surface area, fast electron transfer rate and the evenly distributed amino groups that helped in the Cu^{2+} concentration process.

2.5.3. Silver

Silver has been reported to produce different toxic effects [156], such as the blue–grey discoloration of the skin termed argyria. The following dose-dependent animal toxicity findings have been reported: death, weight loss, hypo-activity, altered neurotransmitter levels, altered liver enzymes, altered blood values, etc. The effects induced by silver particles are mediated via silver ions that are released from the particle surface. WHO does not include Ag^+ in their guidelines for drinking-water quality.

Only two works dealing with Ag^+ determination using G-based electrodes were found in the literature [157,158]. The first work which was based on the Cytosine-Ag-Cytosine (C-Ag-C) metal-base pair achieved a very low LOD (2 pM) [157]. An Au electrode was coated by drop casting with Fe_3O_4/3D-GO nanocomposite. Thereafter, the electrode was immersed in a cytosine-rich DNA solution. The 3-D GO provided a porous structure and wrapped the Fe_3O_4NPs. The formation of the C-Ag-C metal-base pair produced an increase of the charge transfer resistance in the EIS spectrum, due to the formation of a blocking layer. The change in charge transfer resistance was proportional to the concentration of Ag^+ (logarithmic dependence). The 3-D and porous structure obtained provided active sites for attaching more DNA strands and achieve a low LOD.

The other approach proposed in bibliography consists in the deposition of cysteic acid by the electrochemical oxidation of L-cysteine (by CV) on a RGO/GCE electrode [158]. The developed electrode was highly selective towards Ag^+ determination due to the interaction between Ag^+ and the carboxylate and amino groups of cysteic acid. Fig. 17 shows the DPV voltammograms of Ag^+ and the different interfering ions determined (in 10-fold concentration), which demonstrates its selectivity.

47
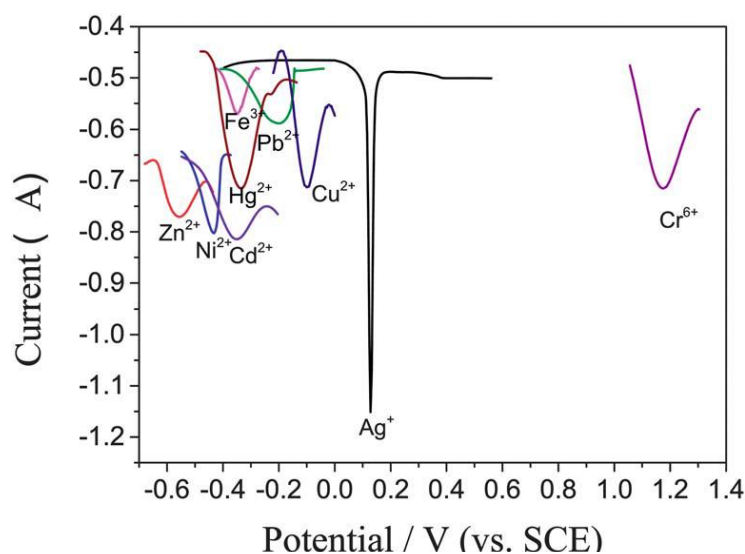
Fig. 17. Differential pulse voltammograms in 0.01 M HNO_3 solution with $6.0 \cdot 10^{-5}$ M different metal ions and $6.0 \cdot 10^{-6}$ M Ag(I). Reproduced from Ref 158 with permission of The Royal Society of Chemistry.

2.5.4. Zinc

The case of Zn^{2+} toxicity is very rare since high doses of Zn^{2+} are needed to produce toxic effects. An excess of Zn^{2+} interferes with the uptake of copper. Zn^{2+} deficiency is widespread and has a detrimental impact on growth, neuronal development, and immunity [159]. The limit established by WHO for Zn^{2+} in drinking water is 3 mg L^{-1}. Zn^{2+} has been determined jointly with other metal ions and the results have been included in previous tables [56,58-60,62,72]. Electrode formulation included Bi [58-60,62,72], Hg [56], Nafion [56,60,62,72], Pani [72] or MWCNTs [62] in addition to G materials.

2.5.5. Thallium

Thallium's most severe effects are produced in the nervous system. Although the exact mechanism of thallium toxicity is as yet unknown, impaired glutathione metabolism, oxidative stress, and disruption of potassium-regulated homeostasis have been pointed out as possible role-players [160]. In the present review, Tl^+ has been determined jointly with other metal ions and the results have been included in previous tables [122,134]. The thallium concentration limit in drinking water is not established by the WHO in their guidelines for drinking water.

Table 5. Determination of other elemental ions by electrochemical methods with graphene-based electrodes.

Electrode (Synthesis technique)	Technique (Accumulation time)	Supporting electrolyte (Metal ion)	LOD	Linear range	Sensitivity	Main interferences (target ion(s) concentration)	Stability (% of initial response) RSD (in calibrating solutions)	Application	[Ref]
AuNPs-chitosan-RGO-PVP/Au (drop casting, electrochemical synthesis)	CV	0.1 M HCl (Cr(VI))	-	5–800 μM (Cr(VI))	-	No interference: Ni^{2+}, Cu^{2+}, Cr^{3+}	-	-	[146]
Fe_3O_4-RGO/GCE (co-precipitation method, drop-casting)	CV	0.1 M PBS Cr^{3+}	-	-	-	-	-	-	[147]
Pani-GQDs/SPCE (electropolymerization)	Stopped flow analysis + LSV (5 s)	1 M HCl (Cr(VI))	1.87 μM (Cr(VI))	1.92–192 μM (Cr(VI))	0.1 μA μM^{-1} (Cr(VI))	No interference: 1-fold Fe^{3+}, 10-fold Pb^{2+}, Cu^{2+}, 100-fold Cd^{2+}, Cr^{3+}, Zn^{2+} (19.2 μM Cr(VI))	RSD: 4.9 % (100 cycles)	Mineral drinking water samples, deteriorated Cr plating solutions	[148]
Rhodamine-B hydrazide-GO/Au (self-assembly)	EIS (50 min adsorption)	5 mM $K_3[Fe(CN)_6]$–$K_4[Fe(CN)_6]$ + PBS + 0.1 M KCl (pH 7.4) (Cu^{2+})	0.061 nM (Cu^{2+})	0.1–50 nM (Cu^{2+})	2.554 kΩ decade^{-1} (C_{Cu2+}, nM)	No interference: 1-fold Hg^{2+}, Ag^+, Cr^{2+}, Fe^{2+}, Pb^{2+} Ba^{2+}, Mn^{2+}, Co^{2+}, Ni^{2+} (10 μM Cu^{2+})	-	-	[150]
AuNPs-ERGO/GCE (electrophoresis, electroreduction)	DPV (180 s)	0.1 M ABS (pH 5) (Cu^{2+})	0.028 nM (Cu^{2+})	5–100 nM (Cu^{2+})	77.9 μA μM^{-1} (Cu^{2+})	No interference: 50-fold Cd^{2+}, Pb^{2+}, Zn^{2+}, Fe^{2+}, Ca^{2+} (50 nM Cu^{2+})	-	-	[151]
Octylamine-GO/Au (drop casting)	SWASV (150 s)	0.1 M ABS (pH 5.3) (Cu^{2+})	2.7 μM (Cu^{2+})	2–50 μM (Cu^{2+}) 50–100 μM (Cu^{2+})	0.178 μA μM^{-1} (2-50 μM) (Cu^{2+})	Interference: 1-fold Pb^{2+} No interference: 1-fold Fe^{3+}, Li^+, Mn^{2+}, Ni^{2+}, Ca^{2+}, Mg^{2+}, Cd^{2+}, Hg^{2+}, Co^{2+}, Zn^{2+} (100 μM Cu^{2+})	-	Deionized water, tap water, lake water	[152]
RGO-CdS/carbon cloth (drop casting)	Chroamperometry (photoelectrochemistry)	0.1 M KCl + 0.5 M TEA (Cu^{2+})	0.05 μM (0.1-1.0 μM) (Cu^{2+}) 0.5 μM (1.0-40 μM) (Cu^{2+})	0.1–1.0 μM (Cu^{2+}) 1.0–40 μM (Cu^{2+})	-	Interference: 1-fold Mg^{2+}, Mn^{2+}, Ni^{2+}, Ag^+ No interference: 1-fold K^+, Na^+, Ba^{2+}, Zn^{2+}, Al^{3+}, Fe^{3+}, Co^{2+} (1 μM Ag$^+$)	-	-	[153]
Nafion-polyethyleneimine-RGO/GCE (drop casting)	DPASV (300 s)	0.1 M ABS (pH 4.0) (Cu^{2+})	0.3 μM (Cu^{2+})	1–70 μM (Cu^{2+})	0.5274 μA μM^{-1} (Cu^{2+})	Interference: 1-fold Pb^{2+} No interference: 1-fold Fe^{3+}, Cd^{2+}, Ni^{2+}, Mg^{2+}, Zn^{2+}, Ca^{2+}, K^+, Na^+ (30 μM Cu^{2+})	RSD: 2.37 % (8 cycles)	-	[154]
Polyallylamine hydrochloride RGO]$_{12}$/GCE (layer-by-layer assembly)	DPASV (420 s)	0.1 ammonium buffer solution (pH 7.0) (Cu^{2+})	0.35 μM (Cu^{2+})	0.5–50 μM (Cu^{2+})	-	No interference: 1-fold Cu^{2+}, Zn^{2+}, Mg^{2+}, Mn^{2+}, Ni^{2+}, Ca^{2+}, Fe^{2+}, Fe^{3+}, Na^+ (0.1 mM Cu^{2+})	-	-	[155]
DNA-Fe_3O_4-3D-GO/Au (drop casting)	EIS (24 h adsorption ocp	0.5 mM $[Fe(CN)_6]^{3-/4-}$ + 0.1 M KCl	2 pM (Ag$^+$)	0.01–100 nM (Ag$^+$)	1033.1 Ω decade^{-1}	No interference: 10-fold Li^+, Cd^{2+}, Zn^{2+}, Ni^{2+}, Mn^{2+},	Stab: 94 % (20 days at 4ºC)	Tap water, river water, spring	[157]

49

	in Ag$^+$ nitrate solution)	(Ag$^+$)			(C$_{Ag+}$, nM)	Cu^{2+}, Co^{2+}, Ca^{2+}, Mg^{2+}, Hg^{2+}, Pb^{2+}, Fe^{2+} (0.1 µM Ag$^+$)	*RSD: 4.4 % (10 cycles)*	water	
Cysteic acid-RGO/GCE (drop casting/ electrochemical synthesis)	DPASV (120 s)	0.01 M HNO$_3$ (Ag$^+$)	1 nM (Ag$^+$)	10 nM–0.2 mM (Ag$^+$)	0.10718 µA µM^{-1} (Ag$^+$)	No interference: 1500-fold (Cr(VI), 1000-fold Zn^{2+}, Ni^{2+}, 500-fold Cd^{2+}, Fe^{3+}, Hg^{2+}, 100-fold Cu^{2+}, Pb^{2+} (6·10^{-6} M Ag$^+$)	Stab: 96.7 % (2 months) *RSD: 3.4 % (7 cycles)*	Lake water, laboratory wastewater	[158]

50

3. Conclusions and perspectives

Anthropogenic activity is increasing the content of hazardous metal ions in different ecosystems and in the food chain, increasing the importance of precise determination of the content of the different metal ions. Electrochemical methods offer advantages over traditional methods used to this aim, such as simplicity, rapidity, flexibility, reliability and simultaneous determination of different metal ions. The most important feature of these techniques is the development of sensitive and selective electrodes. The trend in the design of the electrodes is to develop nanostructured and functionalized electrodes to obtain sensors for *in situ* application. In this sense, graphene-based materials offer several advantages over traditional electrodes in the electrochemical determination of metal ions, such as high surface area, conductivity and easy functionalization. The good electrical conductivity enhances electron transfer rate and the high surface area provides lower detection limits. Graphene can also act as a platform for the functionalization with different materials and/or biomolecules (metal nanoparticles, organic molecules, DNA, etc.) that improve the selectivity of the electrodes. Over the entire family of graphene materials, GO is the most advantageous since it is the cheapest and can be produced industrially in large quantities by an easy chemical oxidation method. The conductivity of GO can be partially restored by chemical, electrochemical, thermal or UV methods to reduce GO to RGO (part of sp^2 carbon domains are restored). The remaining oxygen-containing functional groups after the reduction can be exploited as nucleation/fixation points for nanoparticles or other selective chemicals towards the selective determination of metal ions.

In spite of the work already completed relating to this topic, there is plenty of room for the improvement of graphene-based electrochemical sensors. Graphene materials provide a versatile platform that can be tailored to produce 3-D structures alone or combined with other materials such as carbon nanotubes, conducting polymers, etc. [161]. These 3-D structures show superior surface area since they combine the 2-D structure of graphene materials (with high surface area) into a 3-D structure that is beneficial for lowering the limit of detection. Continuing with the graphene family, graphene quantum dots are also expected in the future to be used for such purpose. Graphene quantum dots provide a good conductivity and very high surface area due to their low dimensions and have been widely used in analytical sciences [162].

Doped graphene has application in materials for energy storage and production [33, 163], sensors [33], photocatalysis [164], etc. Electrochemical sensor performance can be improved by heteroatom doping since the electrochemically active sites introduced are able to facilitate charge transfer, adsorption and activation of analytes, and anchoring of functional moieties or molecules [33]. Elements used to dope graphene structures include B, N, P, O, S, F, Cl, Br, I, Se, etc. However, to date, only nitrogen-doped graphene has been used in metal ions analysis [84, 125]. Thus, there is plenty of room for the research and development of graphene-doped sensors for metal ions analysis.

Once the optimal formulation has been identified, another important factor is the production method. Screen printed electrodes combined with 2-D materials are the simplest and cheapest, and allow mass production with good reproducibility [165-167].

Functionalization with nanoparticles or other chemicals can be easily achieved by means of chemical or electrochemical methods on the screen printed electrodes. There is still the need for the development of flow-automated systems for the on-line determination of metal ions [66,67,148] in a rapid, flexible, reliable and simultaneous way [66]. Electrochemical methods are flexible, rapid and different ions can be detected simultaneously. However, stable, selective and sensitive electrodes should be developed. With this in mind, graphene-based electrodes have shown promising performance as electrode materials (better than other nanomaterials such as CNTs) [82,128]. The combination of graphene materials and electrochemical methods is expected to pave the way towards on-line and in-situ determination of metal ions (for instance in drinking water, river waters, food, etc.). As has been observed throughout the paper, different metal ions can be simultaneously determined with anodic stripping voltammetry techniques. However, if there is the need for specific electrodes for specific metal ions, it would be easy to design the electrochemical cell with different compartments (with specific electrodes) so that each metal ion could be determined with good sensitivity.

Role of the funding source

References:

[1] K. S. Novoselov, V. I. Fal'ko, L. Colombo, P. R. Gellert, M. G. Schwab, K. Kim. Nature 490 (2012) 192-200.

[2] K.S. Novoselov, A.K. Geim, S.V. Morozov, D. Jiang, Y. Zhang, S.V. Dubonos, I.V. Grigorieva, A.A. Firsov. Science 306 (2004) 666–669.

[3] A.K. Geim. Angew. Chem. Int. Ed. 50 (2011) 6967–6985.

[4] A.C. Ferrari, et al. Nanoscale 7 (2015) 4598–4810.

[5] G. Yang, C. Zhu, D. Du, J. Zhu, Y. Lin. Nanoscale 7 (2015) 14217–14231.

[6] T. Kuila, S. Bose, P. Khanra, A.K. Mishra, N.H. Kim, J.H. Lee. Biosens. Bioelectron. 26 (2011) 4637– 4648.

[7] M. Pumera. Mater. Today 14 (2011) 308-315.

[8] Y. Shao, J. Wang, H. Wu, J. Liu, I.A. Aksay, Y. Lin. Electroanal. 22 (2010) 1027–1036.

[9] S. Kochmann, T. Hirsch, O. S. Wolfbeis. Trends Anal. Chem. 39 (2012) 87-113.

[10] Y. Song, Y. Luo, C. Zhu, H. Li, D. Du, Y. Lin. Biosens. Bioelectron. 76(2015)195-212.

[11] S.K. Vashist, J.H.T. Luong. Carbon 84 (2015) 519-550.

[12] X. Gan, H. Zhao. Sensor Mater. 27 (2015) 191-215.

[13] Y. Liu, X. Dong, P. Chen. Chem. Soc. Rev. 41 (2012) 2283–2307.

[14] F. Yavari, N. Koratkar. J. Phys. Chem. Lett. 3 (2012) 1746−1753.

[15] B. Pérez-López, A. Merkoçi. Microchim. Acta 179 (2012) 1–16.

[16] K. Scida, P.W. Stege, G. Haby, G.A. Messina, C.D. García. Anal. Chim. Acta 691 (2011) 6–17.

[17] J. Liu, Z. Liu, C.J. Barrow, W. Yang. Anal. Chim. Acta 859 (2015) 1–19.

[18] A.K. Sundramoorthy, S. Gunasekaran. Trends Anal. Chem. 60 (2014) 36–53.

[19] M. Pumera. Chem. Rec. 9 (2009) 211–223.

[20] A.T. Lawal. Talanta 131 (2015) 424–443.

[21] P. Ramnani, N.M. Saucedo, A. Mulchandani. Chemosphere 143 (2016) 85-98.

[22] O. Moldovan, B. Iñiguez, M.J. Deen, L.F. Marsal. IET Circuits Devices Syst. 9 (2015) 446–453.

[23] S. Sakthinathan, S.-M. Chen. Int. J. Electrochem. Sci. 10 (2015) 6527-6536.

[24] L. MeiJiao, L. Jing, Y. XuYu, Z. ChangAn, Y. Jia, H. Hao, W. XianBao. Chin. Sci. Bull. 58 (2013) 2698-2710.

[25] J. Chang, G. Zhou, E.R. Christensen, R. Heideman, J. Chen. Anal. Bioanal. Chem. 406 (2014) 3957–3975.

[26] G. Aragay, J. Pons, A. Merkoçi. Chem. Rev. 111 (2011) 3433–3458.

[27] A.K. Wanekaya. Analyst 136 (2011) 4383–4391.

[28] G. Aragay, A. Merkoçi. Electrochim. Acta 84 (2012) 49–61.

[29] M.B. Gumpu, S. Sethuraman, U.M. Krishnan, J.B.B. Rayappan. Sens. Actuators, B 213 (2015) 515–533.

[30] G. March, T.D. Nguyen, B. Piro. Biosensors 5 (2015) 241–275.

[31] D.R. Dreyer, S. Park, C.W. Bielawski, R.S. Ruoff. Chem. Soc. Rev. 39 (2010) 228–240.

[32] S. Park, R.S. Ruoff. Nat. Nanotechnol. 4 (2009) 217–224.

[33] X. Wang, G. Sun, P. Routh, D.-H. Kim, W. Huang, P. Chen. Chem. Soc. Rev. 43 (2014) 7067–7098.

[34] Z. Xia-Hong, Z. Ting-Yao, C. Xi. Chin J. Anal. Chem. 43 (2015) 1296–1305.

[35] S. Guo, E. Wang. Nano Today 6 (2011) 240-264.

[36] P.T. Yin, T.-H. Kim, J.-W. Choi, K.-B. Lee. Phys. Chem. Chem. Phys. 15 (2013) 12785-12799.

[37] S. Bai, X. Shen. RSC Adv. 2 (2012) 64–98.

[38] P.V. Kamat. J. Phys. Chem. Lett. 1 (2010) 520–527.

[39] F.W. Campbell, R.G. Compton. Anal. Bioanal. Chem. 396 (2010) 241-259.

[40] X. Wang, B. Liu, Q. Lu, Q. Qu. J. Chromatogr., A 1362 (2014) 1–15.

[41] V. Georgakilas, M. Otyepka, A.B. Bourlinos, V. Chandra, N. Kim, K.C. Kemp, P. Hobza, R. Zboril, K.S. Kim. Chem. Rev. 112 (2012) 6156−6214.

[42] Editorial. Carbon 65 (2013) 1-6.

[43] W.M. Edmunds, K.M. Ahmed, P.G. Whitehead. Environ. Sci.: Process. Impact 17 (2015) 1032-1046.

[44] M.F. Hughes, B.D. Beck, Y. Chen, A.S. Lewis, D.J. Thomas. Toxicol. Sci. 123 (2011) 305–332.

[45] M. Bissen, F.H. Frimmel. Acta Hydroch. Hydrob. 31 (2003) 9–18.

[46] M. Kumaresan, P. Riyazuddin. Curr. Sci. 80 (2001) 837–846.

[47] Z.-G. Liu, X.-J. Huang. Trends Anal. Chem. 60 (2014) 25–35.

[48] W.-W. Li, F.-Y. Kong, J.-Y. Wang, Z.-D. Chen, H.-L. Fang, W. Wang. Electrochim. Acta 157 (2015) 183–190.

[49] B.J. Sanghavi, N.S. Gadhari, P.K. Kalambate, S.P. Karna, A.K. Srivastava. Microchim. Acta 182 (2015) 1473–1481.

[50] Y. Liu, Z. Huang, Q. Xie, L. Sun, T. Gu, Z. Li, L. Bu, S. Yao, X. Tu, X. Luo, S. Luo. Sens. Actuators, B 188 (2013) 894–901.

[51] R. Kempegowda, D. Antony, P. Malingappa. International Journal of Smart and Nano Materials 5 (2014) 17-32.

[52] R.A. Dar, N.G. Khare, D.P. Cole, S.P. Karna, A.K. Srivastava. RSC Adv. 4 (2014) 14432–14440.

[53] G.K. Ramesha, S. Sampath. Sens. Actuators, B 160 (2011) 306–311.

[54] S. Kumar, G. Bhanjana, N. Dilbaghi, R. Kumar, A. Umar. Sens. Actuators, B 227 (2016) 29–34.

[55] A. Sarkar, G. Ravindran, V. Krishnamurthy. International Journal of Bio-Technology and Research 3 (2013) 17-36.

[56] C.M. Willemse, K. Tlhomelang, N. Jahed, P. G. Baker, E.I. Iwuoha. Sensors 11 (2011) 3970-3987.

[57] J. Li, S. Guo, Y. Zhai, E. Wang. Electrochem. Commun. 11 (2009) 1085–1088.

[58] P.K. Sahoo, Bharati Panigrahy, S. Sahoo, A.K. Satpati, Dan Li, D. Bahadur. Biosens. Bioelectron. 43 (2013) 293–296.

[59] K. Pokpas, S. Zbeda, N. Jahed, N. Mohamed, P.G. Baker, E.I. Iwuoha. Int. J. Electrochem. Sci. 9 (2014) 736 – 759.

[60] S. Lee, S. Bong, J. Ha, M. Kwak, S.-K. Park, Y. Piao. Sens. Actuators, B 215 (2015) 62–69.

[61] J. Li, S. Guo, Y. Zhai, E. Wang. Anal. Chim. Acta 649 (2009) 196–201.

[62] H. Huang, T. Chen, X. Liu, H. Ma. Anal. Chim. Acta 852 (2014) 45–54.

[63] J. Ping, Y. Wang, J. Wu, Y. Ying. Food Chem. 151 (2014) 65–71.

[64] C. Huangfu, L. Fu, Y. Li, X. Li, H. Du, J. Ye. Electroanal. 25 (2013) 2238–2243.

[65] Z. Wang, H. Wang, Z. Zhang, G. Liu. Sens. Actuators, B 199 (2014) 7–14.

[66] G. Zhao, Y. Si, H. Wang, G. Liu. Int. J. Electrochem. Sci. 11 (2016) 54–64.

[67] W. Wonsawat, S. Chuanuwatanakul, W. Dungchai, E. Punrat, S. Motomizu, O. Chailapakul. Talanta 100 (2012) 282–289.

[68] A.F. Al-Hossainy, A.A.I. Abd-Elmageed, A.Th.A. Ibrahim. Arabian J. Chem. (2015) http://dx.doi.org/10.1016/j.arabjc.2015.06.020, in press.

[69] Z. Li, L. Chen, F. He, L. Bu, X. Qin, Q. Xie, S. Yao, X. Tu, X. Luo, S. Luo. Talanta 122 (2014) 285–292.

[70] M. Lv, X. Wang, J. Li, X. Yang, C. Zhang, J. Yang, H. Hu. Electrochim. Acta 108 (2013) 412– 420.

[71] L. Zhu, L. Xu, B. Huang, N. Jia, L. Tan, S. Yao. Electrochim. Acta 115 (2014) 471– 477.

[72] N. Ruecha, N. Rodthongkum, D.M. Cate, J. Volckens, O. Chailapakul, C.S. Henry. Anal. Chim. Acta 874 (2015) 40–48.

[73] N. Promphet, P. Rattanarat, R. Rangkupan, O. Chailapakul, N. Rodthongkum. Sens. Actuators, B 207 (2015) 526–534.

[74] X. Yuan, Y. Zhang, L. Yang, W. Deng, Y. Tan, M. Ma, Q. Xie. Analyst 140 (2015) 1647–1654.

[75] Z. Wang, H. Wang, Z. Zhang, X. Yang, G. Liu. Electrochim. Acta 120 (2014) 140–146.

[76] P.M. Lee, Z. Chen, L. Li, E. Liu. Electrochim. Acta 174 (2015) 207–214.

[77] W. Zhou, C. Li, C. Sun, X. Yang. Food Chem. 192 (2016) 351–357.

[78] S. Muralikrishna, K. Sureshkumar, Thomas S. Varley, D. H. Nagaraju, T. Ramakrishnappa. Anal. Methods 6 (2014) 8698–8705.

[79] V.K. Gupta, M.L. Yola, N. Atar, Z. Ustundag, A.O. Solak. Electrochim. Acta 112 (2013) 541– 548.

[80] S.-M. Choi, D.-M. Kim, O.-S. Jung, Y.-B. Shim. Anal. Chim. Acta 892 (2015) 77-84.

[81] W. Bin, C. Yan-hong, Z. Lin-jie. New Carbon Mater. 26 (2011) 31-35.

[82] L. Wu, X. Fu, H. Liu, J. Li, Y. Song. Anal. Chim. Acta 851 (2014) 43–48.

[83] G. Liu, J. Chen, X. Hou, W. Huang. Anal. Methods 6 (2014) 5760–5765.

[84] H. Xing, J. Xu, X. Zhu, X. Duan, L. Lu, W. Wang, Y. Zhang, T. Yang. J. Electroanal. Chem. 760 (2016) 52–58.

[85] Y.-L. Xie, S.-Q. Zhao, H.-L. Ye, J. Yuan, P. Song, S.-Q. Hu. J. Electroanal. Chem. 757 (2015) 235-242.

[86] C. Gao, X.-Y. Yu, R.-X. Xu, J.-H. Liu, X.-J. Huang. ACS Appl. Mater. Interfaces 4 (2012) 4672−4682.

[87] Y. Wei, C. Gao, F.-L. Meng, H.-H. Li, L. Wang, J.-H. Liu, X.-J. Huang. J. Phys. Chem. C 116 (2012) 1034–1041.

[88] Y.-F. Sun, W.-K. Chen, W.-J. Li, T.-J. Jiang, J.-H. Liu, Z.-G. Liu. J. Electroanal. Chem. 714-715 (2014) 97–102.

[89] S. Xiong, B. Yang, D. Cai, G. Qiu, Z. Wu. Electrochim. Acta 185 (2015) 52–61.

[90] D.A.C. Brownson, C. E. Banks. Electrochem. Commun. 13 (2011) 111–113.

[91] RA. Bernhoft. J. Environ. Public Health Volume 2012 (2012) Article ID 460508.

[92] N. Zhou, J. Li, H. Chen, C. Liao, L. Chen. Analyst 138 (2013) 1091–1097.

[93] J. Gong, T. Zhou, D. Song, L. Zhang. Sens. Actuators, B 150 (2010) 491–497.

[94] L. Ding, Y. Liu, J. Zhai, A.M. Bond, J. Zhang. Electroanal. 26 (2014) 121–128.

[95] N. Zhou, H. Chen, J. Li, L. Chen. Microchim. Acta 180 (2013) 493–499.

[96] D. Martín-Yerga, M.B. González-García, A. Costa-García. Sens. Actuators, B 165 (2012) 143–150.

[97] S. Luong Ting, S.J. Ee, A. Ananthanarayanan, K.C. Leong, P. Chen. Electrochim. Acta 172 (2015) 7–11.

[98] P.K. Sahoo, S. Sahoo, A.K. Satpati, D. Bahadur. Electrochim. Acta 180 (2015) 1023–1032.

[99] A. Shirzadmehr, A. Afkhami, T. Madrakian. J. Mol. Liq. 204 (2015) 227–235.

[100] Y. Zhang, J. Xie, Y. Liu, P. Pang, L. Feng, H. Wang, Z. Wu, W. Yang. Electrochim. Acta 170 (2015) 210–217.

[101] Y. Yang, M. Kang, S. Fang, M. Wang, L. He, J. Zhao, H. Zhang, Z. Zhang. Sens. Actuators, B 214 (2015) 63–69.

[102] M. Wang, S. Liu, Y. Zhang, Y. Yang, Y. Shi, L. He, S. Fang, Z. Zhang. Sens. Actuators, B 203 (2014) 497–503.

[103] Z. Zhang, X. Fu, K. Li, R. Liu, D. Peng, L. He, M. Wang, H. Zhang, L. Zhou. Sens. Actuators, B 225 (2016) 453–462.

[104] N. Wang, M. Lin, H. Dai, H. Ma. Biosens. Bioelectron. 79 (2016) 320–326.

[105] M. Wang, S. Zhang, Z. Ye, D. Peng, L. He, F. Yan, Y. Yang, H. Zhang, Z. Zhang. Microchim. Acta 182 (2015) 2251–2258.

[106] H. Park, S.-J. Hwang, K. Kim. Electrochem. Commun. 24 (2012) 100–103.

[107] Y. Zhang, H. Zhao, Z. Wu, Y. Xue, X. Zhang, Y. He, X. Li, Z. Yuan. Biosens. Bioelectron. 48 (2013) 180–187.

[108] S. Fang, X. Dong, Y. Zhang, M. Kang, S. Liu, F. Yan, L. He, X. Feng, P. Wang, Z. Zhang. New J. Chem. 38 (2014) 5935-5942.

[109] H. Zhou, X. Wang, P. Yu, X. Chena, L. Mao. Analyst 137 (2012) 305–308.

[110] Z.-Q. Zhao, X. Chen, Q. Yang, J.-H. Liu, X.-J. Huang. Chem. Commun. 48 (2012) 2180–2182.

[111] N.G.Yasri, A.K. Sundramoorthy, W.-J. Chang, S. Gunasekaran. Front. Mater. 1 (2014) 33.

[112] G. Flora, D. Gupta, A. Tiwari. Interdiscip. Toxicol. 5 (2012) 47–58.

[113] Z. Wang, L. Li, E. Liu. Thin Solid Films 544 (2013) 362–367.

[114] Z. Wang, E. Liu. Talanta 103 (2013) 47–55.

[115] Z. Wang, P.M. Lee, E. Liu. Thin Solid Films 544 (2013) 341–347.

[116] D.A. C. Brownson, C.E. Banks. RSC Advances 2 (2012) 5385–5389.

[117] N. Kong, J. Liu, Q. Kong, R. Wang, C.J. Barrow, W. Yang. Sens. Actuators, B 178 (2013) 426–433.

[118] K. Hamsawahini, P. Sathishkumar, R. Ahamad, A.R.M. Yusoff. Talanta 144 (2015) 969–976.

[119] X. Gong, Y. Bi, Y. Zhao, G. Liu, W.Y. Teoh. RSC Adv. 4 (2014) 24653-24657.

[120] Y. Zhang, M. Qi, G. Liu. Electroanal. 27 (2015) 1110–1118.

[121] J.-T. Zhang, Z.-Y. Jin, W.-C. Li, W. Dong, A.-H. Lu. J. Mater. Chem. A 1 (2013) 13139–13145.

[122] L. Cui, J. Wu, H. Ju. Chem. Eur. J. 21 (2015) 11525–11530.

[123] Z. Lu, S. Yang, Q. Yang, S. Luo, C. Liu, Y. Tang. Microchim. Acta 180 (2013) 555–562.

[124] P.M. Lee, Z. Wang, X. Liu, Z. Chen, E. Liu. Thin Solid Films 584 (2015) 85–89.

[125] Y.-m. Cheng, H.-b. Fa, W. Yin, C.-j. Hou, D.-q. Huo, F.-m. Liu, Y. Zhang, C. Chen. J. Solid State Electrochem. 20(2016) 327-335.

[126] C. Zhou, W. Jiang, B.K. Via. Colloids Surf., B 118 (2014) 72–76.

[127] H. Zhu, Y. Xu, A. Liu, N. Kong, F. Shan, W. Yang, C.J.Barrow, J. Liu. Sens. Actuators, B 206 (2015) 592–600.

[128] Q. Zhao, Y. Chai, R. Yuan, J. Luo. Sens. Actuators, B 178 (2013) 379–384.

[129] B. Wang, B. Luo, M. Liang, A. Wang, J. Wang, Y. Fang, Y. Chang, L. Zhi. Nanoscale 3 (2011) 5059-5066.

[130] M.R. Mahmoudian, Y. Alias, W.J. Basirun, Pei Meng Woi, M. Sookhakian, Farid Jamali-Sheini. Electrochim. Acta 169 (2015) 126–133.

[131] Y. Sun, W. Zhang, H. Yu, C. Hou, D.-s. Li, Y. Zhang, Yaqing Liu. J. Alloys Compd. 638 (2015) 182–187.

[132] L. Yuan-Yuan, C. Meng-Ni, G. Yi-Li, Y. Jian-Mao, M. Xiao-Yu, L. Jian-Yun. Chin. J. Anal. Chem. 43 (2015) 1395–1401.

[133] S. Smarzewska, W. Ciesielski. Food Anal. Methods 8 (2015) 635–642.

[134] H. Bagheri, A. Afkhami, H. Khoshsafar, M. Rezaei, S.J. Sabounchei, M. Sarlakifar. Anal. Chim. Acta 870 (2015) 56–66.

[135] J.-M. Jian, Y.-Y. Liu, Y.-L. Zhang, X.-S. Guo, Q. Cai. Sensors 13 (2013) 13063-13075.

[136] W. Feng, L. Hong-Wei, Y. Xin, C. Di-Zhao. Int. J. Electrochem. Sci., 8 (2013) 7702-7712.

[137] X. Hu, D. Pan, M. Lin, H. Han, F. Li. ECS Electrochem. Lett. 4 (2015) H43-H45.

[138] R. Seenivasan, W.-J. Chang, S. Gunasekaran. ACS Appl. Mater. Interfaces 7 (2015) 15935−15943.

[139] Z.-Q. Zhao, X. Chen, Q. Yang, J.-H. Liu, X.-J. Huang. Electrochem. Commun. 23 (2012) 21–24.

[140] C. Yanhong, W. Bin, L. Hui, Z. Linjie. IEEE (2010) 978-1-4244-7161-4/10.

[141] M. Chen, M. Chao, X. Ma. J. Appl. Electrochem. 44 (2014) 337–344.

[142] A.A. Abraham, M. Rezayi, N.S.A. Manan, L. Narimani, A.N.B. Rosli, Y. Alias. Electrochim. Acta 165 (2015) 221–231.

[143] K. Hamsawahini, P. Sathishkumar, R. Ahamad, A.R.M. Yusoff. Talanta 148 (2016) 101–107.

[144] D. Wang, F. Zhang, J. Tang. Electrochem. 83 (2015) 84–90.

[145] K. Shekhawat, S. Chatterjee, B. Joshi. Int. J. Adv. Res. 3 (2015) 167-172.

[146] C. Santhosh, M. Saranya, R. Ramachandran, S. Felix, V. Velmurugan, A.N. Grace. J. Nanotechnol 2014, Article ID 304526.

[147] A. Prakash, S. Chandra, D. Bahadur. Carbon 50 (2012) 4209-4219.

[148] E. Punrat, C. Maksuk, S. Chuanuwatanakul, W. Wonsawat, O. Chailapakul. Talanta 150 (2016) 198–205.

[149] B. Ashish, K. Neeti, K. Himanshu. Res. J. Recent Sci. 2 (2013) 58-67.

[150] M. Kang, D. Peng, Y. Zhang, Y. Yang, L. He, F. Yan, S. Sun, S. Fang, P. Wang, Z. Zhang. New J. Chem., 2015, 39, 3137-3144.

[151] S. Wang, Y. Wang, L. Zhou, J. Li, S. Wang, H. Liu. Electrochim. Acta 132 (2014) 7–14.

[152] W. Zhang, J. Wei, H. Zhu, K. Zhang, F. Ma, Q. Mei, Z. Zhang, S. Wang. J. Mater. Chem. 22 (2012) 22631–22636.

[153] C.Y. Foo, H.N. Lim, A. Pandikumar, N.M. Huang, Y.H. Ng. J. Hazard. Mater. 304 (2016) 400–408.

[154] R. Hu, H. Gou, Z. Mo, X. Wei, Y. Wang. Ionics 21 (2015) 3125–3133.

[155] H. Liu, S. Li, D. Sun, Y. Chen, Y. Zhou, T. Lu. J. Mater. Chem. B 2 (2014) 2212–2219.

[156] N. Hadrup, H.R. Lam. Regul. Toxicol. Pharm. 68 (2014) 1–7

[157] Y. Yang, M. Kang, S. Fang, M. Wang, L. He, X. Feng, J. Zhao, Z. Zhang, H. Zhang. J. Alloys Compd. 652 (2015) 225-233

[158] L. Liu, C. Wang, G. Wang. Anal. Methods 5 (2013) 5812-5822.

[159] L.M. Plum, L. Rink, H. Haase. Int. J. Environ. Res. Public Health 7 (2010) 1342-1365.

[160] P. Cvjetko, I. Cvjetko, M. Pavlica. Arh. Hig. Rada. Toksikol. 61 (2010) 111-119.

[161] Y. Shen, Q. Fang, B. Chen. Environ. Sci. Technol. 49 (2015) 67−84.

[162] S. Benítez-Martínez, M. Valcárcel. Trends Anal. Chem. 72 (2015) 93–113.

[163] J. Duan, S. Chen, M. Jaroniec, S.Z. Qiao. ACS Catal. 5 (2015) 5207−5234.

[164] L.K. Putri, W.-J. Ong, W.S. Chang, S.-P. Chai. Appl. Surf. Sci. 358 (2015) 2–14.

[165] A. Hayat, J.L. Marty. Sensors 14 (2014) 10432-10453.

[166] K. Duarte, C.I.L. Justino, A.C. Freitas, A.M.P. Gomes, A.C. Duarte, T.A.P. Rocha-Santos. Trends Anal. Chem. 64 (2015) 183–190.

[167] F. Tan, J.P. Metters, C.E. Banks. Sens. Actuators, B 181 (2013) 454–462.